



HAL
open science

The syn-rift tectono-stratigraphic record of rifted margins (Part II): A new model to break through the proximal/distal interpretation frontier

Pauline Chenin, Gianreto Manatschal, Jean-François Ghienne, Peng Chao

► To cite this version:

Pauline Chenin, Gianreto Manatschal, Jean-François Ghienne, Peng Chao. The syn-rift tectono-stratigraphic record of rifted margins (Part II): A new model to break through the proximal/distal interpretation frontier. Basin Research, In press, 10.1111/bre.12628 . insu-03473206

HAL Id: insu-03473206

<https://insu.hal.science/insu-03473206>

Submitted on 9 Dec 2021

HAL is a multi-disciplinary open access archive for the deposit and dissemination of scientific research documents, whether they are published or not. The documents may come from teaching and research institutions in France or abroad, or from public or private research centers.

L'archive ouverte pluridisciplinaire **HAL**, est destinée au dépôt et à la diffusion de documents scientifiques de niveau recherche, publiés ou non, émanant des établissements d'enseignement et de recherche français ou étrangers, des laboratoires publics ou privés.

1
2
3
4
5
6
7
8
9
10
11
12
13
14
15
16
17
18
19
20
21
22
23

The syn-rift tectono-stratigraphic record of rifted margins (Part II):

A new model to break through the proximal/distal interpretation frontier

Pauline Chenin^{1*}, Gianreto Manatschal¹, Jean-François Ghienne¹, Peng Chao¹

[1] Université de Strasbourg, CNRS, ITES UMR 7063, 5 rue Descartes, 67084 Strasbourg,
France

* corresponding author: chenin@unistra.fr

Keywords: hyperextended margin, rifting, tectono-stratigraphic record

Highlights

- A new tectono-stratigraphic model to help break through the proximal/distal interpretation frontier
- Each rift domain is associated with specific structures and sedimentary architectures
- Each rift domain displays a specific ratio of vertical vs horizontal accommodation space creation
- Rift deformation localizes sequentially, inducing a younging of the base of passive infill oceanward
- The early syn-rift stratigraphic record is largely discontinuous/broken up in the distal margin

24 Abstract

25 One fundamental lesson from the last decades research into rifted margins is that
26 stratigraphic horizons cannot be simply correlated from the proximal into distal domain, which
27 makes the interpretation of poorly calibrated and largely inaccessible distal margins difficult.
28 In this contribution, we propose a new tectono-stratigraphic model to help break through the
29 proximal/distal interpretation frontier. After reviewing the scientific advances on rifted margins
30 achieved during the last century, we describe the primary spatio-temporal evolution of active
31 deformation during rifting. We show that different rift domains are associated with specific
32 (1) periods of active deformation; (2) tectonic structures and related stratigraphic
33 architecture; (3) amounts of accommodation creation owing to specific ranges of horizontal
34 widening and vertical deepening; and (4) depositional environments. We demonstrate that
35 the sequential localization of extension during rifting results in a younging of the base of
36 passive infill (i.e., sediment deposited in a non-tectonic setting) oceanward. We propose a
37 panel of few to few tens of My time intervals related to specific tectonic events – our *Tectonic*
38 *Sequences* – that may be correlated more or less easily and continuously across rifted
39 margins. This study underlines the value of an iterative approach between fieldwork on fossil
40 rifted margins and offshore geophysical studies, where field studies offer easy-to-access and
41 high-resolution calibration of dismembered rifted margin remnants, while geophysical studies
42 provide comparatively low-resolution imaging of entire, intact but largely inaccessible, rifted
43 margins. It also highlights the necessity of jettisoning outdated dogma on rifted margins and
44 changing our routines when interpreting seismic sections and outcrops.

45

46 1. Introduction

47 Rifting is a process involving extension of the crust and upper mantle, during which
48 accommodation is created by both horizontal widening and vertical deepening. The
49 involved sedimentary systems record the timing, location and type of tectonic

50 deformation, the distribution of depocenters, the reorganization of sedimentary sources,
51 and the evolution of water depths. Yet, distal parts of present-day rifted margins have
52 remained largely inaccessible to date, including to drilling, which makes the interpretation
53 of their syn-rift stratigraphic architecture, the determination of their sedimentary facies,
54 and their correlation with more proximal parts of the margin difficult.

55 Over the last decades, the scientific community has made significant progress in
56 understanding the processes at play during rifting. The iterative workflow between
57 onshore and offshore studies, together with the improvement of imaging, dating and
58 modelling techniques, enabled us to identify the characteristics common to rift systems,
59 and to recognize a systematic deformation sequence during their formation. The ensuing
60 question is: does a comparable formation history among rift systems imply a similar
61 tectono-stratigraphic record, despite the differences in their local sedimentary sources
62 and depositional environments?

63 In this contribution, we propose a new conceptual tectono-stratigraphic model
64 synthesizing the evolution of deformation over space and time during rifting. We review
65 *when, where* and *how* accommodation is created, and show that specific domains of
66 rifted margins are associated with specific (1) periods of tectonic activity; (2) style of
67 deformation and tectono-stratigraphic architectures; (3) ratios of horizontal vs vertical
68 accommodation creation; and (4) depositional environments. After briefly summarizing
69 the historical evolution of models for rifted margins, we describe our tectono-stratigraphic
70 model and compare it with observations from both present-day and fossil rifted margins.
71 Then, we discuss how this template can help interpreting seismic sections in poorly
72 calibrated rift systems and to correlate remnants of dismembered margins embedded in
73 orogens (e.g., Alps, Pyrenees, Oman, Timor, Zagros). Finally, we examine the limitations
74 of our model, in particular the correlation of timelines/time intervals both along dip and
75 strike of rifted margins, the effect of sedimentation rates with respect to the rates of

76 subsidence, the impact of magma, and the challenge of including a three-dimensional
77 perspective at segmented and multiphase rift systems.

78

79 2. Historical overview

80 Rifting has always been regarded as a process creating accommodation space that is
81 filled with sediments and/or volcanic products and/or water, both during and after the
82 termination of deformation (McKenzie, 1978). However, our understanding of *when*,
83 *where* and *how* accommodation is created and filled has been significantly evolving over
84 the last decades (e.g., Bond and Kominz, 1988; De Graciansky *et al.*, 2011; Gawthorpe
85 *et al.*, 1994; Gawthorpe and Leeder, 2000; Olsen and Morgan, 2006; Schlische, 1995;
86 Withjack *et al.*, 2002).

87

88 2.1. The Geosyncline Theory (from the late 1850's to the 1960's)

89 The premise of tectonics emerged from the work of Hall (1859), who first recognized
90 the existence of vertical movements (subsidence and uplift) of the Earth surface and
91 the folding of sedimentary series (Figure 1a). Hall suggested that folding occurred at
92 the *axis* of *synclinal* structures that resulted from Earth surface deformation. Dana
93 (1873) suggested that the subsidence of *Geosynclines* (which corresponded to Hall's
94 synclinal axis) was balanced by the rising of adjacent *Geanticlines*, both resulting
95 from Earth contraction-driven lateral compression. A few decades later, Haug (1900)
96 introduced the distinction between shallow- and deep-water facies, and emphasized
97 their lateral change between the margins and the axial part of a Geosyncline. He also
98 suggested that Geosynclines were mobile zones located at the boundary between
99 two stable continental masses. These basic concepts were further developed during
100 subsequent decades with the work of Argand (1916), Kay (1951), Kober (1923) and

101 Stille (1913, 1924, 1936), among others. For further details on the birth and evolution
102 of the Geosyncline Theory see the review by Aubouin (1965).

103

104 2.2. The early stages of Plate Tectonic Theory: Pure-Shear vs Simple-Shear models and
105 the birth of seismic stratigraphy (from the 1970's to the early 1990's)

106 Based on the first reflection seismic sections at rifted margins (e.g., Montadert *et al.*
107 1979), rift systems and rifted margins were envisioned as essentially comprising
108 oceanward-dipping, high-angle (ca. 60 °) normal faults separating a series of tilted
109 fault blocks and associated half-graben/graben whose size decreased oceanward
110 (Figure 1b). The oceanic crust was supposed to start directly where thinned
111 continental crust terminated, which implied a localized and instantaneous breakup
112 related to the onset of steady-state magma emplacement. McKenzie (1978) and
113 Jarvis and McKenzie (1980) envisioned rifting as Pure-Shear (depth-uniform) thinning
114 of the lithosphere, resulting in both rapid (“instantaneous”) subsidence associated
115 with crustal thinning, and subsequent protracted, progressively decreasing
116 subsidence related to thermal relaxation of the thinned lithospheric mantle.

117 A few years later, Lemoine *et al.* (1987) suggested that Wernicke's (1985) alternative
118 Simple-Shear Model would better explain the ancient Alpine Tethys rift system
119 (Figure 1c). Indeed, observations from the Alpine Tethys margins exposed in the Alps
120 diverged from the Pure-Shear Model predictions in that: (1) the topographic and
121 thermal evolution of the former conjugate margins appeared to be largely asymmetric
122 (Lemoine, 1985), contrasting with the predictions of the symmetrical Pure-Shear
123 Model; (2) at least one of the two margins was uplifted during rifting (e.g., the
124 Briançonnais Block; Lemoine *et al.*, 1986), while the Pure-Shear model only predicted
125 subsidence; and (3) no evidence for a Penrose-type oceanic crust could be found;
126 instead, Alpine geologists had evidenced exhumation of subcontinental mantle to the
127 seafloor (Decandia and Elter, 1972, 1969).

128 Contemporaneously, Falvey (1974) laid the ground for modern rifted margin
129 stratigraphy. He stated that the onset of rifting was marked by an unconformity
130 generated by a phase of thermal doming, which he named the *Rift Onset*
131 *Unconformity (ROU)*. He also mentioned the existence of a so-called *Breakup*
132 *Unconformity (BU)*, associated with the onset of rapid subsidence of the entire
133 margin. This phase of rapid subsidence, modelled a few years later as an isostatic
134 adjustment following the mechanical breakup of the lithosphere by Braun and
135 Beaumont (1989), was thought to be expressed by the progradation of sedimentary
136 deposits over the shelf and continental slope.

137 Hubbard (1988) introduced the term “megasequence”, which he defined as a “major
138 sedimentary package” bounded by “the most prominent regional unconformities”. He
139 suggested that these prominent regional unconformities “record the principal periods
140 of change in basin geometry and polarity”. Hubbard (1988), and then Prosser (1993),
141 recognized three types of megasequences, namely pre-, syn- and post-rift
142 megasequences, deposited respectively prior to the onset of rifting, during rifting and
143 after the termination of rifting.

144 In the 1980’s–early 1990’s, the architecture of the pre-, syn and post-rift
145 megasequences were conceptualized with the help of analytical (Barr, 1991, 1987),
146 analogue (Buchanan and McClay, 1991), and numerical modelling (Hardy, 1993).
147 The pre-rift megasequence was supposed to be coupled to the underlying basement,
148 except in the presence of low frictional, efficiently decoupling materials like salt or
149 clays. In the absence of pre-rift tectonic events, pre-rift deposits are essentially
150 comprised of parallel strata (i.e., without growth structures; violet sediments in
151 Figures 1b and 1c).

152 The syn-rift megasequence was regarded as comprised of wedge-shape sedimentary
153 deposits that thicken toward the adjacent normal fault (blue sediments in Figures 1b
154 and 1c). However, the nature of the isostatic compensation (none, local or regional),

155 the geometry of the normal fault involved (planar or listric), sedimentation rates and
156 climate may result in various stratal geometries of these syn-rift deposits (e.g., Barr,
157 1991; Buchanan and McClay, 1991; Prosser, 1993).

158 The post-rift megasequence was interpreted to be made of un-extended sedimentary
159 packages that drape or onlap against preexisting topography, or downlap onto
160 oceanic crust (green sediments in Figures 1b and 1c). In isolated basins, when the
161 sedimentation rate is very low compared to the rate of subsidence, these deposits are
162 parallel and horizontal. Otherwise, they display clinofold shapes (e.g., significant
163 thickening of strata toward the basin center; Fig. 5 of Waltham *et al.*, 1993).

164 In the “rigid domino fault blocks” models for rifted margins (Figures 1b and 1c), all
165 faults and intervening tilted blocks are required to move and stop moving
166 simultaneously, and thus the syn-rift megasequence is synchronous across the entire
167 margin (blue sediments in Figures 1b and 1c; Waltham *et al.*, 1993). Both the base
168 and top of the syn-rift megasequence are therefore ideally marked by an isochronous
169 change in stratal dip across the entire margin, either between parallel pre-rift deposits
170 and wedge-shape syn-rift deposits in the former case, or between wedge-shape syn-
171 rift deposits and parallel post-rift deposits in the latter.

172

173

174 2.3. Toward a Polyphase Rifting Model (from the 1990's to the early 2010's)

175 Stratigraphic studies from both the Alps (Froitzheim and Eberli, 1990) and the Iberia–
176 Newfoundland margins (Murillas *et al.*, 1990; Tucholke *et al.*, 2007; Wilson *et al.*,
177 2001) highlighted that Alpine Tethys and southern North-Atlantic rifting were achieved
178 via two main, distinct and successive extensional phases. During the first phase,
179 numerous and broadly distributed half-graben depocenters, bounded by high-angle
180 normal faults, formed over a wide region (dark blue sediments in Figure 1d). At this

181 stage, crustal and lithospheric thinning were minor ($1/\beta \ll 1.5$, where $1/\beta$
182 corresponds to the ratio *crust thickness prior to extension / crust thickness at the end*
183 *of extension*; McKenzie, 1978). During the second phase, tectonic activity was
184 localized only in the future distal margins. There, significant crustal thinning
185 ($1.5 < 1/\beta < \infty$) was achieved via both normal and extensional detachment faulting, as
186 well as via the attenuation of ductile middle- and/or lower crustal layers (Manatschal
187 *et al.* 2001; light blue sediments in Figure 1d). Crustal thinning was accompanied by
188 significant lithospheric thinning.

189 Using numerical models, Lavier and Manatschal (2006) suggested that rifting was
190 achieved via successive and distinct deformation modes, which we call here
191 *Polyphase Rifting*. In their model, deformation evolved from initially distributed
192 extension with limited crustal and lithospheric thinning (the so-called *stretching*
193 *phase*) to increasingly localized deformation with significant crustal and lithospheric
194 thinning (the so-called *thinning* and (*mantle*) *exhumation* phases). At the shift
195 between the *stretching* and *thinning* phases, deformation stopped in the future
196 proximal domain while rifting was still active in the future distal domain. This
197 numerical model was consistent with the observation of passive infill sedimentation in
198 the proximal domain at a time when rifting was not achieved yet, as in the Alpine
199 Tethys (Froitzheim and Eberli, 1990; Masini *et al.*, 2013) and in Iberia–Newfoundland
200 (Manatschal and Bernoulli, 1999; Murillas *et al.*, 1990; Péron-Pinvidic *et al.*, 2007;
201 Tucholke *et al.*, 2007).

202 The observation of passive infill deposits emplaced during rifting required the
203 refinement of the term *syn-rift*. Following Masini *et al.* (2013), we here restrict the use
204 of *syn-rift* to its temporal dimension with respect to the overall rifting event, and use
205 the terms *pre-tectonic*, *syn-tectonic* and *post-tectonic* to characterize the architecture
206 of sedimentary deposits with respect to local tectonic activity (Figures 2a–2d). In this
207 perspective, pre-rift sediments are necessarily pre-tectonic and post-rift sediments

208 are necessarily post-tectonic. However, syn-rift sediments may be either pre-, syn- or
209 post-tectonic (Figure 2e).

210 In the absence of pre-rift tectonic events and inherited topography, pre-tectonic
211 sediments display horizontal and parallel strata of constant thickness (Figure 2a).
212 Syn-tectonic sediments are usually wedge-shaped, but their architecture varies
213 depending on the type of fault they are associated with (Figure 2f). Indeed, while
214 normal faults generate only minor horizontal extension (< 5 km), extensional
215 detachment faults may exhume basement over more than 15 km (e.g., Epin and
216 Manatschal, 2018). We qualify deposits as *half-graben wedge-shaped* when
217 associated with a high-angle normal fault (Figure 2b) and *supra-detachment wedge-*
218 *shaped* when related to an extensional detachment fault (Figure 2c). Note that the
219 development of such growth structures is conditional on a sufficient syn-tectonic
220 sedimentation rate. Extensional detachment faults are generally associated with
221 cataclastic breccias and black gouges (Chester and Logan, 1986; Froitzheim and
222 Eberli, 1990; Manatschal *et al.*, 2000), and, when exhumed to the seafloor, their
223 surface is typically overlain by tectono-sedimentary breccias (e.g., Collettini, 2011,
224 and references therein; Masini *et al.*, 2011). Post-tectonic deposits (Figure 2d) are
225 either made of strata onlapping against, downlapping onto, or draping residual rift-
226 related topography. Away from rift-related faults and/or in the absence of rift-related
227 topography or intervening syn-tectonic deposits, pre- and post-tectonic deposits may
228 practically be indistinguishable and only a paraconformity might capture the
229 intervening syn-tectonic stage.

230

231 3. Building a stratigraphic model for idealized rifted margins

232 Over the last decade, the intense iterative workflow between field studies at remnants
233 of rifted margins exposed on land (e.g., Andersen *et al.*, 2012; Masini *et al.*, 2013;

234 Mohn *et al.*, 2010; Epin *et al.*, 2017; Gawthorpe *et al.*, 2018; Ribes *et al.*, 2019b;
235 Serck *et al.*, 2021; Stockli and Bosworth, 2018), interpretation of rifted margin seismic
236 sections with ever higher resolutions (e.g., Causer *et al.*, 2020; Clerc *et al.*, 2018;
237 Gillard *et al.*, 2016; Hauptert *et al.*, 2016; Lymer *et al.*, 2019; Osmundsen *et al.*, 2016;
238 Whiting *et al.*, 2020; Yang and Welford, 2021; Zhang *et al.*, 2019) and numerical
239 modelling (e.g., Huismans and Beaumont, 2011; Brune *et al.*, 2014; Chenin *et al.*,
240 2020; Duretz *et al.*, 2020; Jourdon *et al.*, 2020; Naliboff *et al.*, 2017; Pérez-Gussinyé
241 *et al.*, 2020; Petri *et al.*, 2019) have allowed to considerably improve our
242 understanding of the architecture and evolution of rifted margins.

243 3.1. Benefits and pitfalls of using a template to guide interpretation

244 In this contribution, we propose a tectono-stratigraphic model to guide seismic
245 and field interpretations in correlating observations from proximal margins into
246 their distal continuation. Although model-driven approaches have historically
247 caused significant misinterpretations and remain problematic when blindly
248 applied (e.g., review by Manatschal *et al.*, 2021), having a first-order template
249 may help when attempting to unravel the tectono-stratigraphic-record of
250 uncalibrated distal domains. Indeed, sedimentary facies of given age may vary
251 between the shallow-water proximal domain and deep-water hyperextended
252 domain, and thus one cannot rely on the seismic signature/sedimentary field
253 observations to correlate sedimentary units. Furthermore, as new real estate
254 (i.e., new depositional surface) is created via the exhumation of basement along
255 extensional detachment faults, the stratigraphic record may be largely
256 discontinuous (e.g., sediments older than the age of exhumation are missing
257 over the corresponding new real estate). This implies that seismic/field
258 interpretations should not attempt to find continuous pre-rift or early syn-rift
259 deposits in distal margins, where extensional detachment faults are likely.

260 The tectono-stratigraphic model we propose aims to describe an interpretation
261 philosophy rather than providing a template to be copy-pasted, and we stress
262 that careful seismic observations, rigorous application of the first principles of
263 stratigraphy, and mindful consideration of the local geological history remain
264 crucial to reliable interpretations.

265

266 3.2. Preliminary concepts and definitions

267

268 3.2.1. A spatial framework for rifted margins: definition of rift domains

269 Based on the geometry of top basement and Moho, which are two of the most
270 consensual interfaces observed on seismic sections (red lines on Figure 3a),
271 Sutra *et al.* (2013) identified four systematic rift domains. From the continent to
272 the oceans, these domains are: (1) the *proximal domain*, where top basement
273 and Moho are sub-horizontal and parallel, and where the 30 ± 5 km-thick crust
274 displays only minor thinning. When the lithosphere was equilibrated prior to
275 rifting (i.e. sub-horizontal top basement, Moho and base of the lithosphere),
276 crustal thickness in the proximal domain may be used as a proxy for pre-rift
277 crustal thickness; (2) the *necking domain*, where the crust is thinned from 30 ± 5
278 km to ca. 10 km; (3) the *hyperextended domain*, where the crust is thinned from
279 ca. 10 km to 0 km. Compared with the necking domain, the angle of aperture
280 between top basement and Moho is lower and more consistent in the
281 hyperextended domain (Nirrengarten *et al.*, 2016; Sutra and Manatschal, 2012;
282 Figure 3a); and (4) the *exhumed mantle domain*, where subcontinental
283 lithospheric mantle is exhumed to the seafloor (Figure 3a).

284 Based on a worldwide compilation of seismic sections across magma-poor rifted
285 margins and rift systems (i.e., < 6 km thickness of magmatic addition prior to
286 lithospheric breakup; Tugend *et al.*, 2020), Chenin *et al.* (2017) proposed that

287 each domain displays a typical range of width, specifically: necking domains
288 range between 10 and 100 km, with an average of 55 km; hyperextended
289 domains between 20 and 70 km, with an average of 50 km; and exhumed
290 mantle domains between 20 and 110 km with an average of 60 km (Figure 3b).
291 They highlighted the absence of correlation between the width of the different
292 domains for a given margin (Figure 3c).

293

294 3.2.2. Linking domains to rheological architecture and deformation processes

295 The variability in the angle of aperture between top basement and Moho among
296 the different domains of rifted margins (red lines in Figure 3a) is interpreted to
297 reflect along-dip changes in the rheology of the continental crust and underlying
298 mantle, which may arise from composition, strain-rate, structural and/or
299 temperature evolution during rifting (Chenin *et al.*, 2017; Nirrengarten *et al.*,
300 2016; Sutra and Manatschal, 2012; Brune *et al.*, 2014; Ros *et al.*, 2017; Figures
301 3d and 3e). In the proximal domain, crustal thinning is minor, broadly distributed,
302 and largely accommodated by ductile deformation within the middle- to lower
303 crust, which accounts for the horizontal and parallel position of both top
304 basement and Moho (Sutra *et al.*, 2013). In the necking domain, the
305 convergence between top basement and Moho is interpreted to reflect the
306 progressive removal of ductile layers (Pérez-Gussinyé *et al.*, 2003; Sutra *et al.*,
307 2013). In the hyperextended domain, the lower dip angle of top basement is
308 thought to express the frictional thinning of a fully brittle continental crust over a
309 weak, serpentinized mantle (Nirrengarten *et al.*, 2016).

310 Following Péron-Pinvidic *et al.* (2013), we propose that each domain is linked to
311 a specific deformation mode at play during rifting (Figure 3f): (1) the proximal
312 domain displays numerous and broadly distributed half-graben depocenters
313 formed during the *stretching phase* of Lavier and Manatschal (2006). The

314 tectono-thermal evolution of this domain is essentially ruled by the McKenzie
315 (1978) model; (2) the necking domain is largely shaped by viscoplastic necking
316 of the lithosphere (Chenin *et al.*, 2018). This *necking phase* corresponds to the
317 early thinning phase of Lavier and Manatschal (2006). It is characterized by
318 focusing of deformation into a narrower region compared to the early stretching
319 phase (20–100 km according to the analytical study by Fletcher and Hallet,
320 1983; the seismic observations by Chenin *et al.*, 2017; and the numerical
321 models by Chenin *et al.*, 2018). There, significant crustal thinning is achieved via
322 detachment faulting (Mohn *et al.*, 2012; Osmundsen and Péron-Pinvidic, 2018;
323 Ribes *et al.*, 2020); (3) the hyperextended domain is essentially shaped by
324 Coulomb Wedge-type frictional thinning of fully brittle continental crust
325 (Nirrengarten *et al.*, 2016). Here, crustal thinning is achieved via in-sequence
326 detachment faulting in highly damaged continental crust (Epin and Manatschal,
327 2018; Lymer *et al.*, 2019; Manatschal, 1999). The *hyperextension phase*
328 corresponds to the late thinning phase of Lavier and Manatschal (2006); and (4)
329 the exhumed mantle domain records the exhumation of subcontinental mantle
330 (i.e., the *mantle exhumation phase* of Lavier and Manatschal, 2006) via first in-
331 sequence detachment faulting and then out-of-sequence or “flip-flop”
332 detachment faulting (Epin *et al.*, 2019; Gillard *et al.*, 2016a; Reston and
333 McDermott, 2011). Flip-flop mantle exhumation generates relatively symmetrical
334 mantle exhumation (Gillard *et al.*, 2016b).

335

336

337 3.2.3. Constraining the spatio-temporal evolution of rifting using the stratigraphic
338 record

339 Recently, Ribes *et al.* (2019b) studied the migration of deformation across the
340 Adriatic margin during Alpine Tethys rifting. In each rift domain they identified

341 syn-tectonic sedimentary packages and placed them into a chronostratigraphic
342 time framework by comparing their position with respect to established timelines
343 (i.e., sedimentary markers tied to dated global events; Figure 4). From this
344 analysis, they concluded that: (1) Alpine Tethys rifting was associated with strain
345 localization, namely the region of active deformation (pink color in Figure 4)
346 became narrower as rifting advanced, and finally focused into the region of
347 future breakup; (2) the focusing of deformation was achieved through discrete
348 steps (i.e., *sequential*) rather than progressively (see the staircase architecture
349 of the roof of the syn-tectonic sequence, which climbs up between the proximal,
350 necking, hyperextended and exhumed mantle domain in Figure 4); and (3)
351 significant amounts of *new real estate* were locally created due to basement
352 (crust or mantle) exhumation via extensional detachment faults (Figure 4). This
353 newly exhumed material could only collect sediments that are younger than its
354 exhumation age, which implies a discontinuous stratigraphic record along dip of
355 the margin.

356 Comparable conclusions were drawn from the study of high-resolution reflection
357 seismic sections in the South China Sea by Chao *et al.* (2021) and Luo *et al.*
358 (2021), in the Porcupine Basin by Whiting *et al.* (2020), in the North Atlantic by
359 Sharp *et al.* (2017), and from numerical models by Pérez-Gussinyé *et al.* (2020):
360 all recognized a sequential localization of deformation into the distal domain as
361 rifting progresses, and/or increasing fragmentation of the pre-rift top basement
362 with ever wider domains of new real estate created between older fragments
363 oceanward.

364 Considering that each rift domain (*proximal, necking, hyperextended* and
365 *exhumed mantle domain*) is dominantly controlled by one specific deformation
366 mode (*stretching, necking, hyperextension* and *mantle exhumation*, respectively;
367 Figure 3f), and assuming that these deformation modes are active during distinct

368 periods of time, Ribes *et al.* (2019b) defined four *system tracts*, namely the
369 *stretching, necking, hyperextension* and *mantle exhumation system tracts*. In the
370 following, we will refer to these periods as *Tectonic Sequences (TS)*; see next
371 section for a discussion of terminology-related issues). A *Tectonic Sequence*
372 encompasses all the sediments deposited during the period of activity of the
373 corresponding deformation mode.

374

375 3.2.4. A short discussion on the complexity of finding accurate and illustrative
376 terminology in an already jargon-rich field

377 In seismic interpretation calibrated by well data, it is common to map seismic
378 *sequences* along rifted margins and to assign them a non-interpretive name
379 linked to their relative age (e.g., J10, J20, J30, K19, K20, etc.; for instance Alves
380 *et al.*, 2003). In contrast, in field studies or in interpretation of seismic images
381 where chronostratigraphic constraints are lacking, it is common to map *system*
382 *tracts/depositional sequences* or seismic *packages* according to the
383 characteristic structures they display (e.g., Posamentier and Vail, 1988; Prosser,
384 1993; Ribes *et al.*, 2019b). Both these "non-interpretative" and "sequence
385 stratigraphy" approaches are equivalent in 2D, however differences arise when it
386 comes to analyze the stratigraphy of a propagating or segmented rift system in
387 3D: In the system tract approach, one correlates deformation phases without
388 regard on their timing (i.e., the age of their upper and lower boundary may
389 change ages across the rift system). In contrast, in the non-interpretative
390 approach, one correlates timelines/isochronous seismic packages without
391 regard to the tectonic processes they record (i.e., one package of given age may
392 display the characteristic deformation patterns of the stretching phase in one
393 segment, and of the hyperextension phase in the adjacent segment).

394 While the term *sequence* often has a time connotation, the term *system tract*
395 rather relies on sedimentary architectures (e.g., stratal terminations). The term
396 *package* is probably the most neutral term that can be used to present
397 observations. Here we chose to use the term *Tectonic Sequence (TS)* to refer to
398 the sediment body deposited during a given deformation phase to underline that
399 (1) they are related to and coeval with a specific deformation mode; and (2) the
400 upper- and lower limit of these packages are isochrons along dip of a given
401 rifted margin transect (2D). We discuss in section 6.4.3 the difficulties raised by
402 studying rifted margins in 3D.

403

404 3.3. Characteristic Tectonic Sequences (TSs) of an idealized 2D along-dip transect 405 across a rifted margin

406 In the present section, we describe the characteristics of the TSs of our idealized
407 model (Figure 5a–5g) without going through the details of construction. The
408 observations on which this model was built derive essentially from the Alps and are
409 presented in Part I (companion paper by Manatschal *et al.*, this volume). The present
410 contribution aims to present our idealized model and show its application. Of course,
411 because it is idealized, our model is simplified (see discussion in section 6.1). It aims
412 to capture the first-order structures and patterns that can generally be identified at
413 rifted margins; however, when applying this model, one must always keep in mind
414 that each rift system is unique and builds on its own inheritance.

415 Based on the field and seismic observations, conceptual models and numerical
416 modelling results presented in section 3.2, we present the Wheeler diagram of
417 idealized two-dimensional rifted margins. By *idealized* we mean that the seven
418 following hypotheses are fulfilled: (1) rifting is achieved via **four distinct and**
419 **successive extension phases** that are the stretching, necking, hyperextension and
420 mantle exhumation phases; (2) these extension phases **do not overlap in time,**

421 therefore **each** one is **associated with one single Tectonic Sequence**, namely
422 stretching, necking, hyperextension and mantle exhumation TS; (3) each extension
423 phase is **controlled by a single deformation mode**, namely stretching, necking,
424 hyperextension and mantle exhumation; (4) the **structures** formed during a
425 deformation phase are **characteristic and specific to the corresponding**
426 **deformation mode**; (5) each **deformation mode is spatially restricted to the rift**
427 **domain(s) it affects** (a deformation mode may affect several rift domains); (6) when
428 a **rift domain** is affected by a deformation mode, its **entire width is affected**; and
429 (7) rifting is a localizing process during which the **successive deformation modes**
430 **affect an ever narrower region**.

431

432 3.3.1. The stretching TS

433 The stretching TS records the stretching phase, which is characterized by a low-
434 β ($\beta \ll 1.5$, where β corresponds to the ratio *length prior to extension / length at*
435 *the end of extension*; McKenzie, 1978) pure shear extension of the lithosphere
436 accommodated by broadly distributed, high-angle normal faulting of brittle layers
437 (usually the upper crust and upper mantle) and plastic deformation of ductile
438 ones (usually the middle- and lower crust). The corresponding half-graben
439 depocenters are distributed over the entire rift domain (Figures 5b and 5g1). The
440 **stretching TS** will thus display **comparable depositional characteristics in**
441 **the future proximal, necking and hyperextended domains** (fifth line of Figure
442 6a), although it will be increasingly overprinted and dismembered by subsequent
443 extensional events in the distal domains (fifth line of Figure 6b). In contrast, the
444 stretching TS will be absent in the exhumed mantle domain since no mantle is
445 exhumed to the seafloor during the stretching phase.

446 The stretching TS is characterized by **wedge-shaped sedimentary deposits**
447 that thicken toward the main controlling normal faults (Figure 5g1 and fifth line of

448 Figure 6a). Related deposits often include breccias derived from the adjacent
449 footwall crest and fault plane. Indeed, the activity of a normal fault is usually
450 associated with footwall uplift and erosion due to the rotation of the fault block
451 (Yielding, 1990) and/or to the flexural response of the lithosphere (Kusznir and
452 Ziegler, 1992). Most of the infill is however linked to axial sedimentation
453 (Gawthorpe and Leeder, 2000; Leeder and Gawthorpe, 1987).

454 Accommodation creation during the stretching phase is predominantly created
455 by fault-controlled subsidence within rift basins. No significant lithospheric
456 thinning occurs during this stage, so that only limited accommodation is created
457 outside the basins, and only minor subsequent thermal subsidence is recorded
458 across the future proximal domain. Moreover, the usually high ratio between the
459 sedimentation- and accommodation creation rates hampers the formation of
460 significant bathymetry during the stretching phase (fifth line of Figure 6c).

461

462 3.3.2. The necking TS

463 The necking TS records the major phase of crustal thinning, from ca. 30 to
464 10 km ($1.5 < 1/\beta < 3$). During the early stages of the necking phase, a few large-
465 offset (up to few tens of km; e.g., Osmundsen and Péron-Pinvidic, 2018; Ribes
466 *et al.*, 2020; Sutra *et al.*, 2013) detachment faults form on either side of a largely
467 undeformed crustal **keystone** (*H-block* in Lavier and Manatschal, 2006; Figure
468 5c). These major **crustal-scale detachment faults**, which may **exhume mid-**
469 **crustal levels to the seafloor** (Ribes *et al.*, 2020), are specific and
470 characteristic structures of the future necking domains. The isostatic uplift
471 resulting from detachment-related tectonic denudation (Spencer, 1984) may
472 result in **erosion** of the exhumed basement and nearby deposition of
473 **siliciclastic sediments/sandstones** (e.g., the *Grès Singuliers* in the Mont

474 Blanc region; Ribes *et al.*, 2020, and references therein), ideally with a *supra-*
475 *detachment wedge-shaped* architecture.

476 At the same time, most of the normal faults formed during the stretching phase
477 are inactivated outside the necking domain. As a result, **the necking TS**
478 **outside the necking domain is characterized by the sealing of the older**
479 **half-graben depocenters by post-tectonic, passively infilling sediments**
480 (fourth line of Figure 6a; e.g., Masini *et al.*, 2013). As no mantle is exhumed to
481 the seafloor during the necking phase, the necking TS is absent in the exhumed
482 mantle domain.

483 The onset of crustal necking is linked to the yield of the strongest lithospheric
484 layer, which is usually the upper mantle in a thermally equilibrated lithosphere
485 (Figure 3d). When the upper crust is mechanically decoupled from the mantle,
486 the mechanical breakdown of the upper mantle is followed by a flexural rebound
487 that tends to bring the necked system back to isostatic equilibrium (Braun and
488 Beaumont, 1989). This flexural rebound accounts for the shallow-water depth, or
489 even the **uplift and local erosion of the keystone** (i.e., the future necking and
490 hyperextended domains) during the necking phase (see erosional unconformity
491 in Figures 5c, 5d and 5g5; Chenin *et al.*, 2019, 2020). Uplift of the keystone may
492 be further increased by the thermal erosion related to the asthenosphere
493 upwelling beneath the rift system.

494 The late necking phase (Figure 5d) is linked to significant crustal and
495 lithospheric thinning, which will eventually counterbalance the flexural rebound
496 of the lithosphere and cause rapid and significant subsidence (e.g., Ribes *et al.*,
497 2020). The timing of uplift vs subsidence depends strongly on the rheology of
498 the lithosphere (Chenin *et al.*, 2020). Subsidence might be further enhanced by
499 large sediment supply and by subsequent thermal relaxation of the rift system.

500 In summary, **in the necking domain of the final margin, the necking TS** is
501 expressed by (fourth line of Figures 6a–6c): (1) **creation of new real estate** due
502 to the exhumation of upper- to middle crustal rocks to the seafloor via
503 extensional detachment faulting; (2) ***supra-detachment wedge-shaped***
504 **sedimentary deposits of necking phase age** emplaced **directly onto**
505 **exhumed basement**; (3) uplift and **erosion of exhumed basement and pre-**
506 **necking sediments** potentially visible **in both the necking and**
507 **hyperextended domains**; and (4) **contemporaneous deposition of**
508 **basement-derived material in adjacent regions**. These sediments may be
509 “cannibalized” (i.e., remobilized and re-deposited) during the necking phase
510 owing to the progressive exhumation–uplift–rollover of the detachment fault on
511 which the sandstones were deposited.

512

513 3.3.3. The hyperextension TS

514 The hyperextension TS records the localized dismembering of fully brittle
515 continental crust from 10 to 0 km thick ($3 < 1/\beta < \infty$). Hyperextension is the first
516 deformation stage to display a marked asymmetry (Nirrengarten *et al.*, 2016;
517 Ranero and Pérez-Gussinyé, 2010): on the one hand, the future lower-plate
518 margin is extended via in-sequence detachment faulting; and on the other hand,
519 the future conjugate upper-plate margin is delaminated by the slip on the
520 underlying detachment fault (Figures 5e, 5g2 and 5g4; Hauptert *et al.*, 2016).
521 Each of these deformation processes results in a particular morphology of the
522 margin (see below).

523 During hyperextension, the proximal and necking domains are tectonically
524 inactive, which results in continued passive infill in the proximal domain and the
525 sealing of syn-tectonic structures/deposits in the necking domain (third line of

526 Figure 6a). Thus, **in the proximal and necking domains of the future margin,**
527 **the hyperextension TS is characterized by post-tectonic deposits.** Due to
528 the lack of mantle exhumation at this stage, the hyperextension TS is absent in
529 the exhumed mantle domain.

530 The hyperextension phase is associated with **rapid subsidence in both the**
531 **necking and hyperextended domains** (third line of Figure 6c). Subsidence is
532 related to extreme crustal thinning above a mechanically weak mantle (the
533 mechanical breakup of the upper mantle was achieved during the previous
534 necking phase). In the necking domain, subsidence is at this stage essentially
535 driven by thermal relaxation (i.e., lithosphere cooling).

536 In the lower-plate hyperextended domain, each successive in-sequence
537 detachment fault crosscuts the former one, resulting in the typical in-sequence
538 architecture illustrated in Figure 5g2 and 6a (Ranero and Pérez-Gussinyé,
539 2010). These detachment faults create new real estate via the exhumation of
540 basement to the seafloor (Figure 5g2). The amount of basement exhumed by a
541 detachment fault was reckoned to 10–20 km along-dip in the hyperextended
542 domain of the Adriatic lower-plate margin (Alpine Tethys) by Epin and
543 Manatschal (2018). The exhumed basement is typically pre-rift upper- to middle
544 crust. Each detachment fault is associated with a supra-detachment
545 sedimentary basin floored by tectono-sedimentary breccias. These basins are
546 filled with supra-detachment wedge-shaped syn-tectonic sediments emplaced
547 directly onto the detachment surface, getting younger toward the detachment
548 exhumation point (third line of Figure 6a; Masini *et al.*, 2011). As the successive
549 in-sequence detachment faults are active one after another, syn-tectonic
550 sedimentary deposits become younger oceanward (Péron-Pinvidic *et al.*, 2007).
551 Therefore, sedimentary deposits of a given age that are syn-tectonic in one

552 supra-detachment basin are post-tectonic in supra-detachment basins located
553 more continent-ward.

554 In summary, **in the hyperextended domain of the final lower-plate margin,**
555 **the hyperextension TS is expressed by** (third line of Figures 6a– 6c):
556 (1) creation of **new real estate** due to the exhumation of upper- to middle crustal
557 rocks to the seafloor via **in-sequence detachment faults that dip exclusively**
558 **oceanward;** (2) **tectono-sedimentary breccias and overlying supra-**
559 **detachment wedge-shaped sedimentary deposits of hyperextension phase**
560 **age emplaced directly onto exhumed basement;** and (3) a progressive
561 **younging of supra-detachment basins fill oceanward.**

562 The hyperextended domain of upper-plate margins represents the residual part
563 of the initial keystone block (Hauptert *et al.*, 2016; Figure 5g4). Compared with its
564 conjugate, the upper-plate hyperextended domain preserves therefore much
565 more of the stretching and necking-related structures and deposits, namely high-
566 angle normal faults that can dip continent- or oceanward. The base of the outer
567 part of the hyperextended domain is a mantle exhumation fault that may
568 eventually bring lower crustal rocks to the seafloor.

569 Ribes *et al.* (2019a) suggested that the individualization of the upper-plate
570 hyperextended domain is often associated with the formation of a *mega-fault*
571 *scarp* at its boundary with the adjacent necking domain. They defined a *mega-*
572 *fault scarp* as a "topographic ramp [formed by a] system of high-angle faults and
573 facing oceanwards a domain of substantial underfilled accommodation space".
574 They noticed that mega-fault scarps are linked with the emplacement of breccias
575 at their toe, over a wide part of the hyperextended domain (Figure 5g4).

576 In summary, **in the hyperextended domain of the final upper-plate margin,**
577 **the hyperextension TS is expressed by:** (1) creation of **a mega-fault scarp**

578 **and** associated **mega-breccias** at the boundary between the necking and future
579 hyperextended domain; (2) good preservation of earlier sedimentary structures
580 due to the **lack of significant new real estate creation**; and (3) possible
581 **exhumation of lower crustal rocks to the seafloor** at the outer edge of the
582 hyperextended domain.

583

584 3.3.4. The mantle exhumation TS

585 The mantle exhumation TS records the phase of subcontinental mantle
586 exhumation to the seafloor (Figure 5f). Mantle exhumation occurs while tectonic
587 activity has ceased in the continental domains of the future margin, **therefore**
588 **the mantle exhumation TS in the proximal, necking and hyperextended**
589 **domains is characterized by post-tectonic sedimentation** (second line of
590 Figure 6a). The entire margin keeps on subsiding during the mantle exhumation
591 phase.

592 The exhumed mantle domain is entirely comprised of new real estate, except
593 from few potential allochthonous blocks of continental crust and/or pre to syn-rift
594 sediments. Subcontinental mantle exhumation is achieved via out-of-sequence
595 flip-flop detachment faults that develop successively on either side of the future
596 spreading center, generating a relatively symmetrical pattern (Epin *et al.*, 2019;
597 Gillard *et al.*, 2016b; Figure 5g and second line of Figure 6a). The activity of a
598 mantle exhumation fault is associated with the formation of a topographic high at
599 the detachment fault breakaway (Spencer, 1984), and thus characterized by
600 over-tilted sedimentary sequences (see to the very right of Figure 5g3; Gillard *et*
601 *al.*, 2015). As tectonic activity continuously steps toward the locus of future
602 breakup, the age of the over-tilted sequences decreases (youngers) oceanward.
603 The first sediments overlying the exhumed mantle are tectono-sedimentary

604 breccias, and if sedimentary sources are available, the next ones are supra-
605 detachment wedge-shaped syn-tectonic sediments deposited directly onto the
606 detachment surface.

607 The exhumation phase often displays incipient magmatic activity, which results
608 in discontinuous magmatic intrusions and lava flows (Coltat *et al.*, 2019; Epin *et*
609 *al.*, 2019; Gillard *et al.*, 2016b, 2015). Magmatic flows are syn-tectonic, and thus
610 they are interbedded with sediments of exhumation phase age.

611 In summary, **in the exhumed mantle domain of the final margin, the mantle**
612 **exhumation TS is expressed by** (second line of Figures 6a and 6b):
613 (1) **exclusively new real estate basement** comprised of **subcontinental**
614 **lithospheric mantle** exhumed to the seafloor via **out-of-sequence**
615 **detachment faulting**; (2) **tectono-sedimentary breccias** and overlying **supra-**
616 **detachment wedge-shaped sedimentary deposits** of mantle exhumation
617 phase age emplaced directly onto exhumed mantle; (3) **over-tilted**
618 **sedimentary packages** at detachment faults breakaway; and (4) a progressive
619 **younging of supra-detachment basins fill oceanward.**

620

621 4. Illustration of our model with calibrated natural examples

622

623 The best calibrated rifted margins worldwide (i.e., constrained by either outcrop
624 observations or drilling) are by far those of the fossil Alpine Tethys exposed in the Alps.
625 This example is described in detail in the companion paper by Manatschal *et al.* (this
626 volume) and only briefly summarized here (Figures 7c and 7d). Another well calibrated
627 example is the conjugate transect across the Iberia–Newfoundland margins imaged by
628 the TGS–LG 12 and SCREECH 2 reflection seismic profiles, respectively. In addition to
629 drill hole data from the proximal domain and inner part of the necking domain (e.g., Alves
630 *et al.*, 2002, on the Iberian side; Sinclair, 1994 and references therein; Wielens *et al.*,

631 2006, on the Newfoundland one), deep-water drilling was performed in the Iberian
632 hyperextended domain and in the inner part of the Newfoundland exhumed mantle
633 domain, as part of the Ocean Drilling Program (ODP) Legs 149, 173 and 210. Besides,
634 the viability of the tectono-stratigraphic interpretation by Sutra *et al.* (2013) was supported
635 by its surface-conservative kinematic restoration.

636

637 4.1. Geological setting of Mesozoic rifting events in Western Europe

638 The opening of the Alpine Tethys and North-Atlantic Ocean was part of the
639 fragmentation of the Pangea supercontinent, which progressed both from east to
640 west and from south to north via *multistage rifting* (Figure 7a): it initiated with the
641 opening of the Meliata-Vardar domain at the western end of the Neothethys. It
642 continued with the opening of the Ligurian, Piemonte and Valais domains between
643 the Eurasian/Iberian plate and the Adriatic/African plate, ahead of the northward-
644 propagating Central Atlantic rifting, while the Meliata–Vardar domain was closing. It
645 continued with the opening of the Bay of Biscay and southern North-Atlantic Ocean,
646 while extension had ceased in the Alpine Tethys realm (Angrand *et al.*, 2020; Le
647 Breton *et al.*, 2020).

648 A broadly distributed extensional event affected a large part of Western Europe and
649 eastern North America from the Permo-Triassic onward (Leleu *et al.*, 2016, and
650 references therein), and is here regarded as the stretching phase of both the Alpine
651 Tethys and Iberia–Newfoundland rifting. In the Alpine Tethys rift system, the onset of
652 localized deformation (necking phase) started at 185 ± 5 Ma (Sinemurian–
653 Pliensbachian), evolved to hyperextension from 175 ± 5 Ma (Toarcian–Aalenian),
654 and culminated with mantle exhumation from 165 ± 5 Ma onward (Bajocian–
655 Bathonian; Manatschal *et al.*, this volume). Rifting stopped in the Alpine Tethys
656 realm before steady-state seafloor spreading occurred in any branch of the Alpine rift
657 system (Picazo *et al.*, 2016). Then, focused deformation started between Iberia and

658 Newfoundland with the necking phase from Tithonian to Berriasian time, continued
659 with hyperextension from latest Berriasian to Valanginian time, and with mantle
660 exhumation from the Valanginian (Mohn *et al.*, 2015, and references therein) until
661 the late Aptian–early Albian lithospheric breakup (Bronner *et al.*, 2011). Note that the
662 Iberia–Newfoundland rift system comprises three main segments that underwent
663 diachronous extension from south to north (Alves *et al.*, 2009, and references
664 therein). Here we focus on the central segment (i.e., South Iberia Abyssal Plain–
665 Northern Newfoundland Basin).

666

667 4.2. The fossil Alpine Tethys rift system

668 4.2.1. The proximal domains

669 The former proximal domains of the European and Adriatic margins were
670 associated with numerous half-graben depocenters (Figure 7b), among which
671 the best-exposed are the Bourg d’Oisans Basin on the European margin
672 (Chevalier, 2002; Dumont *et al.*, 2008), the Il Motto Basin on the northern
673 Adriatic margin (Conti *et al.*, 1994; Eberli, 1988; Ribes *et al.*, 2019b), and the
674 Monte Generoso Basin on the former southern Adriatic margin (Bernoulli, 1964;
675 Bertotti *et al.*, 1993).

676 The sedimentary record is comparable in the three basins, displaying half-
677 graben wedge-shaped deposits from latest Triassic to Sinemurian–
678 Pliensbachian time (Figures 7c and 7d). In the temporal framework of the Alpine
679 Tethys rifting, this corresponds to the early syn-rift history, namely the *stretching*
680 *phase*. From Pliensbachian–Toarcian time onward, the three basins record
681 passive infill (i.e., post-tectonic deposits belonging to the syn-rift
682 megasequence).

683

684 4.2.2. The necking domains

685 The best described necking domain in the Alps used to belong to the former
686 European margin and now lies in the Mont Blanc region (Ribes *et al.*, 2020;
687 Figure 7b). Necking domains of the former northern- and southern Adriatic
688 margin were respectively identified in the Campo–Grosina region (no
689 sedimentary record available) by Mohn *et al.* (2010), and in the Cusio–Biellese
690 region by Beltrando *et al.* (2015). Besides, the sedimentary record of the
691 intervening keystone block is preserved in the Briançonnais region (Claudel and
692 Dumont, 1999; Hauptert *et al.*, 2016).

693 Observations from the Mont Blanc (Ribes *et al.*, 2020, and references therein)
694 and Cusio–Biellese region (Beltrando *et al.*, 2015, and references therein) show
695 that (Figures 7c and 7d): (1) the base of the necking TS is a tectonic
696 unconformity owing to detachment-related basement exhumation (new real
697 estate) and/or local erosion; (2) the necking domain is a local region of
698 siliciclastic deposits (sandstones) due to local basement exhumation and
699 erosion/deposition; (3) water-depth remained relatively shallow during the
700 necking phase and deposition of related sandstones. Observations from the
701 Briançonnais domain indicate that the keystone block underwent a phase of
702 transient emergence during the necking phase.

703

704 4.2.3. The hyperextended domains

705 The outer edge of a European upper plate is exceptionally well-preserved in the
706 Tasna Nappe of southeastern Switzerland (Manatschal *et al.*, 2006; Ribes *et al.*,
707 2019c; Figure 7b). The distal edge of the northern Adria lower plate is exposed
708 in the Err and Upper Platta nappes (Figure 7b) in Southeast Switzerland (Epin
709 and Manatschal, 2018; Manatschal and Nievergelt, 1997; Masini *et al.*, 2012).

710 The hyperextended domain of South Adria is recognized in the Canavese region
711 of the Southern Alps. It was recently interpreted as an upper plate by Decarlis *et*
712 *al.* (2017).

713 The tectono-sedimentary record of the Tasna, Err and Canavese nappes is
714 comparable in that the three of them display (Figures 7c and 7d):
715 (1) discontinuous pre-rift sediments only present as/over allochthonous blocks;
716 (2) basement exhumation via detachment faults overlain by tectono-sedimentary
717 breccias; and (3) deep-marine syn-tectonic sedimentary deposits. They differ in
718 that no lower crust seems to be exhumed at former lower plates (Err Nappe), in
719 contrast to former upper plates (Tasna Nappe and Canavese Zone).

720

721 4.2.4. The exhumed mantle domains

722 The best-preserved outcrops of an exhumed mantle domain and embryonic
723 seafloor spreading system in the Alps are exposed in the Lower Platta Nappe
724 (Figure 7b) in southeastern Switzerland (Desmurs *et al.*, 2002; Epin *et al.*, 2019;
725 Ribes *et al.*, 2019b) and at the Chenaillet Ophiolite in the French-Italian Alps
726 (Manatschal *et al.*, 2011).

727 The tectono-sedimentary record of the Platta Nappe and Chenaillet Ophiolite
728 shows that (Figures 7c and 7d): (1) mantle exhumation was achieved via
729 successive in-sequence detachment faults; (2) topography was created during
730 mantle exhumation, which resulted in gravitational sliding and/or onlapping of
731 syn-exhumation magmatic products and sediments; (3) the exhumed mantle
732 was affected by normal faults, which served as feeder channels for the overlying
733 volcanic sequences; (4) no pre- and early syn-rift deposits existed in the
734 exhumed mantle domain; and (5) the first sedimentary deposits (radiolarites)
735 were characteristic of abyssal deposition environments.

736

737 4.3. The Iberia–Newfoundland conjugate margins

738 4.3.1. The proximal domains

739 The proximal domains of the Iberia and Newfoundland margins (Figure 8a) are
740 characterized by minor stretching factors ($\beta < 2$; Mohn *et al.*, 2015), except in
741 the northern Jeanne d'Arc Basin that was affected by later extension related to
742 the formation of the Orphan Basin further north (Skogseid, 2010). Moho and top
743 basement are sub-horizontal at the scale of both proximal domains (Sutra *et al.*,
744 2013; Figures 8b and 8b1). Extension formed half-graben depocenters such as
745 the (South) Jeanne d'Arc, Whale and Horseshoe basins on the Newfoundland
746 side, and the Porto and Lusitanian basins on the Iberian side (Tucholke *et al.*,
747 2007).

748 The northern Lusitanian- and Jeanne d'Arc basins (Figure 8a) display a
749 comparable evolution and sedimentary fill indicating discontinuous tectonic
750 activity from Late Triassic to Late Jurassic (Alves *et al.*, 2002; Sinclair, 1993).
751 The first rift-related deposits in both basins are Late Triassic to Pliensbachian
752 continental and/or lacustrine sediments and evaporites, representative of
753 terrestrial to epicontinental sea environments. They show *half-graben wedge-*
754 *shape* sedimentary architectures, indicative of their syn-tectonic setting
755 (*stretching TS*). Subsequent marine sandstones and carbonates alternating with
756 shales were passively deposited from the Pliensbachian–Callovian in the
757 northern Lusitanian Basin (Iberian margin) and from the Tithonian in the central
758 Lusitanian Basin and at the Newfoundland margin. They were interpreted to
759 record post-tectonic thermal relaxation at both margins (Alves *et al.*, 2002; Alves
760 *et al.*, 2003; Enachescu, 1987; Hubbard, 1988; McAlpine, 1990; Sinclair, 1988;
761 Ravnås *et al.*, 1997).

762 On both the Iberian and Newfoundland margins, Callovian–Oxfordian deposits
763 were affected by an erosional unconformity (Ian Sharp personal
764 communication). This unconformity preceded renewed extension, during which
765 marine sandstones were deposited in the northern Lusitanian Basin (Alves *et al.*,
766 2003, 2002; Ravnås *et al.*, 1997). Renewed extension in the Jeanne d’Arc Basin
767 during the Tithonian was preceded or accompanied by erosion (Sinclair, 1993,
768 and references therein) with alternating carbonates and shales being
769 subsequently deposited.

770 In the Lusitanian Basin, the onset of post-tectonic sedimentation occurred in the
771 late Tithonian–early Berriasian (Ravnås *et al.*, 1997). Sediments younger than
772 Kimmeridgian are comprised of shallow-marine to continental units that display
773 post-tectonic architectures and testify to limited thermal subsidence (Alves *et al.*,
774 2003). In the Jeanne d’Arc Basin, the onset of post-tectonic sedimentation was
775 recognized during the Valanginian (CNLOPB, 2010; Enachescu, 1987; Sinclair,
776 1988). Sediments include sandstones and shales. Subsequent tectono-
777 stratigraphic evolution in the Jeanne d’Arc Basin was affected by extensional
778 events in the adjacent Orphan Basin (Skogseid, 2010) and is therefore not
779 discussed here.

780

781 4.3.2. The necking domains

782 Alves *et al.* (2006) interpreted the necking zone of the Iberian margin to be
783 structured by only high-angle normal faults but noticed the lack of evidence for
784 pre-rift sediments in its outer part. Sutra *et al.* (2013) and Mohn *et al.* (2015) also
785 interpreted the inner Iberian necking domain to contain a large normal fault
786 (Figure 8b) but suggested that top basement in the outer part of the necking

787 domain is made of new real estate basement exhumed by a detachment fault
788 (Figure 8b2).

789 The necking domain of the Newfoundland margin has traditionally been
790 regarded as structured by only high-angle normal faults, like the rest of the
791 margin (Causer *et al.*, 2020; Hopper *et al.*, 2006; Welford *et al.*, 2010). However,
792 Péron-Pinvidic and Manatschal (2009), Sutra *et al.* (2013) and Mohn *et al.*
793 (2015) interpreted the inner necking fault of the Newfoundland margin as a high-
794 angle normal fault that started to evolve as a detachment fault (minor amount of
795 basement exhumed at low angle; Figure 8b). Nobody has recognized new real
796 estate creation in the rest of the Newfoundland necking domain so far.

797 Drill holes in the northern part of Carson Basin (Newfoundland margin; Figure
798 8a) indicate a Tithonian unconformity overlain by sandstone deposits, like that
799 reported in the Jeanne d'Arc Basin (Ian Sharp personal communication). A later
800 Albian unconformity in the northern Carson Basin is interpreted to mark the rift to
801 drift transition in the southern segment (Wielens *et al.*, 2006).

802 In the Iberian necking domain (Peniche Basin; Figure 8a), Alves *et al.* (2006)
803 interpreted Triassic–Late Jurassic syn-tectonic deposits in the depocenter
804 adjoining the main necking fault. These would correspond to the sedimentary fill
805 of a stretching phase half-graben depocenter. Such deposits are lacking in the
806 outer part of the necking domain. Latest Berriasian to Aptian sediments cover
807 the entire necking domain and were interpreted as post-tectonic (Alves *et al.*,
808 2006; Mohn *et al.*, 2015). Alves *et al.* (2006) reported toplaps of Albian age,
809 contemporaneous to the erosional unconformity reported in the Carson Basin.

810

811 4.3.3. The hyperextended domains

812 The hyperextended domain of the Iberian margin is consensually interpreted as
813 structured by detachment faults that exhumed upper- to mid-crustal basement to
814 the seafloor (Krawczyk *et al.*, 1996; Manatschal *et al.*, 2001; Reston and
815 McDermott, 2011; Figure 8b3). In contrast, the hyperextended domain of the
816 Newfoundland margin is regarded as essentially controlled by high-angle normal
817 faulting that crosscut the entire crust (Mohn *et al.*, 2015; Péron-Pinvidic and
818 Manatschal, 2009; Sutra *et al.*, 2013). This distinction prompted Manatschal
819 (2004) and Hauptert *et al.* (2016) to interpret the Iberian margin as a lower plate
820 and its Newfoundland conjugate as an upper plate.

821 Drill holes in the hyperextended domain of the Iberian margin indicate upper
822 crustal basement affinities (ODP Sites 639, 901, 1065 and 1069). Exhumed
823 middle- or lower crust has been evidenced only at ODP Sites 900 and 1067
824 (outer edge of the hyperextended domain). No drill hole data from the
825 hyperextended domain of the Newfoundland margin is available.

826 None of the drill holes in the Iberian hyperextended domain penetrated Late
827 Triassic–Early Jurassic sediments. However, since all but one of the deep-water
828 drill holes (ODP Site 639 in the northern segment) stopped before reaching the
829 pre-rift top basement, we cannot exclude that such sequences exist, or existed
830 and were eroded prior to hyperextension.

831 In the Iberian hyperextended domain, pre-rift top basement is overlain by
832 concordant Mid- to Late Jurassic sandstones and conglomerates interpreted as
833 emplaced in an offshore shelf environment (ODP Sites 1065 and 1069; Figure
834 8b2). We consider that these syn-rift deposits, which display pre-tectonic
835 architectures, represent the stretching TS in the hyperextended domain. The
836 subsequent Tithonian–Berriasian deposits are still pre-tectonic in the central
837 segment. They comprise clay, silty clay, coarse sands and conglomerates
838 interpreted to reflect a deepening sequence (up to 500–1000 m; ODP Sites 901,

839 1065 and 1069). We consider that they represent the necking TS in the
840 hyperextended domain. Whether the sands/conglomerates are derived from
841 basement erosion is not resolved to date.

842 The sedimentary fill of supra-detachment basins was only drilled in the
843 hyperextended domain of the northern Iberian segment (ODP Sites 638–641).
844 There, it consists of debris flow, turbidites and slumps alternating with
845 background sedimentation. The overall sedimentary sequence displays a
846 wedge-shaped architecture (Boillot and Winterer, 1988). In the hyperextended
847 domain of the central Iberian segment, Péron-Pinvidic *et al.* (2007) suggested
848 that the lack of obvious growth structures may be related to syn-basement
849 exhumation sedimentation in a largely sediment-starved rift system (i.e., the
850 sediment-starved version of our *supra-detachment wedge-shaped* sediment
851 architecture; see Figure 2f). They also noticed an oceanward younging of in the
852 sedimentary fill of supra-detachment basins, where coeval sedimentary
853 sequences display post-tectonic architectures in the inner part of the
854 hyperextended domain, and syn-tectonic architectures in the outer part
855 (Figure 8b3).

856 At ODP Site 1069, nanofossils (chalk) of late Berriasian to early Valanginian
857 age overlie the tilted (pre-tectonic) Tithonian to older sedimentary sequence.
858 These hemipelagic to pelagic sediments were interpreted as being deposited in
859 open-marine outer-shelf to upper-slope environments (> 1500 m; Urquhart,
860 2001). They highlight the shutdown of the terrigenous input in the outermost part
861 of the hyperextended domain during late hyperextension, possibly due to
862 sediment capture by inner basins (Wilson *et al.*, 2001). Mohn *et al.* (2015)
863 attributed the essentially post-tectonic infill of the supra-detachment basins to
864 the short (5–10 My) duration of the hyperextension phase.

865

866 4.3.4. The exhumed mantle domains

867 Wilson *et al.* (2001) suggested that exhumation of already serpentized mantle
868 started during Valanginian–Hauterivian time. While Manatschal (2004) initially
869 envisioned mantle exhumation via a single detachment fault, Gillard *et al.* (2016)
870 identified four successive in- and out-of-sequence detachment faults on the
871 SCREECH 1 seismic profile further north, across the exhumed mantle domain of
872 the Newfoundland margin.

873 At ODP Site 1068 (mantle exhumation point; Figure 8b2), drilling reported
874 tectono-sedimentary breccias supported by a calcareous chalk matrix of
875 Valanginian–Barremian age deposited onto exhumed mantle (Figure 8b4). The
876 next sediments drilled are much younger Campanian turbidites, which onlap
877 against the tilted tectono-sedimentary breccias. This relationship indicates either
878 that ODP Site 1068 was a topographic high already at the onset of mantle
879 exhumation, or that the tectono-sedimentary breccias were tilted and uplifted
880 after their deposition and prior to Campanian time, and that the adjacent basin
881 was progressively filled by turbidites and pelagic sediments. Comparable
882 relationships were documented by Péron-Pinvidic *et al.* (2007) at the conjugate
883 Newfoundland margin (ODP Site 1277; Figure 8b5): breccias of presumably
884 Aptian age and overlying exhumed mantle are over-tilted compared to the Albian
885 to Cenomanian onlapping, sub-horizontal, passive infill.

886 Magmatic activity contemporaneous with lithospheric breakup is evidenced by
887 diabase sills that were emplaced at the Aptian–Albian boundary (Jagoutz *et al.*,
888 2007; Karner and Shillington, 2005).

889

890 4.3.5. Summary

891 The primary spatio-temporal evolution of deformation in the Iberia–
892 Newfoundland rift system can be deduced from the architecture of the main
893 sedimentary package interfaces (Figure 8b2): in the inner necking domain, the
894 blue interface marks the top of the syn-tectonic succession, while in the
895 hyperextended domain, it marks the top of the pre-tectonic succession. This
896 implies that deformation was active in the inner necking domain when no
897 deformation had occurred in the hyperextended domain yet.

898 In the hyperextended domain, a comparable evolution can be observed
899 (Figure 8b3): in the inner part, the red horizon lies within a post-tectonic
900 succession, while it marks the top of syn-tectonic sequence in the outer part.
901 The overlying green horizon lies within a post-tectonic succession along the
902 entire hyperextended domain, while it marks the top of a syn-tectonic
903 succession in the adjacent exhumed mantle domain. This indicates that active
904 deformation was progressively advancing oceanward.

905 The tectono-stratigraphic history of the Iberia–Newfoundland rift system is
906 summarized in Figure 8c. It is consistent with our idealized model in that: (1) it
907 indicates a sequential localization of deformation oceanward; (2) the proximal
908 domain is only affected by high-angle normal faults whose tectonic activity has
909 largely ceased by the end of the stretching phase; (3) syn-stretching and syn-
910 necking deposits in the outer necking and hyperextended domain of the Iberian
911 margin display shallow-water facies comparable to those of the proximal
912 domain; however, they display pre-tectonic stratigraphic architectures in the
913 distal margin, while they are syn-tectonic in the proximal domain; (4) a syn-
914 necking (Tithonian) unconformity overlain by sandstones exists at least in the
915 proximal and necking domain of the Newfoundland margin; (5) the
916 hyperextended Iberian lower plate is structured by in-sequence detachment
917 faults associated with supra-detachment wedge-shaped deposits that become

918 younger oceanward; and (6) the exhumation domain displays over-tilted syn-rift
919 pre- to syn-tectonic sequences against which post-rift sediments onlap.

920 Debated questions concern (1) the existence of extensional detachment faults in
921 the necking domain of both the Iberian and Newfoundland margins; and (2) the
922 existence of (dismembered) half-graben wedge-shape deposits in the stretching
923 TS of the hyperextended domain.

924

925 5. Application of our model to incompletely calibrated natural examples

926 In the following, we rely on our model to interpret the tectono-stratigraphic record of an
927 uncalibrated transect across conjugate NW-South China Sea margins; and of transects
928 across the distal domain of the Mid-Norwegian and Socotra margins with support of
929 observations and data from their adjacent, better-calibrated proximal domains.

930 5.1. The northwest South China Sea conjugate margins

931 5.1.1. Geological setting

932 The NW South China Sea is an aborted, V-shaped oceanic basin that benefits
933 from extensive seismic coverage and some drill holes in the most distal part of
934 the margin, ca. 200 km east of the transect presented below (International
935 Ocean Discovery Program (IODP) Legs 349, 367 and 368; Figure 9a). The
936 South China Sea differs largely from Atlantic-type rifts in that the rheology of the
937 pre-rift lithosphere was significantly weaker due to the high geothermal gradient
938 related to its back-arc position and orogenic and post-orogenic history (Li *et al.*,
939 2018; Sun *et al.*, 2019).

940 Rifting of the NW South China Sea is considered to have begun at ca. 65 Ma
941 (Xie *et al.*, 2019), although this age is poorly constrained. Besides, because of
942 the propagating nature of extension, rifting was largely diachronous along strike.

943 The onset of seafloor spreading is dated to 30–28 Ma based on the presence of
944 magnetic anomalies in the oceanic crust (Gee and Kent, 2007).

945 The NW South China Sea has been widely studied, for instance by Cameselle,
946 *et al.* (2017); Gao *et al.*, (2016); Larsen *et al.* (2018); Nirrengarten *et al.* (2020);
947 Ren *et al.* (2018); Zhang *et al.* (2021). Here we focus on the CGN-1
948 multichannel high-resolution 2D seismic section, for which Chao *et al.* (2021)
949 recently proposed a detailed tectono-sedimentary interpretation and balanced
950 kinematic restoration. To study the spatio-temporal evolution of deformation
951 during rifting, they grouped seismic packages of same interpreted age along dip
952 into one *Sequence (S)*. In total, they identified five syn-rift *Sequences* (packages
953 of same interpreted age along dip) with distinct evolutions across the conjugate
954 margins.

955

956 5.1.2. The proximal domain of the northern margin

957 The proximal domain of the northern margin is characterized by sub-horizontal
958 top basement and Moho separated by a ca. 22 km-thick continental crust
959 (Figure 9b). Top basement and pre-rift sediments are affected by only minor
960 normal faulting (fault throw < 0.2 sTWT). The faulted top basement is directly
961 overlain by post-rift deposits, which prevents any accurate dating of crustal
962 faulting. The proximal domain of the southern margin is not imaged and thus is
963 not discussed here.

964

965 5.1.3. The necking domains

966 On the northern margin, the inner limit of the necking domain is a crustal-scale
967 high-angle normal fault with a fault throw of 1.5 sTWT. 10–15 km further
968 outboard, a major detachment fault exhumed upper- to mid-crustal basement to

969 the seafloor over more than 15 km along dip (Figures 9b and 9b1; Chao *et al.*,
970 2021). In the outer part of the necking domain, the basement is affected by a
971 series of smaller high-angle normal faults, which created tilted blocks with minor
972 basement exhumation (< 0.5 sTWT fault throw).

973 The oldest sediments reported in the northern margin necking domain (S1) are
974 interpreted as pre-necking, half-graben wedge-shaped deposits that were
975 dismembered during the necking phase (Figure 9b1). They include faulted
976 wedge-shaped remnants capping pre-rift top basement and an allochthonous
977 package overlying the detachment surface itself (Chao *et al.* 2021; see their
978 Fig. 6). The first sedimentary package whose base is not disrupted by tectonic
979 activity is S5, which is thus interpreted as the first post-tectonic package in the
980 necking domain.

981 In-between S1 and S5, sediments of Ss 2–4 are interpreted as syn-tectonic of
982 the necking phase. They overlie the entire necking domain and display various
983 sedimentary architectures: sediments of S2 display a progradational architecture
984 onto the detachment surface and wedge-shaped architectures between the tilted
985 blocks of the outer necking domain. Sediments of S3 and S4 passively overlie
986 those of S2 in the inner part of the necking zone, whereas they are faulted (syn-
987 tectonic) in the outer part.

988 Chao *et al.* (2021) recognized that the tops of Ss 3, 4 and 5 are truncated,
989 suggesting that the necking domain was subaerial or above the storm-wave
990 base during relatively advanced stages of rifting (Figure 9b1). If this assumption
991 is correct, it implies that the necking domain remained at shallow water depths
992 during a large part of the rifting process.

993 On the southern margin, the inner part of necking domain is not imaged. Its
994 outer part is affected high-angle normal faults whose steepness decreases

995 oceanward, ending with a sub-horizontal detachment fault that exhumed upper-
996 to mid-crustal basement to the seafloor over ca. 15 km along dip (Figures 9b
997 and 9b2). The detailed tectono-sedimentary record at this margin is poorly
998 constrained compared to its conjugate because it is not possible to distinguish
999 between deposits related to Ss 1–4 (Chao *et al.* 2021). However, the boundary
1000 between S1–4 and S5 is interpreted as erosional, like along the northern margin.

1001 The careful tectono-stratigraphic restoration by Chao *et al.* (2021) allowed them
1002 to reconstruct the distribution of active faulting through time along the NW-South
1003 China Sea rifted margins: Figure 9c shows that, during the early stages of rifting
1004 (necking phase), faulting was localized into two fault corridors on either side of a
1005 largely undeformed region (active faults shown by red color in Figure 9c). This
1006 event is interpreted as the individualization of a *keystone* block, as predicted by
1007 numerical and analogue models (e.g., McClay 1996; Lavier and Manatschal
1008 2006; Huisman and Beaumont 2011). It ended abruptly with the localization of
1009 deformation and onset of massive sedimentation within the keystone area,
1010 contemporaneous with the abandonment of the former fault corridors on either
1011 side. This rapid switch (< 1 My) was interpreted to mark the transition between
1012 the necking and hyperextension phase (Chao *et al.* 2021).

1013

1014 5.1.4. The hyperextended domains

1015 In contrast to the necking domains, the hyperextended domains of the northern
1016 and southern margins are markedly asymmetrical: on the northern margin, the
1017 hyperextended domain is structured by successive high-angle faults that dip
1018 oceanward and cut through the entire crust (Figures 9b and 9b1). Faults throw
1019 decreases oceanward from 1.5 sTWT to < 0.5 sTWT, together with inter-fault
1020 blocks size. At the southern margin, the hyperextended domain is affected by in-

1021 sequence, oceanward-dipping, low-angle detachment faults that root on one and
1022 the same décollement level (Figures 9b and 9b2). Based on these observations,
1023 Chao *et al.* (2021) suggested that the southern margin is a lower plate. In
1024 contrast, the alternance of ramps and terraces shaping the northern margin tip
1025 the scales in favor of an upper plate.

1026 On the northern margin, the hyperextended domain can be subdivided into three
1027 sub-domains with distinct characteristics: in the inner sub-domain (He1 in
1028 Figure 9b1), the first sediments observed on pre-rift top basement are
1029 concordant (pre-tectonic) sedimentary deposits interpreted to belong to S3
1030 (Figure 9b1). The next sediments to be deposited after S3 belong to S4 and
1031 display a wedge-shaped architecture. These are overlain by passive deposits
1032 interpreted to belong to S5. In the central sub-domain (He2 in Figure 9b1), tilted
1033 blocks are overlain by wedge-shaped magmatic products of unknown age.
1034 Magmatism is however younger than S5 because corresponding sediments
1035 passively overlie this segment. In the outermost sub-domain (He3 in
1036 Figure 9b1), only wedge-shaped magmatic products are recognized over the
1037 pre-rift basement. They are directly overlain by post-rift deposits, suggesting that
1038 magmatism becomes younger oceanward. This hypothesis is consistent with the
1039 conclusion drawn by Zhang *et al.* (2021) further east.

1040 The sedimentary record in the hyperextended domain of the southern margin is
1041 poorly constrained and does not allow us to distinguish between syn-rift Ss 1–4
1042 (Chao *et al.* 2021). S5 is interpreted as syn-tectonic in the entire hyperextended
1043 domain (Figure 9b2).

1044 Looking at the spatio-temporal distribution of active faulting (Figure 9c)
1045 highlights a sudden switch from almost no deformation and no sediment
1046 deposition onto the keystone block (i.e., the future hyperextended domain), to
1047 increasingly localized deformation and significant syn-rift sedimentation limited

1048 to the keystone area until the onset of proto-oceanic seafloor spreading.
1049 Keystone individualization (necking phase) is thus associated with extremely
1050 shallow water depth and/or emergence of the future hyperextended domain,
1051 which causes a lack of sediment deposition (uncovered basement shown by
1052 orange color in Figure 9c).

1053

1054 5.1.5. The proto-oceanic domain:

1055 No exhumed mantle has been evidenced in northwest South China Sea,
1056 instead, a proto-oceanic domain is described by Larsen *et al.* (2018) and Chao
1057 *et al.* (2021). This domain is strongly deformed by high-angle normal faults and
1058 overlain by post-rift sediments (Figure 9b).

1059

1060 5.1.6. Summary and predictions:

1061 When looking at the architecture of the main sedimentary package interfaces,
1062 we can see that the top of S4 is the base of post-tectonic sedimentation in the
1063 necking domains, while it lies within the syn-tectonic sequence in the
1064 hyperextended domains. Similarly, the top of S5 is post-tectonic in the necking
1065 and inner hyperextended domains, while it belongs to the syn-tectonic sequence
1066 further outboard. This indicates a migration of active deformation oceanward as
1067 extension progresses. The same trend can be observed in the study of Ren *et*
1068 *al.* (2018; their Fig. 9), where their T80 horizon is post-tectonic in the inner part
1069 of the margin and syn-tectonic in more distal domains.

1070 Figure 9c highlights an abrupt switch in the spatio-temporal distribution of active
1071 deformation during rifting: deformation is first focused into two fault corridors on
1072 either side of an undeformed keystone block that remained at shallow water

1073 depth, or even emerged. Then, deformation shifted “instantaneously” (< 1My) to
1074 an opposite situation where deformation was limited to the keystone and the
1075 fault corridors became inactive.

1076 The evolution of the NW-South China Sea section described above is
1077 summarized in Figure 9d. It is consistent with our idealized model in that: (1)
1078 successive discrete deformation phases advanced oceanward as extension
1079 progressed; (2) the proximal domain is only structured by high-angle normal
1080 faults; (3) the necking domain of both margins display detachment faults that
1081 exhumed upper- to mid-crustal basement to the seafloor; (4) pre-tectonic
1082 deposits of same age as the necking phase are observed in the hyperextended
1083 domain of the northern margin; (5) an erosional unconformity of necking phase
1084 age is observed throughout the hyperextended domain of both margins; and (6)
1085 extension was achieved via detachment faults in the hyperextended domain of
1086 the lower-plate (southern) margin.

1087 Relying on our model, we expect sediments of the necking TS (S2–S4 in Chao
1088 et al., 2021) in the hyperextended domain to display shallow water facies and
1089 include reworked pre-rift sediments. Deposits on either side of the keystone
1090 (necking domains) should display deeper sedimentary facies and be sourced
1091 from both the continent (siliciclastics) and from the eroded keystone (reworked
1092 pre- to syn-rift sediments).

1093 We expect sediments of the hyperextension TS in both the necking and
1094 hyperextended domains to display rapidly deepening sedimentary facies,
1095 associated with both tectonic and thermal subsidence related to intense crustal
1096 thinning and thermal relaxation beneath the two domains. This hypothesis is
1097 supported by drill hole U1501 published by Larsen *et al.* (2018) and the tectono-
1098 stratigraphic analysis of the Liwan Basin further east by Zhang *et al.* (2019),
1099 both of which indicated a rapid deepening of sedimentary facies from shallow

1100 marine to bathyal depths during the early Oligocene. This time corresponds to
1101 the early stages of hyperextension in Chao *et al.* (2021).

1102

1103 5.2. The Mid-Norwegian margin

1104 5.2.1. Geological setting

1105 Rifting between Norway and Greenland was achieved through complex and
1106 multistage extension that started during the late Paleozoic and resulted in
1107 lithospheric breakup during the Eocene (Péron-Pinvidic and Osmundsen, 2018,
1108 and references therein). At the Mid-Norwegian margin, a broadly distributed
1109 stretching phase took place discontinuously from Permian to Triassic time,
1110 following the Devonian–Carboniferous orogenic collapse of the Caledonian belt
1111 (Péron-Pinvidic and Osmundsen, 2018, and references therein). A first phase of
1112 localized deformation (the necking phase) started during the Late Jurassic
1113 (Tithonian) and ended in the Early Cretaceous (e.g., Brekke, 2000; Doré *et al.*,
1114 1999; Planke *et al.*, 2000). Then, localized deformation stepped further
1115 outboard, creating detachment faults that possibly reached mantle exhumation
1116 in the Møre and Vøring basins during late Early- to Late Cretaceous
1117 (Osmundsen *et al.*, 2016). From the Late Cretaceous to final breakup,
1118 increasing magmatic activity occurred along the outermost margin and formed
1119 the so-called *outer highs* (Péron-Pinvidic and Osmundsen, 2018, and references
1120 therein).

1121 The rift domains of the Mid-Norwegian margin were mapped by Péron-Pinvidic
1122 *et al.* (2013), who placed the termination of the proximal domain at the outer
1123 edge of the Trøndelag Platform (Figure 10a). In their view, the necking domain
1124 corresponds largely to the Halten Terrace and continues further south as a
1125 narrower domain. The Møre and Vøring basins (Figure 10a) belong to the

1126 hyperextended (and possibly exhumed mantle) domain of the mid-Norwegian
1127 margin because they display a crustal thickness of less than 10 km (Funk *et al.*
1128 2017). The nature of the seismic basement beneath these basins is the matter
1129 of much debate, especially about the proportion of pre-rift continental crust with
1130 respect to magmatic underplate, inherited Caledonian basement, altered
1131 continental crust and serpentinized mantle (e.g., Osmundsen *et al.*, 2016;
1132 Péron-Pinvidic and Osmundsen, 2018; Zastrozhnov *et al.*, 2020). The resolution
1133 is especially low in the outer part of the Møre and Vøring basins due to
1134 significant breakup-related magmatic additions.

1135 The Norwegian margin benefited recently from a careful three-dimensional
1136 mapping of major tectonic structures by Osmundsen and Péron-Pinvidic (2018).
1137 These authors suggested that each rift domain is framed by laterally persistent
1138 tectonic structures that allow for significant changes in the margin architecture,
1139 which they termed *breakaway fault complexes*.

1140

1141 5.2.2. The calibrated proximal and necking domains

1142 The tectono-stratigraphy of the Trøndelag Platform was recently reviewed by
1143 Péron-Pinvidic *et al.* (2020). These authors highlighted a complex extensional
1144 history following the post-orogenic collapse of the Caledonian belt. Extension
1145 was accommodated via both normal faulting and extensional reactivation of core
1146 complex structures inherited from the post-orogenic collapse. The Trøndelag
1147 Platform displays post-tectonic sedimentation from Late Triassic onward.

1148 The necking domain width ranges between 20 and 80 km (Figure 10a). It is
1149 framed by two crustal-scale, *breakaway fault complexes*, namely the *inner-* and
1150 *outer necking breakaway complex* at its inner and outer edge, respectively
1151 (Figure 10b; Osmundsen and Péron-Pinvidic, 2018). Both necking breakaway

1152 complexes are often composite structures in that they comprise both high- β
1153 (large fault heave) detachment faults and low- β (minor fault heave) normal
1154 faults.

1155 The main fault of the inner necking breakaway complex roots within the ductile
1156 middle or lower crust and is related to an abrupt but moderate increase in
1157 accommodation (> 20 km of basement exhumation along dip overlain with ca.
1158 2.5 km of Jurassic and Lower Cretaceous sediments in Figure 10b). From south
1159 to north along the Norwegian margin, the inner necking breakaway complex is
1160 represented by the Møre–Trøndelag, Vingleia, Bremstein, and Revfallet Fault
1161 Complexes (Figure 10a). The main fault of the outer necking breakaway
1162 complex cuts through the entire crust, down to the upper lithospheric mantle. It
1163 is usually associated with significant accommodation creation (> 20 km of
1164 basement exhumation along dip overlain with > 4 km of Lower Cretaceous
1165 sediments, in addition to the unknown thickness of Jurassic sediments in Figure
1166 10b). From south to north along the Norwegian margin, it is represented by the
1167 Main Møre Boundary Fault and the Ytreholmen Fault Complex (Figure 10a).
1168 However, the three-dimensional architecture of the inner- and outer necking
1169 breakaway complexes is complicated since the two merge in places, so that the
1170 necking domain locally coincides with a unique breakaway fault complex. This is
1171 the case south of the Halten Terrace (i.e., the Klakk Fault Complex; Figure 10a).

1172 The stratigraphy of the Norwegian necking domain often displays erosional
1173 truncations. For instance, at the outer edge of southern Halten Terrace, the
1174 Jurassic sequence on the inner side of both the Klakk (outer) and Vingleia
1175 (inner) Fault Complexes are deeply eroded before the deposition of deep-marine
1176 Lower Cretaceous sediments (e.g., Bell *et al.*, 2014, and references therein;
1177 Figure 10c). At the northern Halten Terrace, Breivik *et al.* (2010) and
1178 Osmundsen and Péron-Pinvidic (2018) interpreted erosion both at the

1179 Ytreholmen (outer) and Revfallet (inner) Fault Complex. In the inner part of the
1180 Halten Terrace, Elliott *et al.* (2012) highlighted erosion at the Bremstein (inner)
1181 Fault Complex. South of the Halten Terrace, Osmundsen and Ebbing (2008)
1182 reported erosion along the Main Møre Fault (inner breakaway fault complex). In
1183 all cases, erosion is reckoned to be of latest Jurassic–earliest Cretaceous age,
1184 which corresponds to the end of the necking phase. The resulting unconformity
1185 is sealed by a regionally correlatable shale event of early Barremian age (Ian
1186 Sharp personal communication). The latest Jurassic–earliest Cretaceous
1187 unconformity can be linked to the so-called *Base Cretaceous Unconformity* or
1188 *BCU* that is widely recognized across the Norwegian margin (e.g., Brekke,
1189 2000).

1190 Early Jurassic deposits in the necking domain are syn-tectonic sediments
1191 dominated by shallow-marine sandstones (Faleide *et al.*, 2010). Late Jurassic
1192 sedimentary facies indicate rapid deepening, as shown by prevailing first
1193 shallow- and then deep-marine shales. The deepening sequence is interrupted
1194 by an episode of major uplift and erosion that affected the necking domain but
1195 not the inner part of the shallow-water proximal domain, dismissing the
1196 hypothesis of a thermally driven dynamic topography. Indeed, as the latter
1197 process involves uplift over several hundreds of kilometers (Campbell, 2005),
1198 dynamic topography in the necking domain would have necessarily generated
1199 erosion in the adjacent thick-crust proximal domain, and thus shallow-water
1200 proximal domain.

1201

1202 5.2.3. The poorly calibrated hyperextended domain

1203 In the hyperextended domain offshore the mid-Norwegian margin, the thickness
1204 of sedimentary deposits may be over 7 sTWT in the axial part of the Møre and

1205 Vøring basins. Drill holes penetrate only as deep as the Late Cretaceous (e.g.,
1206 Zastrozhnov *et al.*, 2020, and references therein). The base of the Cretaceous
1207 sequence is interpreted to be marked by a strong reflection, supposed to
1208 correspond to both an erosional hiatus and to the base of passive onlap in the
1209 proximal and necking domains (i.e., the *BCU* mentioned above). Underlying
1210 deposits are usually interpreted as undifferentiated pre-Cretaceous sediments.
1211 Basement is consensually interpreted as affected by a series of oceanward-
1212 dipping, in-sequence detachment faults (e.g., Abdelmalak *et al.*, 2017;
1213 Osmundsen *et al.*, 2002; Zastrozhnov *et al.*, 2020), which suggests that the mid-
1214 Norwegian margin is a lower-plate margin (e.g., Mosar *et al.*, 2002). This is
1215 further supported by the shorter along-dip width of the eastern-Greenland
1216 conjugate margin (e.g., Péron-Pinvidic *et al.*, 2013).

1217

1218 5.2.4. Summary and predictions

1219 The evolution of the Norwegian margin is consistent with that of our idealized
1220 model in that: (1) it displays a sequential localization of deformation, starting with
1221 discontinuous Permo–Triassic extension distributed over at least the future
1222 proximal and necking domains, and probably also over the future hyperextended
1223 domain. Distributed deformation stopped in the Late Triassic and focused in the
1224 future necking domain during the Late Jurassic (i.e., necking phase); (2) The
1225 main structures allowing for crustal thinning (the *inner-* and *outer necking*
1226 *breakaway complexes* of Osmundsen and Péron-Pinvidic, 2018) are crustal-
1227 scale detachment faults, possibly associated with minor normal faults; (3) The
1228 necking phase was often associated with erosion at both the inner-and outer
1229 necking breakaway complexes; (4) the late stage of the necking phase was
1230 associated with an erosional unconformity (the *BCU*) that affected both the
1231 future necking domain, and at least the inner part of the hyperextended domain.

1232 Based on our model, we interpret the BCU either as an unconformity that marks
1233 the erosion of the keystone block during the necking phase, comparable with the
1234 unconformity interpreted at the top of the necking TS in the South China Sea; or
1235 as a onlap surface marking the onset of rapid deepening of the hyperextended
1236 domain following extreme crustal thinning and/or the onset of thermal relaxation.
1237 In both cases, we expect that the overlying Early Cretaceous sediments display
1238 sedimentary facies testifying to a rapid deepening associated with the
1239 dismembering of the keystone block during hyperextension. This interpretation is
1240 supported by the massive thickness of Cretaceous deposits (locally > 7 km) in
1241 both the Møre and Vøring basins (Brekke, 2000; Faleide *et al.*, 2010). Besides,
1242 the pattern of subsidence–uplift/erosion–subsidence observed on the Halten
1243 Terrace (necking domain) can be compared to that of the Briançonnais domain
1244 and explained by a flexural rebound following early necking of the upper mantle
1245 with respect to the crust (Chenin *et al.*, 2019).

1246

1247 5.3. The southeastern margin of the Gulf of Aden: the Socotra region

1248 5.3.1. Geological setting

1249 Socotra Island is located at the eastern edge of the Gulf of Aden southern
1250 margin. The western part of the island was interpreted to expose part of a former
1251 necking domain, while its eastern part would correspond to the outer part of a
1252 proximal domain (Ahmed *et al.*, 2014; Nonn *et al.*, 2017). In between, Socotra
1253 Island is crossed by an ENE–WSW transfer zone (Hadibo Transfer Zone; HTZ
1254 on the map of Figure 11). Socotra is one of the rare places in the world where a
1255 necking domain and the outer part of a proximal domain crop out. Emergence of
1256 these regions, which usually lie in relatively deep-marine environments, is

1257 related to a late-rift regional uplift (the *syn-OCT uplift* of Leroy *et al.*, 2012, and
1258 references therein, where *OCT* stands for *Ocean–Continent Transition*).

1259 The oldest sediments recovered in Socotra are Early Triassic and Jurassic in the
1260 eastern part of the island, and Cretaceous in the west (Samuel *et al.*, 1997).
1261 These were deposited during a phase of discontinuous, broadly distributed
1262 extension (stretching phase) that lasted from the Permo-Triassic to the Eocene
1263 in the future Gulf of Aden region. Localized extension (necking) initiated during
1264 the Priabonian (ca. 34 Ma; Leroy *et al.*, 2012, and references therein). The
1265 timing of hyperextension is not constrained. The onset of seafloor spreading
1266 occurred during the Burdigalian (ca. 20 Ma in eastern Socotra; Fournier *et al.*,
1267 2007) and was accompanied by regional uplift and significant erosion of both
1268 conjugate proximal margins (the *syn-OCT uplift* mentioned above).

1269

1270 5.3.2. The calibrated (onshore) proximal and inner necking domains

1271 At Socotra, necking was associated with significant tectonic exhumation and
1272 denudation that removed the entire pre-rift sedimentary cover and part of the
1273 exposed basement both in the east and in the west of the island (Pik *et al.*,
1274 2013) We note that this geometry is compatible with basement exhumation
1275 related to the activity of crustal-scale detachment faults (dotted blue lines on
1276 transects A–A' and C–C' of Figure 11). This episode of tectonic exhumation
1277 occurred earlier in the east (ca. 38 Ma) compared to the west (ca. 32 Ma; Pik *et*
1278 *al.*, 2013).

1279 From late Priabonian to Rupelian time, sediments were deposited in graben-type
1280 depocenters displaying subsidence and progressive deepening adjacent to the
1281 detachment faults (Nonn *et al.*, 2017, and references therein). Subsidence
1282 climax was reached during Rupelian–Chattian time (deep-marine deposits).

1283 Then, a *syn-OCT uplift* brought Socotra Island to emergence (Leroy *et al.*, 2012,
1284 and references therein).

1285

1286 5.3.3. The uncalibrated (offshore) outer necking and hyperextended domains

1287 Offshore Socotra, Nonn *et al.* (2017) recognized usually two crustal-scale
1288 extensional faults that exhumed basement to the seafloor over several
1289 kilometers along dip (up to 10 km in transect B–B' in Figure 11). However, in
1290 easternmost Socotra, they recognized only one major detachment fault that
1291 exhumed basement over 13 km along dip.

1292 Further outboard, top basement deepens abruptly from ca. 2 km to 4 km below
1293 sea level over ca. 10 km. This morphostructural step is interpreted to mark the
1294 transition between the necking and hyperextended domain and can be regarded
1295 as a mega fault scarp (Nonn *et al.*, 2017; Ribes *et al.*, 2019a). The
1296 hyperextended domain is structured by a series of oceanward dipping
1297 detachment faults (transect B–B' and D–D' in Figure 11), which prompted Nonn
1298 *et al.* (2017) to interpret the Socotra margin as a lower plate. This hypothesis is
1299 consistent with their interpretation of a residual keystone and of continent-ward-
1300 dipping faults in the hyperextended domain of the conjugate (Oman) margin.

1301

1302 5.3.4. Summary and predictions

1303 The Socotra necking domain provides thermochronological data testifying to a
1304 phase of necking starting at ca. 34 Ma (Leroy *et al.*, 2012), which was
1305 accompanied with basement exhumation and emergence (Pik *et al.*, 2013) that
1306 presumably occurred along detachment faults. Stratigraphy indicates a rapid
1307 deepening of sedimentary deposits in adjacent depocenters. The climax of

1308 subsidence rate was reached during the Rupelian–Chattian (ca. 28 Ma). Yet,
1309 according to our model, the highest subsidence rates in the necking domain
1310 occur during the hyperextension phase. In the case of Socotra, this would imply
1311 that the necking phase was relatively short (< 34 – 28, namely < 6 My).

1312 The occurrence of a mega-fault scarp at the transition between the necking and
1313 hyperextended domain of a lower-plate margin is not expected in our idealized
1314 model. However, whether this mega-fault scarp formed during
1315 necking/hyperextension or corresponds to a late rift feature associated with the
1316 syn-OCT uplift of the proximal margin described by Leroy *et al.* (2012, and
1317 references therein) remains to be determined. That the Socotra margin is not an
1318 upper plate remains also to be confirmed.

1319 Relying on our model, we expect that the presence of Priabonian (syn-necking)
1320 and older sediments in the hyperextended domain is limited to the top of the
1321 tilted blocks, and that they display shallow-water facies and possibly erosional
1322 unconformities. We expect the hyperextension phase to start during the
1323 Rupelian–Chattian and to be associated with a rapid increase in water depth,
1324 which would be recorded by sedimentary facies both on top and between the
1325 tilted blocks in the hyperextended domain.

1326

1327 6. Discussion

1328 6.1. Tectono-stratigraphic model vs. reality: first-order trends and simplifications

1329 As a generic template, our tectono-stratigraphic model is necessarily simplified with
1330 respect to the evolution of rift systems worldwide. Below, we discuss the relevance of
1331 our simplifications and the reliability of the first-order features we identified as
1332 characteristic of rift phases or domains.

1333 6.1.1. The stretching phase

1334 In our model, we consider that the stretching phase is achieved via broadly
1335 distributed, synchronous extension over the entire rift domains. Yet it has been
1336 proven that, for many rift systems and rifted margins, the stretching phase
1337 included several extension pulses that were offset in time and/or space (e.g.,
1338 Alves *et al.*, 2002; Bosworth *et al.*, 2005; Péron-Pinvidic and Osmundsen, 2018;
1339 Sinclair, 1993). Due to the absence of localized deformation during the
1340 stretching phase, it is very difficult to distinguish stretching-related structures
1341 from those generated by orogenic collapse or far-field effects of other tectonic
1342 events. Conversely, the onset of the subsequent phase of localized deformation
1343 (i.e., necking) is relatively easy to identify.

1344 Besides, the distribution of deformation during the stretching phase is largely
1345 controlled by inheritance (Manatschal *et al.*, 2015), and thus specific to each
1346 tectonic system. As our model aims to provide a template as general as possible
1347 to interpret the tectono-stratigraphic record of distal margins, it is sensible to limit
1348 our description of the stretching phase to a very first-order, considering that the
1349 detailed stretching evolution can only be unraveled on the basis of regional data.

1350

1351 6.1.2. The necking phase

1352 6.1.2.1. Formation of a keystone

1353 The formation of a keystone as part of the necking phase is predicted by
1354 both analogue and numerical models. It has also been suggested in the
1355 balanced kinematic restorations from Sutra *et al.* (2013) and Chao *et al.*
1356 (2021). Several field and seismic studies also provide good evidence for it
1357 (e.g., Hauptert *et al.*, 2016, and references therein). It is, however,
1358 extremely difficult to prove the systematic formation of a keystone during

1359 rifting since this phase is transient and the keystone is thought to be
1360 subsequently dismembered during hyperextension. One exception may be
1361 the Briançonnais domain which, because of its particular position between
1362 two overstepping en-échelon rift segments, may have "fossilized" the
1363 necking stage just prior to the reorganization of the segmented Alpine rift
1364 system into a unique rift basin, and preserved it during later Alpine
1365 convergence (Lescoutre and Manatschal, 2020; Manatschal *et al.*, 2021).

1366

1367 6.1.2.2. Formation of tens of kilometer-scale detachment faults

1368 Although only rarely described until the last decade, a growing body of
1369 evidence suggests the existence of major detachment faults that would
1370 exhume basement over up to several tens of kilometers along dip (Chao *et*
1371 *al.*, 2021; Osmundsen and Péron-Pinvidic, 2018; Ribes *et al.*, 2020; Sutra
1372 and Manatschal, 2012). Reasons why such structures have been seldom
1373 identified so far may be: (1) the poor calibration of the necking domain
1374 because it lies in relatively deep-water settings in thermally equilibrated
1375 rifted margins; (2) our preconceived idea on rifted margins being formed of
1376 tilted blocks (Figure 12a); and (3) the difficulty to distinguish between the
1377 top of pre-rift basement and top of new real estate basement (i.e.,
1378 basement exhumed to the seafloor via an extensional detachment fault).
1379 Further studies are needed to determine whether such structure represent
1380 the rule or the exception at rift systems/rifted margins.

1381

1382 6.1.3. The hyperextension phase: formation of upper- vs. lower plate margins

1383 The formation of upper- vs. lower-plate margins at magma-poor rift systems is
1384 predicted by numerical modelling (Lavie and Manatschal, 2006; Peron-Pinvidic

1385 and Naliboff, 2020) and supported by morphological observations (Hauptert *et*
1386 *al.*, 2016; Nirrengarten *et al.*, 2016; Péron-Pinvidic *et al.*, 2015; Ranero and
1387 Pérez-Gussinyé, 2010; Sutra *et al.*, 2013). Note that flip in the polarity of upper-
1388 vs lower plate margins may occur across transform faults along strike of rift
1389 systems (Decarlis *et al.*, 2017).

1390 Significant thermal weakening prior to/during the hyperextension phase may
1391 instead generate a symmetrical evolution (Buck, 1991). However, magma-
1392 rich/volcanic rift systems are not necessarily symmetrical and may go through a
1393 comparable early rift evolution as magma-poor ones (e.g., Eldholm *et al.*, 1995;
1394 Péron-Pinvidic *et al.*, 2013). Thus, whether magma-rich rift systems develop an
1395 upper- vs. lower-plate architecture remains to be determined.

1396

1397 6.1.4. The mantle exhumation phase: “symmetrical” pattern of detachment faulting

1398 It is generally accepted that mantle exhumation is achieved via extensional
1399 detachment faulting, however the details of this process are difficult to unravel
1400 based on field observations and direct seismic imaging only. Several pieces of
1401 evidence suggest that mantle exhumation is achieved via flip-flop detachment
1402 faulting, rather than via a unique detachment fault, namely: (1) the fact that
1403 seafloor spreading initiates usually in the center of an exhumed mantle or proto-
1404 oceanic domain; (2) the relatively symmetrical pattern of magnetic anomalies
1405 over exhumed mantle with respect to the final seafloor spreading axis (Gillard *et*
1406 *al.*, 2016b, and references therein); (3) the symmetrical pattern of over-tilted
1407 sedimentary sequences in the exhumed mantle domain (Gillard *et al.*, 2016a,
1408 2015).

1409

1410 6.2. Characteristics of rift systems

1411 6.2.1. Spatial and temporal scaling of margin domains and rifting events

1412 In Table 1, we summarize the duration of the rift phases, as well as the width of
1413 the rift domains for the examples presented above. We did not attempt to
1414 provide duration ranges for the stretching phase because it is a phase of diffuse
1415 deformation, and thus hard to distinguish from the "noise" generated by potential
1416 preceding orogenic collapse or far-field effects of adjacent tectonic events. In
1417 most examples, necking appears to have been achieved rapidly (< 10 My). One
1418 exception is the Norwegian rift system, for which a late Mid-Jurassic to latest
1419 Jurassic necking phase (ca. 25 My?; Table 1) is usually considered (Peron-
1420 Pinvidic and Osmundsen, 2018, and references therein). Yet the Norwegian
1421 rifting is often described as a succession of extension phases separated by
1422 tectonic pauses, rather than one continuous polyphase extensional event (see
1423 Fig. 20 in Zastrozhnov *et al.*, 2020). Short necking phase durations are
1424 consistent with numerical models by Chenin *et al.* (2020), which explore a wide
1425 range of crust and mantle rheologies and predict the duration of the necking
1426 phase to range between 3.3 for strong lithospheres and 8 My for weak
1427 lithospheres submitted to a bulk extension rate of 10^{-15} s^{-1} . The necking domain
1428 width of all examples above ranges from 20 to 100 km, consistent with the range
1429 observed by Chenin *et al.* (2017).

1430 Hyperextension also appears to have been achieved rapidly in most examples
1431 (< 10 My). It may have taken longer at the Norwegian margin, however the
1432 transition between the phase of hyperextension and a potential phase of mantle
1433 exhumation is not constrained, which makes it a poorly calibrated example. The
1434 hyperextended domain widths of all examples above (from 25 to 60 km; Table 1)
1435 fall within the range observed by Chenin *et al.* (2017). Considering that the
1436 hyperextended domain is the domain that displays the smaller variability in width
1437 (Chenin *et al.*, 2017) and is characterized by relatively consistent angles of

1438 aperture between top basement and Moho amongst rifted margins (Nirrengarten
1439 *et al.*, 2016), we can also expect the hyperextension phase to be relatively
1440 consistent among rifting events. This hypothesis needs however to be
1441 confirmed.

1442 The duration of the mantle exhumation phase is poorly constrained from the
1443 examples presented above; however, we expect it to be highly variable given
1444 the variability of exhumed mantle domain widths reported by Chenin *et al.*
1445 (2017). At Socotra, the small width (ca. 10 km) of the exhumation domain
1446 reported by Nonn *et al.* (2017) falls below the range observed by Chenin *et al.*
1447 (2017). We can either conclude that the latter range is underestimated because
1448 mantle exhumation can occur over a very short period/distance; or that mantle
1449 may not have been exhumed at the Socotra margin, and thus that the domain
1450 between the hyperextended crust and first mature oceanic crust may rather be
1451 interpreted as a proto-oceanic domain like in the South China Sea. The latter
1452 interpretation may be supported by the presence of outer highs, which are
1453 regarded as magmatic extrusions by Nonn *et al.* (2017). The duration of mantle
1454 exhumation may be largely controlled by the capacity of underlying
1455 asthenosphere to produce magma (temperature, fertility, upwelling rate
1456 conditions), and thus the rapidity of steady-state seafloor spreading to take over,
1457 however these hypotheses need to be tested.

1458

1459 6.2.2. Spatio-temporal evolution of accommodation and related sedimentary facies

1460 There are two ways to create accommodation, namely vertical deepening and
1461 horizontal widening. Accommodation space is more or less efficiently and rapidly
1462 filled with sediments depending on the ratio between sedimentation- vs.
1463 accommodation creation rate (Tugend *et al.*, 2014). In the following, we describe

1464 the relative contribution of vertical vs horizontal accommodation creation in the
1465 different rift domains and provide insight into the likely evolution of depositional
1466 environment. For the sake of simplicity, we consider a sediment-rich, siliciclastic-
1467 dominated setting like in the NW-South China Sea, for which the tectonic history
1468 is efficiently captured by the sedimentary record and its relationship to tectonic
1469 structures (e.g., faults; Figure 12). Sediment-starved rift systems will be
1470 discussed in section 6.4.1.

1471 6.2.2.1. The proximal domain

1472 The proximal domain is well-calibrated by drilling, seismic imaging, and
1473 field data. The low heave and throw of normal faults and associated limited
1474 crustal thinning (continental crust remains usually > 25 km thick; Figure 3a)
1475 results in limited tectonic accommodation creation (grey curves in Figure
1476 13a). Besides, minor lithospheric thinning beneath the proximal domain
1477 accounts for the lack of significant thermal subsidence.

1478 The proximal domain is usually characterized by accommodation-limited
1479 settings during the entire rifting period, which means an excess of
1480 sediments with respect to the overall available accommodation space
1481 (Prosser, 1993). As a result, facies usually range between subaerial and
1482 shallow-marine *sensu lato*, while a significant part of sediments bypass the
1483 domain and feed more distal basinal areas. Most common sediments within
1484 proximal half-graben depocenters include siliciclastic, salt and/or carbonate
1485 platform deposits. Massive salt deposition may also characterize proximal
1486 domain depocenters, in particular in arid rift settings (Prosser, 1993).

1487

1488 6.2.2.2. The necking domain

1489 The necking domain is characterized by both moderate horizontal widening
1490 (up to a few tens kilometers; e.g., Figure 8b2) due to the creation of new
1491 real estate via extensional detachment faults, and moderate- to high crustal
1492 (30–10 km) and lithospheric thinning (blue curves in Figure 13a). The
1493 necking stage is thought to display a largely undeformed keystone block
1494 between two crustal-scale necking faults (Figure 5c).

1495 The tectono-stratigraphic evolution during the necking phase is complex
1496 and may vary among rift systems depending on the inherited rheological
1497 architecture of the involved lithosphere. In the early stages of necking, the
1498 necking domain remains in shallow water (e.g., Iberia margin; Mohn *et al.*,
1499 2015, and references therein, mid-Norwegian margin; Faleide *et al.*, 2010,
1500 and references therein, northern North Sea; McLeod *et al.*, 2002) or may
1501 even be locally and temporarily uplifted above sea level (e.g., Socotra
1502 margin; Pik *et al.*, 2013, Campos Basin; Lewis *et al.*, 2014, East-India
1503 margin; Hauptert *et al.*, 2016, Mont Blanc; Ribes *et al.*, 2020, Porcupine
1504 Basin; Whiting *et al.*, 2020, NW-South China Sea; Chao *et al.* 2021). At this
1505 stage, the necking domain is confined and may still be accommodation-
1506 limited. Sediment deposits may include shallow-marine carbonates and/or
1507 shallow-marine- or terrestrial sandstones (e.g., Newfoundland margin;
1508 Wielens *et al.*, 2006, Norwegian margin; Faleide *et al.*, 2010, Porcupine
1509 Basin; Whiting *et al.*, 2020). Syn-necking sandstones are possibly derived
1510 from immediately adjacent exhumed basement domes/core complexes
1511 (e.g., the *Grès Singuliers* close to Mont Blanc; Ribes *et al.*, 2020). They
1512 may contrast with those deposited during the stretching TS, which are
1513 usually sourced from more regional sources.

1514 Subsequently, when significant new real estate has been created and/or
1515 significant thermal subsidence has occurred and/or the flexural rebound of

1516 the underlying lithospheric mantle has stopped, the necking domain may
1517 rapidly evolve into open-marine and sediment-limited settings (Figure 6c).
1518 Depositional environments evolve from continental and/or shallow-marine
1519 during the stretching and early necking TS, to deep marine/continental
1520 slope environments during the late necking/hyperextension and
1521 subsequent TS (e.g., shale deposition over the syn-necking shallow-water
1522 *Grès Singulier* in the Alpine necking domain, Ribes *et al.*, 2020; turbidites
1523 deposition over syn-necking (Tithonian) shallow-water deposits in the distal
1524 Iberian margin, Mohn *et al.*, 2015; Upper Jurassic deep-marine shales
1525 deposited over shallow marine sand-dominated Bathonian deposits and
1526 Callovian shallow-marine shales in the necking zone of the Norwegian
1527 margin, Faleide *et al.*, 2010 and Bell *et al.*, 2014, early Cretaceous shales
1528 in the Newfoundland necking domain, Wielens *et al.*, 2006; sediment
1529 starvation contemporaneous with strain localization at the Horda Platform
1530 in the North Sea; Tillmans *et al.*, 2021).

1531 Note that the deposits of the stretching TS are partially dismembered an
1532 potentially tilted by syn-necking detachment and normal faults, whereas
1533 deposits of the late necking TS are continuous.

1534

1535 6.2.2.3. The hyperextended domain

1536 The hyperextended domain is characterized by substantial horizontal
1537 widening, especially on the lower plate, due to the creation of new real
1538 estate via successive, in-sequence detachment faults (red curves in Figure
1539 13a; see also Fig. 7 in Manatschal *et al.*, 2001, and Figs. 10c and 10d in
1540 Epin and Manatschal, 2018). It also displays extreme crustal thinning from
1541 ca. 10 to > 0 km (Figure 3a), which is accompanied by immediate tectonic

1542 subsidence, and followed by significant thermal subsidence owing to major
1543 lithosphere thinning.

1544 The hyperextended domains of conjugate margins correspond to the
1545 former keystone blocks that used to be framed by the two major necking
1546 faults during the necking phase (Lavier and Manatschal, 2006; Chao *et al.*
1547 2021). At that time (necking TS), the keystone was at shallow water depths
1548 or even emerged (cf. previous section; Figure 6c). During the subsequent
1549 hyperextension phase, it was intensively delaminated via extensional
1550 detachment faults. As a result, both the stretching and necking TS are
1551 largely dismembered in the hyperextended domain (Figure 6b). From the
1552 late necking or early hyperextension TS onward, sediment deposits testify
1553 to a switch from an accommodation-limited to a sediment-limited
1554 environment, which is expressed by a rapid deepening of sedimentary
1555 facies up to deep-marine or abyssal conditions (Figure 6c; e.g., Masini *et*
1556 *al.*, 2011; Mohn *et al.*, 2015). The available accommodation during
1557 subsequent rift stages is thus essentially inherited from the unfilled
1558 accommodation created during hyperextension, and to a lesser extent due
1559 to lithosphere thermal relaxation.

1560 The sediments of the late hyperextension TS are the first to be continuous
1561 along dip of the hyperextended domain.

1562

1563 6.2.2.4. The exhumed mantle domain

1564 The exhumed mantle domain is characterized by extreme horizontal
1565 widening since this domain is entirely made of new real estate. When the
1566 distal rift basin is not isolated, mantle is exhumed in deep-marine or
1567 abyssal settings (e.g., Epin *et al.*, 2021; Steinmann, 1905) and is

1568 subjected to significant thermal subsidence once it has moved away from
1569 the spreading center.

1570 The first sediments deposited onto the exhumed mantle belong to the
1571 mantle exhumation TS (Figure 6a). Siliciclastic sedimentary sources may
1572 be lacking since the exhumed mantle domain is usually more than 100 km
1573 away from the emerged continent (Chenin *et al.*, 2017). Instead, deposition
1574 may be dominated by axial sedimentation (i.e., perpendicular to the margin
1575 dip-direction). Deposits may either arise from local gravitational reworking,
1576 turbidity or contour currents, pelagic sedimentation, or chemical
1577 precipitation (e.g., oversaturated SiO₂ rich fluids precipitating cherts), all of
1578 which usually characterize abyssal depositional environments (below the
1579 Carbonate Compensation Depth or CCD). Exceptions may occur at
1580 transform margins, where the exhumed mantle domain may be directly fed
1581 by the adjacent continent.

1582

1583 6.3. Projections and correlations from proximal to distal domains

1584 6.3.1. New aspects of the interpretation of distal domains

1585 Due to the significantly greater depth of the distal margin with respect to the
1586 proximal domain, the necking zone has for a long time represented an
1587 “interpretation frontier” between a well-calibrated domain continent-ward, and a
1588 much more enigmatic and largely inaccessible domain oceanward (Doran and
1589 Manatschal, 2017). The first attempts of distal margin interpretation naturally
1590 considered that observations made at the proximal domain can be transposed to
1591 the distal one (Figure 12a). Therefore, rift-related deformation was regarded as
1592 synchronous along the entire margin and achieved via planar high angle normal
1593 faulting between rigid tilted blocks (Waltham *et al.*, 1993). The understanding of

1594 where, when and how deformation and sediments are distributed during rifting
1595 underwent a significant paradigm shift since the 1990's (Figure 12b). It is now
1596 generally acknowledged that rifting is a localizing process that focuses toward
1597 the locus of future lithospheric breakup (Pérez-Gussinyé *et al.*, 2020; Ribes *et*
1598 *al.*, 2019b; Whiting *et al.*, 2020; Luo *et al.*, 2021; Chao *et al.* 2021), and thus the
1599 base of post-tectonic deposits should be regarded as younging oceanward.
1600 Practically, (1) syn-tectonic sediments of the distal domain are likely to
1601 correspond (timewise) to post-tectonic deposits in the proximal domain; and (2)
1602 sediment deposits of early rift phases are going to be increasingly fragmented
1603 oceanward (Figure 12b).

1604

1605 6.3.2. Correlating timelines across rifted margins

1606 In our tectono-stratigraphic model, we associated each of the successive
1607 deformation phases at play during rifting to one Tectonic Sequence (TS). A
1608 Tectonic Sequence encompasses all stratigraphic packages synchronous to the
1609 corresponding deformation phase, therefore the base and the top of each TS
1610 are by definition timelines along-dip of a given transect. Due to the polyphase
1611 and localizing nature of rifting, their correlation across the margin is difficult.
1612 Below we provide a set of characteristic timelines that may be generally
1613 recognized at rifted margins and discuss what the formerly defined *Rift Onset*
1614 *Unconformity* and *Breakup Unconformity* (Falvey, 1974) and *Necking*
1615 *Unconformity* (Chenin *et al.*, 2015) become in our new model.

1616 6.3.2.1. The Base of the Syn-Rift megasequence vs. the Rift Onset

1617 Unconformity

1618 In the mid-1970's, the onset of rifting was thought to be immediately
1619 preceded by a phase of large-scale (several hundreds of km)

1620 doming/arching of the continental crust that produces widespread erosion
1621 in the future region of rifting and breakup (Falvey, 1974). By the late
1622 1970's, such a phase of thermal doming/dynamic topography was thought
1623 to be characteristic of the onset of *active/volcanic rifting* only, while
1624 *passive/magma-poor rifting* was supposed to start with subsidence (Sengör
1625 and Burke, 1978), as predicted by the Pure-Shear Model of McKenzie
1626 (1978). More recently, Menzies *et al.* (2002) concluded that pre-rift dynamic
1627 topography was not systematic enough to be diagnostic of volcanic rifting.
1628 Dynamic topography produces a major unconformity over a wide domain
1629 (> 600 km; Campbell, 2005; Figure 13b). This unconformity can be used as
1630 a proxy for the Base Syn-Rift timeline (BSR in Figures 6, 12a and 12b)
1631 when the related doming precedes the stretching phase.

1632 Whether or not initial doming takes place, the stretching phase is
1633 characterized by widely distributed normal faulting that forms numerous
1634 half-graben depocenters. In sediment-rich rift systems, the BSR
1635 corresponds within the basins to a shift from pre-tectonic to half-graben
1636 wedge-shaped deposits. Such a shift may be identifiable on both seismic
1637 sections and at the outcrop scale.

1638 The formation of high-angle normal faults is often associated with the uplift
1639 of the corresponding footwall and local erosion of its crest (Yielding, 1990)
1640 over a width usually less than 5 km (Figure 13b). This erosional
1641 unconformity and its correlative conformities can be used as a proxy for the
1642 age of the BSR.

1643

1644 6.3.2.2. The Base of the Necking Tectonic Sequence vs. the Necking

1645 Unconformity

1646 Chenin *et al.* (2015) defined the necking unconformity as the transition from
1647 syn- to post-tectonic deposits in the proximal domain (for sufficiently
1648 sediment-rich rift systems). In our model this “unconformity” corresponds to
1649 the timeline at the base of the necking TS (BNk in Figures 6 and 12a and
1650 12b).

1651 The “necking unconformity” is difficult to correlate across more distal
1652 domains. In the future necking and hyperextended domains, we notice that
1653 the necking phase is often associated with the formation of erosional
1654 unconformities. In the necking domain, erosion occurs at the breakaway of
1655 the necking fault (e.g., Norwegian margin; Bell *et al.*, 2014) and/or along
1656 upper- to mid-crustal basement exhumed by this fault (e.g., Mont Blanc;
1657 Ribes *et al.*, 2020). The new real estate created by activity on detachment
1658 faults corresponds also to a discordance since sedimentary deposits
1659 cannot be older than local basement exhumation age. Distinguishing
1660 between exhumed basement and eroded top basement may be difficult,
1661 especially because one does not exclude the other.

1662 In-between the main necking fault systems, the keystone block (future
1663 hyperextended domains) seems to remain at shallow water depths during
1664 (part of) the necking phase, or to be even temporarily emergent. Illustrative
1665 examples include the early Jurassic karst of the Briançonnais (section
1666 4.2.2; Claudel and Dumont, 1999), Tithonian offshore shelf deposits at the
1667 Iberian hyperextended domain (section 4.3.3; Mohn *et al.*, 2015, and
1668 references therein), lack of deposition in the central part of the
1669 northwestern South China sea (section 5.1.4 and Figure 9e; Chao *et al.*
1670 *subm*), shallow water deposits on the Halten Terrace at the mid-Norwegian
1671 margin (section 5.2.2; Bell *et al.*, 2014), and basement subaerial
1672 exhumation at the Socotra margin (section 5.3.2; Pik *et al.*, 2013). The

1673 width of such necking-related uplift is of the order of a few tens of
1674 kilometers (Figure 13b; Chenin *et al.*, 2019, and references therein).

1675 Thus, the necking phase may be associated with several unconformities
1676 and/or discordances in both the necking and hyperextended domains.
1677 Although these may not be synchronous, they are largely limited to the
1678 necking TS, which seems to usually encompass only a short period of time
1679 (section 6.2.1), and thus can be reasonably correlated with the “necking
1680 unconformity” of the proximal domain.

1681

1682 6.3.2.3. The Base of the Post-Rift megasequence vs. the Breakup

1683 Unconformity

1684 Falvey (1974) suggested that continental breakup results in a rapid
1685 increase in the subsidence rate at the two conjugate margins. The resulting
1686 rapid marine transgression produces either a backstep of the onlapping
1687 sediments towards the continent when accommodation creation rate
1688 dominates over sedimentation rate at the coast, or a progressive onlap
1689 otherwise. In both cases it would produce an unconformity, often named
1690 the *Breakup Unconformity*. This hypothesis was supported by dynamic
1691 thermo-mechanical modelling (Braun and Beaumont, 1989). Although the
1692 existence of such discordance has been highlighted in several margins
1693 (e.g., Iberia–Newfoundland; Tucholke *et al.*, 2007, Santos Basin, Grand
1694 Banks and Beaufort Sea; Hubbard, 1988, Amerasian Basin; Embry and
1695 Dixon, 1990), its cause and synchronicity became debated from the 2000’s
1696 (e.g., Masini *et al.*, 2013; Wilson *et al.*, 2001). Gillard *et al.* (2015)
1697 highlighted that, in the exhumed mantle domain, each detachment fault
1698 was associated with a specific discordance, ruling out the existence of a
1699 unique *breakup unconformity* at the scale of an entire margin. More

1700 recently, Pérez-Gussinyé *et al.* (2020) advocated, based on dynamical
1701 thermo-mechanical numerical modeling, that the “breakup unconformity”
1702 was restricted to the most distal part of the margin because lithospheric
1703 breakup is not associated with a sudden stress drop.

1704 The Base of the Post-rift timeline (BPR in Figures 6, 12a and 12b) and
1705 onset of seafloor spreading are often difficult to define, either because of
1706 scattered and sporadic incipient magmatic activity in magma-poor rift
1707 systems (Bronner *et al.*, 2011; Epin *et al.*, 2019; Epin *et al.*, 2021; Jagoutz
1708 *et al.*, 2007), or because of excess magma prior to onset of steady-state
1709 seafloor spreading in magma-rich rift systems (Tugend *et al.*, 2020). When
1710 the first-formed oceanic crust can be identified, the age of breakup
1711 corresponds to the age of the first overlying sediments in most sediment-
1712 rich rift systems (in sediment-starved systems the first overlying sediments
1713 provide only a minimum age). On seismic sections, the corresponding
1714 seismic reflection could theoretically be correlated across the entire margin.
1715 It may correspond to a discordance in the most distal part of the margin
1716 since it expresses the transition from syn- to post tectonic settings,
1717 however it is likely a conformable reflection in the proximal domain since
1718 deformation therein ceased earlier than the time of breakup. In the field, the
1719 BPR is practically impossible to identify based on geometrical criteria. In
1720 the past, it was considered to be marked by the biostratigraphic hiatus
1721 related to the backstep/progressive onlap mentioned above. However,
1722 given that breakup is not associated with a sudden stress drop in the
1723 proximal domain (Pérez-Gussinyé *et al.*, 2020), the contemporality
1724 between this paraconformity recorded in the proximal domain and the BPR
1725 is unlikely.

1726 It is important not to automatically interpret unconformities at proximal
1727 margins as marking the BPR because numerous unconformities in the
1728 proximal domain may relate either to local tectonic events, or to large-
1729 scale, unrelated processes (e.g., climate, or far-field influence of a large-
1730 scale tectonic event). Indeed, as the top of the proximal domain remains at
1731 shallow depths due to its thick crust (30 ± 5 km) and the absence of
1732 significant lithospheric thinning, it may be very sensitive to eustatic
1733 changes (Prosser, 1993). Therefore, the timing of breakup cannot be
1734 accurately determined from seismic reflector relationship the proximal and
1735 necking domains.

1736

1737 6.4. Model limitations

1738 The tectono-stratigraphic evolution presented in this contribution provides a powerful
1739 template to guide the seismic interpretation of distal margins and to unravel the
1740 complexity of rift systems exposed in orogens, where they are usually dismembered
1741 by thrust tectonics. However, as a model it remains a simplification, and thus it
1742 should not be used without taking the regional specificities of individual rift systems.
1743 Below we briefly review the main potential pitfalls to keep in mind when using this
1744 template:

1745 6.4.1. Completeness and quality of the tectono-stratigraphic record

1746 The efficient record of the tectono-stratigraphic evolution depends primarily on
1747 the ratio between sedimentation- and accommodation creation rate (e.g.,
1748 Ravnås and Steel, 1998 and references therein; Martins-Neto and Catuneanu,
1749 2010). A sediment-starved system will incompletely or even not record syn-
1750 tectonic deformation (Figure 14a; e.g., Barr, 1991). Note that the sedimentary
1751 budget available during rifting depends largely on the climate, in that humid

1752 conditions favor increased erosion, and hence prolific sediment sources,
1753 conversely to arid climates that favor sediment starvation (Prosser, 1993).

1754 The presence of pre- or syn-rift low frictional materials like salt and/or clay may
1755 also be a problem since they can induce deformation and accommodation
1756 creation not necessarily related to the rifting event itself (e.g., Rowan and Ratliff,
1757 2012).

1758

1759 6.4.2. Presence of magmatic systems

1760 The presence of magmatic systems may represent a difficulty because
1761 (1) magmatic crust may be hard to distinguish from pre-rift continental crust
1762 (Osmundsen et al., 2016; Tugend et al., 2020); (2) magmatic intrusions may
1763 perturb or overprint the tectono-sedimentary record, rendering its unravelling
1764 difficult (Zhang et al., 2021); and (3) magma-related heat may modify the
1765 rheology of the lithosphere involved, and thus lead to different deformation
1766 modes compared to magma-poor rifting; in particular, significant magmatic
1767 activity and related diiking may trigger both crustal and lithospheric breakup
1768 before the continental crust was thinned to 0 km (Bialas et al., 2010; Ebinger
1769 and Casey, 2001; Sun et al., 2019). Otherwise, magmatic lava flows may
1770 behave comparably to sediments, and can thus be interpreted in a similar way
1771 (e.g., Chao et al., 2021)

1772

1773 6.4.3. The three-dimensional aspect of rift systems

1774 Rift systems are often segmented by transform faults (Figure 14b1), especially
1775 during crustal thinning (necking and hyperextension; Nirrengarten *et al.*, 2018).
1776 Transform systems can separate segments with distinct margin architectures, as

1777 exemplified by the differing domains width between the northern and central
1778 segment of the Iberia margin (Sutra and Manatschal, 2012) and between the
1779 southern (Møre), central (Vøring) and northern (Lofoten) segment of the mid-
1780 Norwegian margin (Péron-Pinvidic and Osmundsen, 2018). Transfer faults can
1781 also delimit segments with different timings of extension (e.g., the sequential
1782 northward propagation of crustal extension along the Iberian margin; Alves *et*
1783 *al.*, 2009, the sequential evolution along the Norwegian–Greenland conjugate
1784 margins; Gernigon *et al.*, 2020, or the westward younging of extension across
1785 the transform fault of the Socotra margin; Pik *et al.*, 2013). Therefore, the timing
1786 of necking, hyperextension and mantle exhumation, as well as the age of the
1787 various unconformities mentioned above, vary presumably from one segment to
1788 another (Nirrengarten *et al.*, 2018; Péron-Pinvidic *et al.*, 2013).

1789 Individual faults have a limited extent along strike (Lescoutre and Manatschal,
1790 2020; Lymer *et al.*, 2019; Nonn *et al.*, 2017; Péron-Pinvidic *et al.*, 2007) and
1791 major structures may change their tectonic role along the margin (e.g., local
1792 merging of breakaway complexes in Osmundsen and Péron-Pinvidic, 2018;
1793 Figure 10a).

1794 The correlation of timelines is particularly tricky in propagating rift systems (e.g.,
1795 the V-shaped South China Sea, Gulf of Aden, Bay of Biscay, Porcupine Basin,
1796 early stages of the southern North-Atlantic rifting, etc.; Nirrengarten *et al.*, 2018,
1797 and references therein; Luo *et al.*, 2021). Indeed, the migration of deformation
1798 toward both the rift center and the tip of the propagator renders timelines oblique
1799 to the conjugate margins (Figure 14b2).

1800

1801 6.4.4. Multistage rifting (out-of-sequence deformation)

1802 Rifting may not always initiate on a thermally and gravitationally equilibrated
1803 lithosphere (Manatschal *et al.*, 2021; Zhang *et al.*, 2020) and/or the pre-rift
1804 sediments may display variable thicknesses inherited from previous tectonic
1805 events. In Western Europe, for instance, the Alpine Tethys rifting overprinted an
1806 area that was formerly affected by the Meliata-Vardar rifting, which is expressed
1807 by a thickening of the pre-Alpine Tethys rifting sedimentary sequence to the east
1808 (Manatschal *et al.*, this vol. and references therein). In Grand Banks, the Jeanne
1809 d'Arc stretching basin underwent post-Iberia–Newfoundland rifting extension
1810 related to the opening of the Orphan Basin (e.g., Skogseid, 2010). We refer to
1811 these spatially overprinting but temporally distinct extension phases as
1812 *multistage rifting* (Cadenas *et al.*, 2020). The consequence of multistage rifting
1813 may be the local incorporation and/or reactivation of older tectono-stratigraphic
1814 features into the ongoing rift system (Figure 14c). Examples include the Permian
1815 and Triassic basins incorporated in the Jurassic hyperextended domain of the
1816 Alpine rift system (Epin and Manatschal, 2018); and Jurassic salt-bearing basins
1817 in the Cretaceous hyperextended domain of the Basque-Cantabrian basin
1818 (Manatschal *et al.*, 2021; Miró *et al.*, 2021).

1819

1820 7. Conclusion

1821

1822 In this contribution, we propose a tectono-stratigraphic model describing the primary
1823 spatio-temporal evolution of active deformation during rifting. We show that the different
1824 rift domains of rifted margins are associated with specific (1) periods of tectonic activity;
1825 (2) styles of deformation and related tectono-stratigraphic architecture; (3) amounts of
1826 horizontal and vertical accommodation creation; and (4) depositional environments. We
1827 demonstrate that the sequential localization of extension during rifting results in both a
1828 younging of the base of passive infill and an increasing fragmentation of early rift-related

1829 deposits oceanward. We propose a panel of Tectonic Sequences that may be correlated
1830 more or less easily and continuously across rifted margins. This model provides a new
1831 template to help correlate observations made at the well-calibrated and understood
1832 proximal domain with the more inaccessible and enigmatic distal domain. It highlights the
1833 necessity of jettisoning outdated dogma on rifted margins and changing our routines
1834 when interpreting seismic sections and correlating remnants of dismembered rifted
1835 margins exposed in orogens.

1836

1837 Acknowledgments: The authors are grateful to C.A.L. Jackson, I. Sharp, L. Whitting, and an
1838 anonymous reviewer for thorough, constructive and stimulating reviews that helped
1839 improving the manuscript. We also thank Editor K. Gallagher for handling both the present
1840 manuscript and its companion. The concepts presented in this work benefited from fruitful
1841 discussions with Garry Karner. M. Nirrengarten is acknowledged for providing the NW-SCS
1842 domain map shown in Figure 9a.

1843

1844 Author contributions:

1845 Pauline Chenin: Writing – original draft, Conceptualization, Investigation

1846 Gianreto Manatschal: Writing – review & editing, Conceptualization, Investigation, Funding
1847 acquisition

1848 Jean-François Ghienne: Writing – review & editing, Conceptualization, Investigation

1849 Peng Chao: Writing – review & editing, Conceptualization, Investigation

1850

1851 Data Availability Statement:

1852 Data sharing is not applicable to this article as no new data were created or analyzed in this
1853 study.

REFERENCES

- 1854
1855
- 1856 Abdelmalak, M.M., Faleide, J.I., Planke, S., Gernigon, L., Zastrozhnov, D., Shephard, G.E., Myklebust,
1857 R., 2017. The T-Reflection and the Deep Crustal Structure of the Vøring Margin, Offshore mid-
1858 Norway. *Tectonics* 36, 2497–2523. <https://doi.org/10.1002/2017TC004617>
- 1859 Ahmed, A., Leroy, S., Keir, D., Korostelev, F., Khanbari, K., Rolandone, F., Stuart, G., Obrebski, M.,
1860 2014. Crustal structure of the Gulf of Aden southern margin: Evidence from receiver functions on
1861 Socotra Island (Yemen). *Tectonophysics* 637, 251–267.
1862 <https://doi.org/10.1016/j.tecto.2014.10.014>
- 1863 Alves, T., Moita, C., Cunha, T., Ullnaess, M., Myklebust, R., Monteiro, J.H., Manuppella, G., 2009.
1864 Diachronous evolution of Late Jurassic–Cretaceous continental rifting in the northeast Atlantic
1865 (west Iberian margin). *Tectonics* 28, n/a-n/a. <https://doi.org/10.1029/2008TC002337>
- 1866 Alves, T.M., Gawthorpe, R.L., Hunt, D.W., Monteiro, J.H., 2003. Post-Jurassic tectono-sedimentary
1867 evolution of the Northern Lusitanian Basin (western Iberian margin). *Basin Res.* 15, 227–249.
1868 <https://doi.org/10.1046/j.1365-2117.2003.00202.x>
- 1869 Alves, T.M., Gawthorpe, R.L., Hunt, D.W., Monteiro, J.H., 2002. Jurassic tectono-sedimentary
1870 evolution of the Northern Lusitanian Basin (offshore Portugal). *Mar. Pet. Geol.* 19, 727–754.
1871 [https://doi.org/10.1016/S0264-8172\(02\)00036-3](https://doi.org/10.1016/S0264-8172(02)00036-3)
- 1872 Alves, T.M., Moita, C., Sandnes, F., Cunha, T., Monteiro, J.H., Pinheiro, L.M., 2006. Mesozoic-
1873 Cenozoic evolution of North Atlantic continental-slope basins: The Peniche basin, western
1874 Iberian margin. *Am. Assoc. Pet. Geol. Bull.* 90, 31–60. <https://doi.org/10.1306/08110504138>
- 1875 Andersen, T.B., Corfu, F., Labrousse, L., Osmundsen, P.-T., 2012. Evidence for hyperextension along
1876 the pre-Caledonian margin of Baltica. *J. Geol. Soc. London.* 169, 601–612.
1877 <https://doi.org/10.1144/0016-76492012-011>
- 1878 Angrand, P., Mouthereau, F., Masini, E., Asti, R., 2020. A reconstruction of Iberia accounting for
1879 Western Tethys-North Atlantic kinematics since the late-Permian-Triassic. *Solid Earth* 11, 1313–
1880 1332. <https://doi.org/10.5194/se-11-1313-2020>
- 1881 Argand, E., 1916. Sur l'arc des Alpes occidentales. Bridel, G.
- 1882 Aubouin, J., 1965. Geosynclines. Elsevier Publishing Company, Amsterdam - London - New York.
- 1883 Barr, D., 1991. Subsidence and sedimentation in semi-starved half-graben: A model based on North
1884 Sea data. *Geol. Soc. Spec. Publ.* 56, 17–28. <https://doi.org/10.1144/GSL.SP.1991.056.01.02>
- 1885 Barr, D., 1987. Structural/stratigraphic models for extensional basins of half-graben type. *J. Struct.*
1886 *Geol.* 9, 491–500. [https://doi.org/10.1016/0191-8141\(87\)90124-6](https://doi.org/10.1016/0191-8141(87)90124-6)
- 1887 Bell, R.E., Jackson, C.A.L., Elliott, G.M., Gawthorpe, R.L., Sharp, I.R., Michelsen, L., 2014. Insights
1888 into the development of major rift-related unconformities from geologically constrained
1889 subsidence modelling: Halten Terrace, offshore mid Norway. *Basin Res.* 26, 203–224.
1890 <https://doi.org/10.1111/bre.12049>
- 1891 Beltrando, M., Stockli, D.F., Decarlis, A., Manatschal, G., 2015. A crustal-scale view at rift localization
1892 along the fossil Adriatic margin of the Alpine Tethys preserved in NW Italy. *Tectonics* 34, 1927–
1893 1951. <https://doi.org/10.1002/2015TC003973>
- 1894 Bernoulli, D., 1964. Zur Geologie des Monte Generoso (Lombardische Alpen): ein Beitrag zur
1895 Kenntnis der südalpinen Sedimente.
- 1896 Bertotti, G., Picotti, V., Bernoulli, D., Castellarin, A., 1993. From rifting to drifting: tectonic evolution of
1897 the South-Alpine upper crust from the Triassic to the Early Cretaceous. *Sediment. Geol.* 86, 53–
1898 76. [https://doi.org/10.1016/0037-0738\(93\)90133-P](https://doi.org/10.1016/0037-0738(93)90133-P)
- 1899 Bialas, R.W., Buck, W.R., Qin, R., 2010. How much magma is required to rift a continent? *Earth*
1900 *Planet. Sci. Lett.* 292, 68–78. <https://doi.org/10.1016/J.EPSL.2010.01.021>
- 1901 Boillot, G., Winterer, E.L., 1988. Drilling on the Galicia margin: retrospect and prospect 1, Scientific

- 1902 Results.
- 1903 Bond, G.C., Kominz, M.A., 1988. Evolution of thought on passive continental margins from the origin
1904 of geosynclinal theory (~1860) to the present. *Bull. Geol. Soc. Am.* 100, 1909–1933.
1905 [https://doi.org/10.1130/0016-7606\(1988\)100<1909:EOTOPC>2.3.CO;2](https://doi.org/10.1130/0016-7606(1988)100<1909:EOTOPC>2.3.CO;2)
- 1906 Bosworth, W., Huchon, P., McClay, K., 2005. The Red Sea and Gulf of Aden Basins. *J. African Earth
1907 Sci.* 43, 334–378. <https://doi.org/10.1016/j.jafrearsci.2005.07.020>
- 1908 Braun, J., Beaumont, C., 1989. A physical explanation of the relation between flank uplifts and the
1909 breakup unconformity at rifted continental margins. *Geology* 17, 760–764.
1910 [https://doi.org/10.1130/0091-7613\(1989\)017<0760:APEOTR>2.3.CO](https://doi.org/10.1130/0091-7613(1989)017<0760:APEOTR>2.3.CO)
- 1911 Breivik, A., Mjelde, R., Raum, T., 2010. Crustal structure beneath the Trøndelag Platform and adjacent
1912 areas of the Mid-Norwegian margin, as derived from wide-angle seismic and potential field data.
1913 *Nor. J. Gology* 90, 141–161.
- 1914 Brekke, H., 2000. The tectonic evolution of the Norwegian Sea continental margin, with emphasis on
1915 the Voring and More basins. *Spec. Publ. Soc. London* 167, 327–378.
- 1916 Bronner, A., Sauter, D., Manatschal, G., Péron-Pinvidic, G., Munsch, M., 2011. Magmatic breakup as
1917 an explanation for magnetic anomalies at magma-poor rifted margins. *Nat. Geosci.* 4, 549–553.
- 1918 Brune, S., Heine, C., Pérez-Gussinyé, M., Sobolev, S. V., 2014. Rift migration explains continental
1919 margin asymmetry and crustal hyper-extension. *Nat. Commun.* 5, 4014.
1920 <https://doi.org/10.1038/ncomms5014>
- 1921 Buchanan, P.G., McClay, K.R., 1991. Sandbox experiments of inverted listric and planar fault systems.
1922 *Tectonophysics* 188, 97–115. [https://doi.org/10.1016/0040-1951\(91\)90317-L](https://doi.org/10.1016/0040-1951(91)90317-L)
- 1923 Buck, W.R., 1991. Modes of continental lithospheric extension. *J. Geophys. Res.* 96, 20,161-20,178.
- 1924 Cadenas, P., Manatschal, G., Fernández-Viejo, G., 2020. Unravelling the architecture and evolution of
1925 the inverted multi-stage North Iberian-Bay of Biscay rift. *Gondwana Res.* 88, 67–87.
1926 <https://doi.org/10.1016/j.gr.2020.06.026>
- 1927 Comeselle, A.L., Ranero, C.R., Franke, D., Barckhausen, U., 2017. The continent-ocean transition on
1928 the northwestern South China Sea. *Basin Res.* 29, 73–95. <https://doi.org/10.1111/bre.12137>
- 1929 Campbell, I.H., 2005. Large Igneous Provinces and the Mantle Plume Hypothesis. *Elements* 1, 265–
1930 269. <https://doi.org/10.2113/gselements.1.5.265>
- 1931 Causer, A., Pérez-Díaz, L., Adam, J., Eagles, G., 2020. Uncertainties in break-up markers along the
1932 Iberia-Newfoundland margins illustrated by new seismic data. *Solid Earth* 11, 397–417.
1933 <https://doi.org/10.5194/se-11-397-2020>
- 1934 Chao, P., Manatschal, G., Chenin, P., Ren, J., Zhang, C., Pang, X., Zheng, J., Yang, L., Kuznir, N.J.,
1935 2021. The tectono-stratigraphic and magmatic evolution of conjugate rifted margins: insights
1936 from the NW South China Sea. *J. Geodyn.*
- 1937 Chenin, P., Manatschal, G., Decarlis, A., Schmalholz, S.M., Duretz, T., Beltrando, M., 2019. Emersion
1938 of distal domains in advanced stages of continental rifting explained by asynchronous crust and
1939 mantle necking. *Geochemistry, Geophys. Geosystems* 20, 2019GC008357.
1940 <https://doi.org/10.1029/2019GC008357>
- 1941 Chenin, P., Manatschal, G., Lavier, L.L., Erratt, D., 2015. Assessing the impact of orogenic inheritance
1942 on the architecture, timing and magmatic budget of the North Atlantic rift system: a mapping
1943 approach. *J. Geol. Soc. London.* 172, 711–720. <https://doi.org/10.1144/jgs2014-139>
- 1944 Chenin, P., Manatschal, G., Picazo, S., Müntener, O., Karner, G.D., Johnson, C., Ulrich, M., 2017.
1945 Influence of the architecture of magma-poor hyperextended rifted margins on orogens produced
1946 by the closure of narrow versus wide oceans. *Geosphere* 13, 1–18.
1947 <https://doi.org/10.1130/GES01363.1>
- 1948 Chenin, P., Schmalholz, S.M., Manatschal, G., Duretz, T., 2020. Impact of crust–mantle mechanical
1949 coupling on the topographic and thermal evolutions during the necking phase of ‘magma-poor’

- 1950 and 'sediment-starved' rift systems: A numerical modeling study. *Tectonophysics* 228472.
1951 <https://doi.org/10.1016/j.tecto.2020.228472>
- 1952 Chenin, P., Schmalholz, S.M., Manatschal, G., Karner, G.D., 2018. Necking of the lithosphere: A
1953 reappraisal of basic concepts with thermo-mechanical numerical modeling. *J. Geophys. Res.*
1954 *Solid Earth* 123, 5279–5299. <https://doi.org/10.1029/2017JB014155>
- 1955 Chester, F.M., Logan, J.M., 1986. Implications for mechanical properties of brittle faults from
1956 observations of the Punchbowl fault zone, California. *Pure Appl. Geophys. PAGEOPH* 124, 79–
1957 106. <https://doi.org/10.1007/BF00875720>
- 1958 Chevalier, F., 2002. Vitesse et cyclicité de fonctionnement des failles normales de rift: implication sur
1959 le remplissage stratigraphique des bassins et sur les modalités d'extension d'une marge passive
1960 fossile: application au demi-graben liasique de Bourg d'Oisans (Alpes occid. Université de
1961 Bourgogne.
- 1962 Claudel, M.E., Dumont, T., 1999. A record of multistage continental break-up on the Briançonnais
1963 marginal plateau (Western Alps): Early and Middle-Late Jurassic rifting. *Eclogae Geol. Helv.* 92,
1964 45–61.
- 1965 Clerc, C., Ringenbach, J.C., Jolivet, L., Ballard, J.F., 2018. Rifted margins: Ductile deformation,
1966 boudinage, continentward-dipping normal faults and the role of the weak lower crust. *Gondwana*
1967 *Res.* 53, 20–40. <https://doi.org/10.1016/j.gr.2017.04.030>
- 1968 CNLOPB, C.-N.-L.O.P.B., 2010. Jeanne d'Arc Basin lithostratigraphy [WWW Document]. URL
1969 https://www.cnlopb.ca/wp-content/uploads/maps/xdb_lith.pdf%0A
- 1970 Colletini, C., 2011. The mechanical paradox of low-angle normal faults: Current understanding and
1971 open questions. *Tectonophysics*. <https://doi.org/10.1016/j.tecto.2011.07.015>
- 1972 Coltat, R., Boulvais, P., Branquet, Y., Collot, J., Epin, M.E., Manatschal, G., 2019. Syntectonic
1973 carbonation during synmagmatic mantle exhumation at an ocean-continent transition. *Geology*
1974 47, 183–186. <https://doi.org/10.1130/G45530.1>
- 1975 Conti, P., Manatschal, G., Pfister, M., 1994. Synrift sedimentation, Jurassic and Alpine tectonics in the
1976 central Ortler nappe (Eastern Alps, Italy). *Eclogae Geol. Helv.* 87, 63–90.
- 1977 Dana, J.D., 1873. On some results of the Earth's contraction from cooling including a discussion of the
1978 origin of mountains and the nature of the Earth's interior. *Am. J. Sci.* 3, 423–443.
- 1979 De Graciansky, P.C., Roberts, D.G., Tricart, P., 2011. The Western Alps, from rift to passive margin to
1980 orogenic belt: an integrated geoscience overview, *Developments in Earth Surface Processes* 14.
1981 Elsevier.
- 1982 Decandia, F.A., Elter, P., 1972. La "zona" ofiolitifera del Bracco nel settore compreso fra Levente e la
1983 Val Graveglia (Appennino ligure). *Mem. Soc. Geol. Ital.* 11, 503–530.
- 1984 Decandia, F.A., Elter, P., 1969. Riflessioni sul problema delle ofioliti nell'Appennino settentrionale
1985 (nota preliminare). *Atti della Soc. Toscana di Sci. Nat.*
- 1986 Decarli, A., Beltrando, M., Manatschal, G., Ferrando, S., Carosi, R., 2017. Architecture of the Distal
1987 Piedmont-Ligurian Rifted Margin in NW Italy: Hints for a Flip of the Rift System Polarity.
1988 *Tectonics* 36, 2388–2406. <https://doi.org/10.1002/2017TC004561>
- 1989 Deemer, S., Hall, J., Solvason, K., Lau, K.W.H., Loudon, K., Srivastava, S., Sibuet, J.C., 2009.
1990 Structure and development of the southeast Newfoundland continental passive margin: Derived
1991 from SCREECH Transect 3. *Geophys. J. Int.* 178, 1004–1020. <https://doi.org/10.1111/j.1365-246X.2009.04162.x>
- 1993 Desmurs, L., Müntener, O., Manatschal, G., 2002. Onset of magmatic accretion within a magma-poor
1994 rifted margin: a case study from the Platta ocean-continent transition, eastern Switzerland.
1995 *Contrib. to Mineral. Petrol.* 144, 365–382. <https://doi.org/10.1007/s00410-002-0403-4>
- 1996 Doran, H., Manatschal, G., 2017. Breaking up is never easy: The complexities that create
1997 opportunities in the distal domain. *GeoExPro* 58–61.

- 1998 Doré, A.G., Lundin, E.R., Jensen, L.N., Birkelan, Ø., Eliassen, P.E., Fichler, C., 1999. Principal
1999 tectonic events in the evolution of the northwest European Atlantic margin, in: Fleet, A.J., Boldy,
2000 S.A.R. (Eds.), *Petroleum Geology of Northwest Europe: Proceedings of the 5th Conference*. The
2001 Geological Society, London, pp. 41–61.
- 2002 Dumont, T., Champagnac, J.D., Crouzet, C., Rochat, P., 2008. Multistage shortening in the Dauphiné
2003 zone (French Alps): The record of Alpine collision and implications for pre-Alpine restoration, in:
2004 *Swiss Journal of Geosciences*. SpringerOpen, pp. 89–110. [https://doi.org/10.1007/s00015-008-](https://doi.org/10.1007/s00015-008-1280-2)
2005 1280-2
- 2006 Duretz, T., Asti, R., Lagabrielle, Y., Brun, J.P., Jourdon, A., Clerc, C., Corre, B., 2019. Numerical
2007 modelling of Cretaceous Pyrenean Rifting: The interaction between mantle exhumation and syn-
2008 rift salt tectonics. *Basin Res.* 32, 0–1. <https://doi.org/10.1111/bre.12389>
- 2009 Eberli, G.P., 1988. The evolution of the southern continental margin of the Jurassic Tethys Ocean as
2010 recorded in the Allgäu Formation of the Austroalpine Nappes of Graubünden (Switzerland).
2011 *Eclogae Geol. Helv.* 81, 175–214.
- 2012 Ebinger, C.J., Casey, M., 2001. Continental breakup in magmatic provinces: An Ethiopian example.
2013 *Geology* 29, 530.
- 2014 Eldholm, O., Skogseid, J., Planke, S., Gladchenko, T.P., 1995. Volcanic margin concepts, in: Banda,
2015 E., Torné, M., Talwani, M. (Eds.), *Rifted Ocean-Continent Boundaries*. Springer, Dordrecht, pp.
2016 1–16. https://doi.org/10.1007/978-94-011-0043-4_1
- 2017 Elliott, G.M., Wilson, P., Jackson, C.A. -L., Gawthorpe, R.L., Michelsen, L., Sharp, I.R., 2012. The
2018 linkage between fault throw and footwall scarp erosion patterns: an example from the Bremstein
2019 Fault Complex, offshore Mid-Norway. *Basin Res.* 24, 180–197. [https://doi.org/10.1111/J.1365-](https://doi.org/10.1111/J.1365-2117.2011.00524.X)
2020 2117.2011.00524.X
- 2021 Embry, A.F., Dixon, J., 1990. The breakup unconformity of the Amerasia Basin, Arctic Ocean:
2022 evidence from Arctic Canada. *Geol. Soc. Am. Bull.* 102, 1526–1534.
2023 [https://doi.org/10.1130/0016-7606\(1990\)102<1526:TBUOTA>2.3.CO;2](https://doi.org/10.1130/0016-7606(1990)102<1526:TBUOTA>2.3.CO;2)
- 2024 Enachescu, M.E., 1987. Tectonic and Structural Framework of the Northeast Newfoundland
2025 Continental Margin, in: *Sedimentary Basins and Basin-Forming Mechanisms — Memoir 12*.
2026 CSPG Special Publications, pp. 117–146.
- 2027 Epin, M.-E., Manatschal, G., Amann, M., Ribes, C., Clause, A., Guffon, T., Lescanne, M., 2019.
2028 Polyphase tectono-magmatic evolution during mantle exhumation in an ultra-distal, magma-poor
2029 rift domain: example of the fossil Platta ophiolite, SE Switzerland. *Int. J. Earth Sci.*
2030 <https://doi.org/10.1007/s00531-019-01772-0>
- 2031 Epin, M.-E., Manatschal, G., Sapin, F., Rowan, M.G., 2021. The tectono-magmatic and subsidence
2032 evolution during lithospheric breakup in a salt-rich rifted margin: Insights from a 3D seismic
2033 survey from southern Gabon. *Mar. Pet. Geol.* 128, 105005.
2034 <https://doi.org/10.1016/j.marpetgeo.2021.105005>
- 2035 Epin, M.E., Manatschal, G., 2018. Three-dimensional architecture, structural evolution, and role of
2036 inheritance controlling detachment faulting at a hyperextended distal margin: the example of the
2037 Err detachment system (SE Switzerland). *Tectonics* 37, 4494–4514.
2038 <https://doi.org/10.1029/2018TC005125>
- 2039 Epin, M.E., Manatschal, G., Amann, M., 2017. Defining diagnostic criteria to describe the role of rift
2040 inheritance in collisional orogens: the case of the Err-Platta nappes (Switzerland). *Swiss J.*
2041 *Geosci.* 110, 419–438. <https://doi.org/10.1007/s00015-017-0271-6>
- 2042 Faleide, J.I., Bjorlykke, K., Gabrielsen, R.H., 2010. Geology of the norwegian continental shelf, in:
2043 *Petroleum Geoscience: From Sedimentary Environments to Rock Physics*. Springer Berlin
2044 Heidelberg, pp. 467–499. https://doi.org/10.1007/978-3-642-02332-3_22
- 2045 Falvey, D.A., 1974. The development of continental margins in Plate Tectonics theory. *APPEA J.* 14,
2046 95. <https://doi.org/10.1071/aj73012>
- 2047 Fletcher, R.C., Hallet, B., 1983. Unstable extension of the lithosphere: A mechanical model for Basin-

- 2048 and-Range structure. *J. Geophys. Res.* 88, 7457. <https://doi.org/10.1029/JB088iB09p07457>
- 2049 Fournier, M., Huchon, P., Khanbari, K., Leroy, S., 2007. Segmentation and along-strike asymmetry of
2050 the passive margin in Socotra, eastern Gulf of Aden: Are they controlled by detachment faults?
2051 *Geochemistry, Geophys. Geosystems* 8, n/a-n/a. <https://doi.org/10.1029/2006GC001526>
- 2052 Froitzheim, N., Eberli, G.P., 1990. Extensional detachment faulting in the evolution of a Tethys passive
2053 continental margin, Eastern Alps, Switzerland. *Geol. Soc. Am. Bull.* 102, 1297–1308.
2054 [https://doi.org/10.1130/0016-7606\(1990\)102](https://doi.org/10.1130/0016-7606(1990)102)
- 2055 Gao, J., Wu, S., McIntosh, K., Mi, L., Liu, Z., Spence, G., 2016. Crustal structure and extension mode
2056 in the northwestern margin of the South China Sea. *Geochemistry, Geophys. Geosystems* 17,
2057 2143–2167. <https://doi.org/10.1002/2016GC006247>
- 2058 Gawthorpe, R.L., Fraser, A.J., Collier, R.E.L., 1994. Sequence stratigraphy in active extensional
2059 basins: implications for the interpretation of ancient basin-fills. *Mar. Pet. Geol.* 11, 642–658.
2060 [https://doi.org/10.1016/0264-8172\(94\)90021-3](https://doi.org/10.1016/0264-8172(94)90021-3)
- 2061 Gawthorpe, R.L., Leeder, M.R., 2000. Tectono-sedimentary evolution of active extensional basins.
2062 *Basin Res.* 12, 195–218. <https://doi.org/10.1111/j.1365-2117.2000.00121.x>
- 2063 Gawthorpe, R.L., Leeder, M.R., Kranis, H., Skourtsos, E., Andrews, J.E., Henstra, G.A., Mack, G.H.,
2064 Muravchik, M., Turner, J.A., Stamatakis, M., 2018. Tectono-sedimentary evolution of the Plio-
2065 Pleistocene Corinth rift, Greece. *Basin Res.* 30, 448–479. <https://doi.org/10.1111/bre.12260>
- 2066 Gee, J.S., Kent, D. V., 2007. Source of oceanic magnetic anomalies and the geomagnetic polarity time
2067 scale. <https://doi.org/10.7916/D8DV1V8P>
- 2068 Gernigon, L., Franke, D., Geoffroy, L., Schiffer, C., Foulger, G.R., Stoker, M., 2020. Crustal
2069 fragmentation, magmatism, and the diachronous opening of the Norwegian-Greenland Sea.
2070 *Earth-Science Rev.* <https://doi.org/10.1016/j.earscirev.2019.04.011>
- 2071 Gillard, M., Autin, J., Manatschal, G., 2016a. Fault systems at hyper-extended rifted margins and
2072 embryonic oceanic crust: Structural style, evolution and relation to magma. *Mar. Pet. Geol.* 76,
2073 51–67. <https://doi.org/10.1016/j.marpetgeo.2016.05.013>
- 2074 Gillard, M., Autin, J., Manatschal, G., Sauter, D., Munschy, M., Schaming, M., 2015. Tectonomagmatic
2075 evolution of the final stages of rifting along the deep conjugate Australian-Antarctic magma-poor
2076 rifted margins: Constraints from seismic observations. *Tectonics* 34, 753–783.
2077 <https://doi.org/10.1002/2015TC003850>.Received
- 2078 Gillard, M., Manatschal, G., Autin, J., 2016b. How can asymmetric detachment faults generate
2079 symmetric Ocean Continent Transitions? *Terra Nov.* 28, 27–34. <https://doi.org/10.1111/ter.12183>
- 2080 Hall, J., 1859. Description and Figures of the Organic Remains of the Lower Helderberg Group and
2081 Orinskany Sandstone. *Natural History of New-York, Paleontology.* *Geol. Surv. N.Y., Albany.*
- 2082 Hardy, S., 1993. Numerical modelling of the response to variable stretching rate of a domino fault
2083 block system. *Mar. Pet. Geol.* 10, 145–152. [https://doi.org/10.1016/0264-8172\(93\)90019-O](https://doi.org/10.1016/0264-8172(93)90019-O)
- 2084 Haug, E., 1900. Les géosynclinaux et les aires continentales: contribution à l'étude des transgressions
2085 et des regressions marines. *Au siège de la Société géologique de France.*
- 2086 Hauptert, I., Manatschal, G., Decarlis, A., Unternehr, P., 2016. Upper-plate magma-poor rifted margins:
2087 stratigraphic architecture and structural evolution. *Mar. Pet. Geol.* 69, 241–261.
2088 <https://doi.org/10.1016/j.marpetgeo.2015.10.020>
- 2089 Hopper, J.R., Funck, T., Tucholke, B.E., Loudon, K.E., Holbrook, W.S., Larsen, H.C., 2006. A deep
2090 seismic investigation of the Flemish Cap margin: Implications for the origin of deep reflectivity
2091 and evidence for asymmetric break-up between Newfoundland and Iberia. *Geophys. J. Int.* 164,
2092 501–515. <https://doi.org/10.1111/j.1365-246X.2006.02800.x>
- 2093 Hubbard, R.J., 1988. Age and significance of sequence boundaries on Jurassic and Early Cretaceous
2094 rifted continental margins. *Am. Assoc. Pet. Geol. Bull.* 72, 49–72.
2095 <https://doi.org/10.1306/703c81c8-1707-11d7-8645000102c1865d>

- 2096 Huismans, R., Beaumont, C., 2011. Depth-dependent extension, two-stage breakup and cratonic
2097 underplating at rifted margins. *Nature* 473, 74–78. <https://doi.org/10.1038/nature09988>
- 2098 Jagoutz, O., Müntener, O., Manatschal, G., Rubatto, D., Péron-Pinvidic, G., Turrin, B.D., Villa, I.M.,
2099 2007. The rift-to-drift transition in the North Atlantic: A stuttering start of the MORB machine?
2100 *Geology* 35, 1087–1090. <https://doi.org/10.1130/G23613A.1>
- 2101 Jarvis, G.T., McKenzie, D.P., 1980. Sedimentary basin formation with finite extension rates. *Earth*
2102 *Planet. Sci. Lett.* 48, 42–52. [https://doi.org/10.1016/0012-821X\(80\)90168-5](https://doi.org/10.1016/0012-821X(80)90168-5)
- 2103 Jourdon, A., Le Pourhiet, L., Mouthereau, F., May, D., 2020. Modes of Propagation of Continental
2104 Breakup and Associated Oblique Rift Structures. *J. Geophys. Res. Solid Earth* 125,
2105 e2020JB019906. <https://doi.org/10.1029/2020JB019906>
- 2106 Karner, G.D., Shillington, D.J., 2005. Basalt sills of the U reflector, Newfoundland basin: A
2107 serendipitous dating technique. *Geology* 33, 985–988. <https://doi.org/10.1130/G21971.1>
- 2108 Kay, M., 1951. North American geosynclines. Geological Society of America.
- 2109 Kober, L., 1923. *Bau und Entstehung der Alpen*. Berlin.
- 2110 Krawczyk, C.M., Reston, T.J., Boillot, G., Beslier, M.-O., 1996. Evidence for detachment tectonics on
2111 the Iberia Abyssal Plain rifted margin, Proceedings of the Ocean Drilling Program: Scientific
2112 Results.
- 2113 Kuszniir, N.J., Ziegler, P.A., 1992. The mechanics of continental extension and sedimentary basin
2114 formation: A simple-shear/pure-shear flexural cantilever model. *Tectonophysics* 215, 117–131.
2115 [https://doi.org/10.1016/0040-1951\(92\)90077-J](https://doi.org/10.1016/0040-1951(92)90077-J)
- 2116 Larsen, H.C., Mohn, G., Nirrengarten, M., Sun, Z., Stock, J., Jian, Z., Klaus, A., Alvarez-Zarikian, C.A.,
2117 Boaga, J., Bowden, S.A., Briais, A., Chen, Y., Cukur, D., Dadd, K., Ding, W., Dorais, M., Ferré,
2118 E.C., Ferreira, F., Furusawa, A., Gewecke, A., Hinojosa, J., Höfig, T.W., Hsiung, K.H., Huang, B.,
2119 Huang, E., Huang, X.L., Jiang, S., Jin, H., Johnson, B.G., Kurzawski, R.M., Lei, C., Li, B., Li, L.,
2120 Li, Y., Lin, J., Liu, C., Liu, C., Liu, Z., Luna, A.J., Lupi, C., McCarthy, A., Ningthoujam, L., Osono,
2121 N., Peate, D.W., Persaud, P., Qiu, N., Robinson, C., Satolli, S., Sauermilch, I., Schindlbeck, J.C.,
2122 Skinner, S., Straub, S., Su, X., Su, C., Tian, L., van der Zwan, F.M., Wan, S., Wu, H., Xiang, R.,
2123 Yadav, R., Yi, L., Yu, P.S., Zhang, C., Zhang, J., Zhang, Y., Zhao, N., Zhong, G., Zhong, L.,
2124 2018. Rapid transition from continental breakup to igneous oceanic crust in the South China Sea.
2125 *Nat. Geosci.* 11, 782–789. <https://doi.org/10.1038/s41561-018-0198-1>
- 2126 Lavier, L.L., Manatschal, G., 2006. A mechanism to thin the continental lithosphere at magma-poor
2127 margins. *Nature* 440, 324–328. <https://doi.org/10.1038/nature04608>
- 2128 Le Breton, E., Brune, S., Ustaszewski, K., Zahirovic, S., Seton, M., Müller, R.D., 2020. Kinematics and
2129 extent of the Piemont-Liguria Basin – implications for subduction processes in the Alps. *Solid*
2130 *Earth Discuss.* 1–42. <https://doi.org/10.5194/se-2020-161>
- 2131 Leeder, M.R., Gawthorpe, R.L., 1987. Sedimentary models for extensional tilt-block/half-graben
2132 basins, in: Coward, M.P., Dewey, J.F., Hancock, P.L. (Eds.), *Continental Extensional Tectonics*.
2133 Geological Society of London, Special publications No. 28, pp. 139–152.
2134 <https://doi.org/10.1144/gsl.sp.1987.028.01.11>
- 2135 Leleu, S., Hartley, A.J., van Oosterhout, C., Kennan, L., Ruckwied, K., Gerdes, K., 2016. Structural,
2136 stratigraphic and sedimentological characterisation of a wide rift system: The Triassic rift system
2137 of the Central Atlantic Domain. *Earth-Science Rev.*
2138 <https://doi.org/10.1016/j.earscirev.2016.03.008>
- 2139 Lemoine, M., 1985. Structuration jurassique des Alpes occidentales et paléogéographie de la Téthys
2140 ligurienne. *Bull. la Soc. Geol. Fr.* 8, 126–137.
- 2141 Lemoine, M., Bas, T., Arnaud-Vanneau, A., Arnaud, H., Dumont, T., Gidon, M., Bourbon, M., de
2142 Graciansky, P.C., Rudkiewicz, J.L., Megard-Galli, J., Tricart, P., 1986. The continental margin of
2143 the Mesozoic Tethys in the Western Alps. *Mar. Pet. Geol.* 3, 179–199.
2144 [https://doi.org/10.1016/0264-8172\(86\)90044-9](https://doi.org/10.1016/0264-8172(86)90044-9)

- 2145 Lemoine, M., Tricart, P., Boillot, G., 1987. Ultramafic and gabbroic ocean floor of the Ligurian Tethys
2146 (Alps, Corsica, Apennines): In search of a genetic model. *Geology* 15, 622–625.
2147 [https://doi.org/10.1130/0091-7613\(1987\)15](https://doi.org/10.1130/0091-7613(1987)15)
- 2148 Leroy, S., Razin, P., Autin, J., Bache, F., d'Acremont, E., Watremez, L., Robinet, J., Baurion, C.,
2149 Denèle, Y., Bellahsen, N., Lucazeau, F., Rolandone, F., Rouzo, S., Kiel, J.S., Robin, C.,
2150 Guillocheau, F., Tiberi, C., Basuyau, C., Beslier, M.O., Ebinger, C., Stuart, G., Ahmed, A.,
2151 Khanbari, K., Al Ganad, I., de Clarens, P., Unternehr, P., Al Toubi, K., Al Lazki, A., 2012. From
2152 rifting to oceanic spreading in the Gulf of Aden: A synthesis. *Arab. J. Geosci.* 5, 859–901.
2153 <https://doi.org/10.23919/RADIO.2017.8242234>
- 2154 Lescoutre, R., Manatschal, G., 2020. Role of rift-inheritance and segmentation for orogenic evolution:
2155 example from the Pyrenean-Cantabrian system. *Bull. la Soc. Geol. Fr.* 191.
- 2156 Lewis, D.S., Ross, E., Leander, M., 2014. New insights into late synrift subsidence from detailed well
2157 ties and seismic mapping, Campos Basin, Brazil, in: Pindell, J., Horn, B., Rosen, N., Weimer, P.,
2158 Dinkleman, M., Lowrie, A., Fillon, R., Granath, J., Kennan, L. (Eds.), *Sedimentary Basins: Origin,
2159 Depositional Histories and Petroleum Systems*. SEPM Society for Sedimentary Geology,
2160 Houston, pp. 98–115.
- 2161 Li, F., Sun, Z., Yang, H., 2018. Possible Spatial Distribution of the Mesozoic Volcanic Arc in the
2162 Present-Day South China Sea Continental Margin and Its Tectonic Implications. *J. Geophys.
2163 Res. Solid Earth* 123, 6215–6235. <https://doi.org/10.1029/2017JB014861>
- 2164 Luo, P., Manatschal, G., Ren, J., Zhao, Z., Wang, H., Tong, D., 2021. Tectono-magmatic and
2165 stratigraphic evolution of final rifting and breakup: evidence from the tip of the southwestern
2166 propagator in the South China Sea. *Mar. Pet. Geol.* 105079.
2167 <https://doi.org/10.1016/J.MARPETGEO.2021.105079>
- 2168 Lymer, G., Cresswell, D.J.F., Reston, T.J., Bull, J.M., Sawyer, D.S., Morgan, J.K., Stevenson, C.,
2169 Causer, A., Minshull, T.A., Shillington, D.J., 2019. 3D development of detachment faulting during
2170 continental breakup. *Earth Planet. Sci. Lett.* 515, 90–99.
2171 <https://doi.org/10.1016/j.epsl.2019.03.018>
- 2172 Manatschal, G., 2004. New models for evolution of magma-poor rifted margins based on a review of
2173 data and concepts from West Iberia and the Alps. *Int. J. Earth Sci.* 93, 432–466.
2174 <https://doi.org/10.1007/s00531-004-0394-7>
- 2175 Manatschal, G., 1999. Fluid- and reaction-assisted low-angle normal faulting: evidence from rift-related
2176 brittle fault rocks in the Alps (Err Nappe, eastern Switzerland). *J. Struct. Geol.* 21, 777–793.
2177 [https://doi.org/10.1016/S0191-8141\(99\)00069-3](https://doi.org/10.1016/S0191-8141(99)00069-3)
- 2178 Manatschal, G., Bernoulli, D., 1999. Architecture and tectonic evolution of nonvolcanic margins:
2179 Present-day Galicia and ancient Adria. *Tectonics* 18, 1099–1119.
2180 <https://doi.org/10.1029/1999TC900041>
- 2181 Manatschal, G., Chenin, P., Ghienne, J.-F., Ribes, C., Masini, E., n.d. A tectono-stratigraphic model
2182 for the syn-rift sequence of a magma-poor rifted margin (Part 1): insights from the Alpine Tethys.
2183 *Basin Res.*
- 2184 Manatschal, G., Chenin, P., Lescoutre, R., Miró, J., Cadenas, P., Saspiturry, N., Masini, E., Chevrot,
2185 S., Ford, M., Jolivet, L., Mouthereau, F., Thinon, I., Issautier, B., Calassou, S., 2021. The role of
2186 inheritance in forming rifts and rifted margins and building collisional orogens: a Biscay-Pyrenean
2187 perspective. *Bull. la Société Géologique Fr.*
- 2188 Manatschal, G., Engström, A., Desmurs, L., Schaltegger, U., Cosca, M., Müntener, O., Bernoulli, D.,
2189 2006. What is the tectono-metamorphic evolution of continental break-up: The example of the
2190 Tasna Ocean-Continent Transition. *J. Struct. Geol.* 28, 1849–1869.
2191 <https://doi.org/10.1016/j.jsg.2006.07.014>
- 2192 Manatschal, G., Froitzheim, N., Rubenach, M., Turrin, B.D., 2001. The role of detachment faulting in
2193 the formation of an ocean-continent transition: Insights from the Iberia Abyssal Plain. *Geol. Soc.
2194 Spec. Publ.* 187, 405–428. <https://doi.org/10.1144/GSL.SP.2001.187.01.20>
- 2195 Manatschal, G., Lavier, L.L., Chenin, P., 2015. The role of inheritance in structuring hyperextended rift

- 2196 systems: Some considerations based on observations and numerical modeling. *Gondwana Res.*
2197 27, 140–164. <https://doi.org/10.1016/j.gr.2014.08.006>
- 2198 Manatschal, G., Marquer, D., Früh-Green, G.L., 2000. Channelized fluid flow and mass transfer along
2199 a rift-related detachment fault (Eastern Alps, Southeast Switzerland). *Bull. Geol. Soc. Am.* 112,
2200 21–33. [https://doi.org/10.1130/0016-7606\(2000\)112<21:CFFAMT>2.0.CO;2](https://doi.org/10.1130/0016-7606(2000)112<21:CFFAMT>2.0.CO;2)
- 2201 Manatschal, G., Müntener, O., 2009. A type sequence across an ancient magma-poor ocean--
2202 continent transition: the example of the western Alpine Tethys ophiolites. *Tectonophysics* 473, 4–
2203 19. <https://doi.org/10.1016/j.tecto.2008.07.021>
- 2204 Manatschal, G., Nievergelt, P., 1997. A continent-ocean transition recorded in the Err and Platta
2205 nappes (Eastern Switzerland). *Eclogae Geol. Helv.* 90, 3–27.
- 2206 Manatschal, G., Sauter, D., Karpoff, A.M., Masini, E., Mohn, G., Lagabriele, Y., 2011. The Chenaillet
2207 Ophiolite in the French/Italian Alps: An ancient analogue for an Oceanic Core Complex? *Lithos*
2208 124, 169–184. <https://doi.org/10.1016/j.lithos.2010.10.017>
- 2209 Martins-Neto, M.A., Catuneanu, O., 2010. Rift sequence stratigraphy. *Mar. Pet. Geol.* 27, 247–253.
2210 <https://doi.org/10.1016/J.MARPETGEO.2009.08.001>
- 2211 Masini, E., Manatschal, G., Mohn, G., 2013. The Alpine Tethys rifted margins: Reconciling old and
2212 new ideas to understand the stratigraphic architecture of magma-poor rifted margins.
2213 *Sedimentology* 60, 174–196. <https://doi.org/10.1111/sed.12017>
- 2214 Masini, E., Manatschal, G., Mohn, G., Ghienne, J.F., Lafont, F., 2011. The tectono-sedimentary
2215 evolution of a supra-detachment rift basin at a deep-water magma-poor rifted margin: The
2216 example of the Samedan Basin preserved in the Err nappe in SE Switzerland. *Basin Res.* 23,
2217 652–677. <https://doi.org/10.1111/j.1365-2117.2011.00509.x>
- 2218 Masini, E., Manatschal, G., Mohn, G., Unternehr, P., 2012. Anatomy and tectono-sedimentary
2219 evolution of a rift-related detachment system: The example of the Err detachment (central Alps,
2220 SE Switzerland). *Bull. Geol. Soc. Am.* 124, 1535–1551. <https://doi.org/10.1130/B30557.1>
- 2221 McAlpine, K.D., 1990. Mesozoic stratigraphy, sedimentary evolution, and petroleum potential of the
2222 Jeanne d'Arc Basin, Grands Banks of Newfoundland.
- 2223 McKenzie, D., 1978. Some remarks on the development of sedimentary basins. *Earth Planet. Sci. Lett.*
2224 40, 25–32. [https://doi.org/10.1016/0012-821X\(78\)90071-7](https://doi.org/10.1016/0012-821X(78)90071-7)
- 2225 McLeod, A.E., Underhill, J.R., Davies, S.J., Dawers, N.H., 2002. The Influence of Fault Array Evolution
2226 on Synrift Sedimentation Patterns: Controls on Deposition in the Strathspey-Brent-Statfjord Half
2227 Graben, Northern North Sea. *Am. Assoc. Pet. Geol. Bull.* 86, 1061–1093.
2228 <https://doi.org/10.1306/61EEDC24-173E-11D7-8645000102C1865D>
- 2229 Menzies, Martin A, Klemperer, Simon L, Ebinger, Cynthia J, Baker, Joel, 2002. Characteristics of
2230 volcanic rifted margins, in: Menzies, M. A., Klemperer, S. L., Ebinger, C. J., Baker, J. (Eds.),
2231 Volcanic Rifted Margins. Geological Society of America Special Paper 362, Boulder, Colorado,
2232 pp. 1–14.
- 2233 Merino-Perez, I., 2016. Stratigraphic evolution of a segmented hyper-extended rifted margin: The
2234 example of the Western Iberia Margin (Master Thesis). Université de Strasbourg.
- 2235 Miró, J., Cadenas, P., Manatschal, G., Muñoz, J.A., 2021. Reactivation of a hyperextended rift system:
2236 the Basque-Cantabrian Pyrenees case. *Basin Res.* 00, 1–25. <https://doi.org/10.1111/bre.12595>
- 2237 Miró, J., Cadenas, P., Manatschal, G., Muñoz, J.A., n.d. Reactivation of a hyperextended rift system:
2238 the Basque-Cantabrian Pyrenees case.
- 2239 Mohn, G., Karner, G.D., Manatschal, G., Johnson, C.A., 2015. Structural and stratigraphic evolution of
2240 the Iberia–Newfoundland hyper-extended rifted margin: a quantitative modelling approach. *Geol.*
2241 *Soc. London, Spec. Publ.* 413, 53–89. <https://doi.org/10.1144/SP413.9>
- 2242 Mohn, G., Manatschal, G., Beltrando, M., Masini, E., Kusznir, N., 2012. Necking of continental crust in
2243 magma-poor rifted margins: Evidence from the fossil Alpine Tethys margins. *Tectonics* 31,
2244 TC1012. <https://doi.org/10.1029/2011TC002961>

- 2245 Mohn, G., Manatschal, G., Müntener, O., Beltrando, M., Masini, E., 2010. Unravelling the interaction
2246 between tectonic and sedimentary processes during lithospheric thinning in the Alpine Tethys
2247 margins. *Int. J. Earth Sci.* 99, 75–101. <https://doi.org/10.1007/s00531-010-0566-6>
- 2248 Montadert, L., de Charpal, O., Roberts, D., Guennoc, P., Sibuet, J.-C., 1979. Northeast Atlantic
2249 passive continental margins: Rifting and subsidence processes, in: Talwani, M., Hay, W., Ryan,
2250 W.B.F. (Eds.), *Deep Drilling Results in the Atlantic Ocean: Continental Margins and*
2251 *Paleoenvironment, Volume 3. American Geophysical Union (AGU)*, pp. 154–186.
2252 <https://doi.org/10.1029/me003p0154>
- 2253 Mosar, J., Eide, E. a., Osmundsen, P.T., Sommaruga, A., Torsvik, T.H., 2002. Greenland - Norway
2254 separation: A geodynamic model for the North Atlantic. *Nor. Geol. Tidsskr.* 82, 281–298.
- 2255 Murillas, J., Mougénot, D., Boulot, G., Comas, M.C., Banda, E., Mauffret, A., 1990. Structure and
2256 evolution of the Galicia Interior Basin (Atlantic western Iberian continental margin).
2257 *Tectonophysics* 184, 297–319. [https://doi.org/10.1016/0040-1951\(90\)90445-E](https://doi.org/10.1016/0040-1951(90)90445-E)
- 2258 Naliboff, J.B., Buitter, S.J.H., Péron-Pinvidic, G., Osmundsen, P.T., Tetreault, J., 2017. Complex fault
2259 interaction controls continental rifting. *Nat. Commun.* 8. [https://doi.org/10.1038/s41467-017-](https://doi.org/10.1038/s41467-017-00904-x)
2260 [00904-x](https://doi.org/10.1038/s41467-017-00904-x)
- 2261 Nirrengarten, M., Manatschal, G., Tugend, J., Kuszniir, N., Sauter, D., 2018. Kinematic Evolution of the
2262 Southern North Atlantic: Implications for the Formation of Hyperextended Rift Systems.
2263 *Tectonics* 37, 89–118. <https://doi.org/10.1002/2017TC004495>
- 2264 Nirrengarten, M., Manatschal, G., Yan, X., Kuszniir, N., Millot, B., 2016. Application of the critical
2265 Coulomb wedge theory to hyper-extended, magma-poor rifted margins. *Earth Planet. Sci. Lett.*
2266 442, 121–132.
- 2267 Nirrengarten, M., Mohn, G., Kuszniir, N.J., Sapin, F., Despinois, F., Pubellier, M., Chang, S.P., Larsen,
2268 H.C., Ringenbach, J.C., 2020. Extension modes and breakup processes of the southeast China-
2269 Northwest Palawan conjugate rifted margins. *Mar. Pet. Geol.* 113, 104123.
2270 <https://doi.org/10.1016/j.marpetgeo.2019.104123>
- 2271 Nonn, C., Leroy, S., Khanbari, K., Ahmed, A., 2017. Tectono-sedimentary evolution of the eastern Gulf
2272 of Aden conjugate passive margins: Narrowness and asymmetry in oblique rifting context.
2273 *Tectonophysics* 721, 322–348. <https://doi.org/10.1016/j.tecto.2017.09.024>
- 2274 Olsen, K.H., Morgan, P., 2006. Introduction: Progress in understanding continental rifts. *Dev.*
2275 *Geotecton.* [https://doi.org/10.1016/S0419-0254\(06\)80005-4](https://doi.org/10.1016/S0419-0254(06)80005-4)
- 2276 Osmundsen, P.T., Ebbing, J., 2008. Styles of extension offshore mid-Norway and implications for
2277 mechanisms of crustal thinning at passive margins. *Tectonics* 27.
2278 <https://doi.org/10.1029/2007TC002242>
- 2279 Osmundsen, P.T., Péron-Pinvidic, G., 2018. Crustal-scale fault interaction at rifted margins and the
2280 formation of domain-bounding breakaway complexes: Insights from offshore Norway. *Tectonics*
2281 37, 935–964.
- 2282 Osmundsen, P.T., Péron-Pinvidic, G., Ebbing, J., Erratt, D., Fjellanger, E., Bergslien, D., Syvertsen,
2283 S.E., 2016. Extension, hyperextension and mantle exhumation offshore Norway: a discussion
2284 based on 6 crustal transects. *Nor. J. Gology* 96, 343–372. <https://doi.org/10.17850/njg96-4-05>
- 2285 Osmundsen, P.T., Sommaruga, A., Skilbrei, J.R., Olesen, O., 2002. Deep structure of the Mid Norway
2286 rifted margin. *Nor. J. Geol.* 82, 205–224.
- 2287 Pérez-Gussinyé, M., Andrés-Martínez, M., Araújo, M., Xin, Y., Armitage, J., Morgan, J.P., 2020.
2288 Lithospheric Strength and Rift Migration Controls on Synrift Stratigraphy and Breakup
2289 Unconformities at Rifted Margins: Examples From Numerical Models, the Atlantic and South
2290 China Sea Margins. *Tectonics* 39, e2020TC006255. <https://doi.org/10.1029/2020TC006255>
- 2291 Pérez-Gussinyé, M., Ranero, C.R., Reston, T.J., 2003. Mechanisms of extension at nonvolcanic
2292 margins: Evidence from the Galicia interior basin, west of Iberia. *J. Geophys. Res.* 108.
2293 <https://doi.org/10.1029/2001JB000901>

- 2294 Péron-Pinvidic, G., Manatschal, G., 2009. The final rifting evolution at deep magma-poor passive
 2295 margins from Iberia-Newfoundland: A new point of view. *Int. J. Earth Sci.* 98, 1581–1597.
 2296 <https://doi.org/10.1007/s00531-008-0337-9>
- 2297 Péron-Pinvidic, G., Manatschal, G., Masini, E., Sutra, E., Flament, J.M., Hauptert, I., Unternehr, P.,
 2298 2015. Unravelling the along-strike variability of the Angola – Gabon rifted margin: a mapping
 2299 approach. *Geol. Soc. London, Spec. Publ.* 438. <https://doi.org/10.1144/SP438.1> #
- 2300 Péron-Pinvidic, G., Manatschal, G., Minshull, T. a., Sawyer, D.S., 2007. Tectonosedimentary evolution
 2301 of the deep Iberia-Newfoundland margins: Evidence for a complex breakup history. *Tectonics* 26,
 2302 n/a-n/a. <https://doi.org/10.1029/2006TC001970>
- 2303 Péron-Pinvidic, G., Manatschal, G., Osmundsen, P.T., 2013. Structural comparison of archetypal
 2304 Atlantic rifted margins: A review of observations and concepts. *Mar. Pet. Geol.* 43, 21–47.
 2305 <https://doi.org/10.1016/j.marpetgeo.2013.02.002>
- 2306 Peron-Pinvidic, G., Naliboff, J., 2020. The exhumation detachment factory. *Geology* 48, 635–639.
 2307 <https://doi.org/10.1130/G47174.1>
- 2308 Péron-Pinvidic, G., Osmundsen, P.T., 2018. The Mid Norwegian - NE Greenland conjugate margins:
 2309 Rifting evolution, margin segmentation, and breakup. *Mar. Pet. Geol.*
 2310 <https://doi.org/10.1016/j.marpetgeo.2018.08.011>
- 2311 Péron-Pinvidic, G., Osmundsen, P.T., Bunkholt, H., 2020. The proximal domain of the Mid-Norwegian
 2312 rifted margin: The Trøndelag Platform revisited. *Tectonophysics* 790, 228551.
 2313 <https://doi.org/10.1016/j.tecto.2020.228551>
- 2314 Petri, B., Duretz, T., Mohn, G., Schmalholz, S.M., Karner, G.D., Müntener, O., 2019. Thinning
 2315 mechanisms of heterogeneous continental lithosphere. *Earth Planet. Sci. Lett.* 512, 147–162.
 2316 <https://doi.org/10.1016/J.EPSL.2019.02.007>
- 2317 Picazo, S., Müntener, O., Manatschal, G., Bauville, A., Karner, G.D., Johnson, C., 2016. Mapping the
 2318 nature of mantle domains in Western and Central Europe based on clinopyroxene and spinel
 2319 chemistry: evidence for mantle modification during an extensional cycle. *Lithos.*
 2320 <https://doi.org/10.1016/j.lithos.2016.08.02>
- 2321 Pik, R., Bellahsen, N., Leroy, S., Denèle, Y., Razin, P., Ahmed, A., Khanbari, K., 2013. Structural
 2322 control of basement denudation during rifting revealed by low-temperature (U-Th-Sm)/He
 2323 thermochronology of the Socotra Island basement-Southern Gulf of Aden margin.
 2324 *Tectonophysics* 607, 17–31. <https://doi.org/10.1016/j.tecto.2013.07.038>
- 2325 Planke, S., Symonds, P.A., Alvestad, E., Skogseid, J., 2000. Seismic volcanosratigraphy of large-
 2326 volume basaltic extrusive complexes on rifted margins. *J. Geophys. Res.* 105, 19,335-19,351.
- 2327 Posamentier, H.W., Vail, P.R., 1988. Eustatic controls on clastic deposition II—sequence and systems
 2328 tract models. *Spec. Publ. SEPM* 42.
- 2329 Prosser, S., 1993. Rift-related linked depositional systems and their seismic expression, in: Williams,
 2330 G.D., Dobb, A. (Eds.), *Tectonics and Seismic Sequence Stratigraphy*. Geological Society Special
 2331 Publication. pp. 35–66.
- 2332 Ranero, C.R., Pérez-Gussinyé, M., 2010. Sequential faulting explains the asymmetry and extension
 2333 discrepancy of conjugate margins. *Nature* 468, 294–299. <https://doi.org/10.1038/nature09520>
- 2334 Ravnås, R., Steel, R.J., 1998. Architecture of marine rift-basin successions. *Am. Assoc. Pet. Geol.*
 2335 *Bull.* 82, 110–146. <https://doi.org/10.1306/1D9BC3A9-172D-11D7-8645000102C1865D>
- 2336 Ravnås, R., Windelstad, J., Mellere, D., Nøttvedt, A., Sjøblom, T.S., Steel, R.J., Wilson, R.C.L., 1997.
 2337 A marine Late Jurassic syn-rift succession in the Lusitanian Basin, western Portugal — tectonic
 2338 significance of stratigraphic signature. *Sediment. Geol.* 114, 237–266.
 2339 [https://doi.org/10.1016/S0037-0738\(97\)00068-7](https://doi.org/10.1016/S0037-0738(97)00068-7)
- 2340 Ren, J., Pang, X., Lei, C., Yu, P., Luo, P., 2018. Characteristics and formation mechanism of
 2341 deepwater and ultra-deepwater basins in the northern continental margin of the South China
 2342 Sea. *Chinese J. Geophys.* 61, 4901–4920. <https://doi.org/10.6038/>

- 2344 Reston, T.J., McDermott, K.G., 2011. Successive detachment faults and mantle unroofing at magma-poor rifted margins. *Geology* 39, 1071–1074. <https://doi.org/10.1130/G32428.1>
- 2346 Ribes, C., Ghienne, J.-F., Manatschal, G., Decarlis, A., Karner, G.D., Figueredo, P.H., Johnson, C.A.,
2347 2019a. Long-lived mega fault-scarps and related breccias at distal rifted margins: insights from
2348 present-day and fossil analogues. *J. Geol. Soc. London*. 176, 801–816.
2349 <https://doi.org/10.1144/jgs2018-181>
- 2350 Ribes, C., Ghienne, J.F., Manatschal, G., Dall’Asta, N., Stockli, D.F., Galster, F., Gillard, M., Karner,
2351 G.D., 2020. The Grès Singuliers of the Mont Blanc region (France and Switzerland): stratigraphic
2352 response to rifting and crustal necking in the Alpine Tethys. *Int. J. Earth Sci.* 109, 2325–2352.
2353 <https://doi.org/10.1007/s00531-020-01902-z>
- 2354 Ribes, C., Manatschal, G., Ghienne, J.-F., Karner, G.D., Johnson, C.A., Figueredo, P.H., Incerpi, N.N.,
2355 Epin, M., 2019b. The syn-rift stratigraphic record across a fossil hyper-extended rifted margin:
2356 the example of the northwestern Adriatic margin exposed in the Central Alps. *Int. J. Earth Sci.*
2357 108, 2071–2095. [https://doi.org/DOI: 10.1007/s00531-019-01750-6](https://doi.org/DOI:10.1007/s00531-019-01750-6)
- 2358 Ribes, C., Petri, B., Ghienne, J., Manatschal, G., Galster, F., Karner, G.D., Figueredo, P.H., Johnson,
2359 C.A., Karpoff, A., 2019c. Tectono-sedimentary evolution of a fossil ocean-continent transition:
2360 Tasna nappe, central Alps (SE Switzerland). *Geol. Soc. Am. Bull.* 1–20.
2361 <https://doi.org/10.1130/B35310.1/4863878/b35310.pdf>
- 2362 Ros, E., Pérez-Gussinyé, M., Araújo, M., Thoaldo Romeiro, M., Andrés-Martínez, M., Morgan, J.P.,
2363 2017. Lower crustal strength controls on melting and serpentinization at magma-poor margins:
2364 Potential implications for the South Atlantic. *Geochemistry, Geophys. Geosystems* 18, 4538–
2365 4557. <https://doi.org/10.1002/2017GC007212>
- 2366 Rowan, M.G., Ratliff, R.A., 2012. Cross-section restoration of salt-related deformation: Best practices
2367 and potential pitfalls. *J. Struct. Geol.* <https://doi.org/10.1016/j.jsg.2011.12.012>
- 2368 Samuel, M.A., Harbury, N., Bott, R., Thabet, A.M., 1997. Field observations from the Socotran
2369 platform: Their interpretation and correlation to Southern Oman. *Mar. Pet. Geol.* 14, 661–673.
2370 [https://doi.org/10.1016/s0264-8172\(96\)00033-5](https://doi.org/10.1016/s0264-8172(96)00033-5)
- 2371 Schlische, R.W., 1995. Geometry and Origin of Fault-Related Folds in Extensional Settings. *Am.*
2372 *Assoc. Pet. Geol. Bull.* 79, 1661–1678. [https://doi.org/10.1306/7834DE4A-1721-11D7-
2373 8645000102C1865D](https://doi.org/10.1306/7834DE4A-1721-11D7-8645000102C1865D)
- 2374 Sengör, A.M.C., Burke, K., 1978. Relative timing of rifting and volcanism on Earth and its tectonic
2375 implications. *Geophys. Res. Lett.* 5, 419–421. <https://doi.org/10.1029/GL005i006p00419>
- 2376 Serck, C.S., Braathen, A., Olaussen, S., Osmundsen, P.T., Midtkandal, I., van Yperen, A.E., Indrevær,
2377 K., 2021. Supradetachment to rift basin transition recorded in continental to marine deposition;
2378 Paleogene Bandar Jissah Basin, NE Oman. *Basin Res.* 33, 544–569.
2379 <https://doi.org/10.1111/bre.12484>
- 2380 Sharp, I., Higgins, S., Scott, M., Freitag, U., Allsop, C., Kane, K., Sultan, A., Doubleday, P., Leppard,
2381 C., Bloomfield, J., Cody, J., Rait, G., Haynes, S., 2017. Rift to drift evolution and hyperextension
2382 in the North Atlantic – Insights from a super-regional approach, in: Davies, M., Carlisle, C. (Eds.),
2383 *Atlantic Ireland 2017*. Dublin, pp. 22–23.
- 2384 Sinclair, I.K., 1994. tectonism and sedimentation in the Jeanne d’Arc Basin, Grand Banks of
2385 Newfoundland. University of Aberdeen.
- 2386 Sinclair, I.K., 1993. Tectonism: the dominant factor in mid-Cretaceous deposition in the Jeanne d’Arc
2387 Basin, Grand Banks. *Mar. Pet. Geol.* 10, 530–549. [https://doi.org/10.1016/0264-8172\(93\)90058-
2388 Z](https://doi.org/10.1016/0264-8172(93)90058-Z)
- 2389 Sinclair, I.K., 1988. Evolution of Mesozoic-Cenozoic sedimentary basins in the Grand Banks area of
2390 Newfoundland and comparison with Falvey’s (1974) rift model, *Bulletin of Canadian Petroleum*
2391 *Geology*. GeoScienceWorld.

- 2392 Skogseid, J., 2010. The Orphan Basin - a key to understanding the kinematic linkage between North
2393 and NE Atlantic Mesozoic rifting. II Cent. North Atl. Conjug. Margins Conf. II, 13–23.
- 2394 Spencer, J.E., 1984. Role of tectonic denudation in warping and uplift of low-angle normal faults.
2395 *Geology* 12, 95–98.
- 2396 Steinmann, G., 1905. *Geologische Beobachtungen in den Alpen*. Wagners Universitäts-
2397 Buchdruckerei.
- 2398 Stille, H., 1936. The Present Tectonic State of the Earth. *Am. Assoc. Pet. Geol. Bull.* 20, 849–880.
2399 <https://doi.org/10.1306/3d932dfa-16b1-11d7-8645000102c1865d>
- 2400 Stille, H., 1924. *Grundfragen der vergleichenden Tektonik*. Berlin.
- 2401 Stille, H., 1913. *Evolution und Revolutionen in der Erdgeschichte*. Berlin.
- 2402 Stockli, D.F., Bosworth, W.B., 2018. Timing of extensional faulting along the magma-poor central and
2403 northern red sea rift margin-transition from regional extension to necking along a hyperextended
2404 rifted margin, in: *Geological Setting, Palaeoenvironment and Archaeology of the Red Sea*.
2405 Springer International Publishing, pp. 81–111. https://doi.org/10.1007/978-3-319-99408-6_5
- 2406 Sun, Z., Lin, J., Qiu, N., Jian, Z., Wang, P., Pang, X., Zheng, J., Zhu, B., 2019. The role of magmatism
2407 in the thinning and breakup of the South China Sea continental margin Special Topic: The South
2408 China Sea Ocean Drilling. *Natl. Sci. Rev.* 6, 871–876. <https://doi.org/10.1093/NSR/NWZ116>
- 2409 Sutra, E., Manatschal, G., 2012. How does the continental crust thin in a hyperextended rifted margin?
2410 Insights from the Iberia margin. *Geology* 40, 139–142. <https://doi.org/10.1130/G32786.1>
- 2411 Sutra, E., Manatschal, G., Mohn, G., Unternehr, P., 2013. Quantification and restoration of extensional
2412 deformation along the Western Iberia and Newfoundland rifted margins. *Geochemistry,*
2413 *Geophys. Geosystems* 14, 2575–2597. <https://doi.org/10.1002/ggge.20135>
- 2414 Tillmans, F., Gawthorpe, R.L., Jackson, C.A.L., Rotevatn, A., 2021. Syn-rift sediment gravity flow
2415 deposition on a Late Jurassic fault-terraced slope, northern North Sea. *Basin Res.* 33, 1844–
2416 1879. <https://doi.org/10.1111/bre.12538>
- 2417 Tucholke, B.E., Sawyer, D.S., Sibuet, J., Brest, I.C. De, 2007. Breakup of the Newfoundland–Iberia
2418 rift, in: Karner, G.D., Manatschal, G., Pinheiro, L.M. (Eds.), *Imaging, Mapping and Modelling*
2419 *Continental Lithosphere Extension and Breakup*; Geological Society, London, Special
2420 Publications, 282. The Geological Society of London, pp. 9–46. <https://doi.org/10.1144/SP282.2>
- 2421 Tugend, J., Gillard, M., Manatschal, G., Nirrengarten, M., Harkin, C., Epin, M.-E., Sauter, D., Autin, J.,
2422 Kuszniir, N., McDermott, K., 2020. Reappraisal of the magma-rich versus magma-poor rifted
2423 margin archetypes. *Geol. Soc. London, Spec. Publ.* 476, 23–47. <https://doi.org/10.1144/SP476.9>
- 2424 Tugend, J., Manatschal, G., Kuszniir, N.J., Masini, E., Mohn, G., Thinon, I., 2014. Formation and
2425 deformation of hyperextended rift systems: Insights from rift domain mapping in the Bay of
2426 Biscay-Pyrenees. *Tectonics* 33, 1239–1276. <https://doi.org/10.1002/2014TC003529>
- 2427 Urquhart, E., 2001. Depositional environment of synrift sediments on the Iberia margin, in: AGU Fall
2428 Meeting Abstracts. pp. PP42B-0505.
- 2429 Waltham, D., Hardy, S., Abousetta, A., 1993. Sediment geometries and domino faulting. *Geol. Soc.*
2430 *Spec. Publ.* 71, 67–85. <https://doi.org/10.1144/GSL.SP.1993.071.01.04>
- 2431 Welford, J.K., Smith, J.A., Hall, J., Deemer, S., Srivastava, S.P., Sibuet, J.-C., 2010. Structure and
2432 rifting evolution of the northern Newfoundland Basin from Erable multichannel seismic reflection
2433 profiles across the southeastern margin of Flemish Cap. *Geophys. J. Int.* 180, 976–998.
2434 <https://doi.org/10.1111/j.1365-246X.2009.04477.x>
- 2435 Wernicke, B., 1985. Uniform-sense normal simple shear of the continental lithosphere. *Can. J. Earth*
2436 *Sci.* 22, 108–125. <https://doi.org/10.1139/e85-009>
- 2437 Whiting, L., Haughton, P.D.W., Shannon, P.M., 2020. From rifting to hyperextension: Upper Jurassic–
2438 Lower Cretaceous tectono-stratigraphy of the Porcupine Basin, Irish Atlantic Margin. *Basin Res.*
2439 33, 1662–1696. <https://doi.org/10.1111/bre.12530>

- 2440 Wielens, J.B.W., Jauer, C.D., Williams, G.L., 2006. Is there a viable petroleum system in the Carson
2441 and Salar Basins, offshore Newfoundland? *J. Pet. Geol.* 29, 303–326.
2442 <https://doi.org/10.1111/j.1747-5457.2006.00303.x>
- 2443 Wilson, R.C.L., Manatschal, G., Wise, S., 2001. Rifting along non-volcanic passive margins:
2444 Stratigraphic and seismic evidence from the Mesozoic successions of the Alps and Western
2445 Iberia. *Geol. Soc. London, Spec. Publ.* 187, 429–452.
2446 <https://doi.org/10.1144/gsl.sp.2001.187.01.21>
- 2447 Withjack, M.O., Schlische, R.W., Olsen, P.E., 2002. Rift-Basin Structure and Its Influence on
2448 Sedimentary Systems. *Spec. Publ. SEPM* 57–81.
- 2449 Xie, X., Ren, J., Pang, X., Lei, C., Chen, H., 2019. Stratigraphic architectures and associated
2450 unconformities of Pearl River Mouth basin during rifting and lithospheric breakup of the South
2451 China Sea. *Mar. Geophys. Res.* 40, 129–144. <https://doi.org/10.1007/s11001-019-09378-6>
- 2452 Yang, P., Welford, J.K., 2021. Investigating the Porcupine Atlantic margin, offshore Ireland, through
2453 integration of new seismic reflection and gravity data. *Tectonophysics* 807, 228809.
2454 <https://doi.org/10.1016/j.tecto.2021.228809>
- 2455 Yielding, G., 1990. Footwall uplift associated with Late Jurassic normal faulting in the northern North
2456 Sea. *J. - Geol. Soc.* 147, 219–222. <https://doi.org/10.1144/gsjgs.147.2.0219>
- 2457 Zastrozhnov, D., Gernigon, L., Gogin, I., Planke, S., Abdelmalak, M.M., Polteau, S., Faleide, J.I.,
2458 Manton, B., Myklebust, R., 2020. Regional structure and polyphased Cretaceous-Paleocene rift
2459 and basin development of the mid-Norwegian volcanic passive margin.
2460 <https://doi.org/10.1016/j.marpetgeo.2020.104269>
- 2461 Zhang, C., Manatschal, G., Pang, X., Sun, Z., Zheng, J., Li, H., Sun, L., Zhang, J., Zhao, Y., 2020.
2462 Discovery of Mega-Sheath Folds Flooring the Liwan Subbasin (South China Sea): Implications
2463 for the Rheology of Hyperextended Crust. *Geochemistry, Geophys. Geosystems* 21,
2464 e2020GC009023. <https://doi.org/10.1029/2020GC009023>
- 2465 Zhang, C., Su, M., Pang, X., Zheng, J., Liu, B., Sun, Z., Manatschal, G., 2019. Tectono-Sedimentary
2466 Analysis of the Hyperextended Liwan Sag Basin (Midnorthern Margin of the South China Sea).
2467 *Tectonics* 38, 470–491. <https://doi.org/10.1029/2018TC005063>
- 2468 Zhang, C., Sun, Z., Manatschal, G., Pang, X., Qiu, N., Su, M., Zheng, J., Li, H., Gu, Y., Zhang, J.,
2469 Zhao, Y., 2021. Syn-rift magmatic characteristics and evolution at a sediment-rich margin:
2470 Insights from high-resolution seismic data from the South China Sea. *Gondwana Res.* 91, 81–96.
2471 <https://doi.org/10.1016/j.gr.2020.11.012>
- 2472

2473
2474
2475

TABLE CAPTION

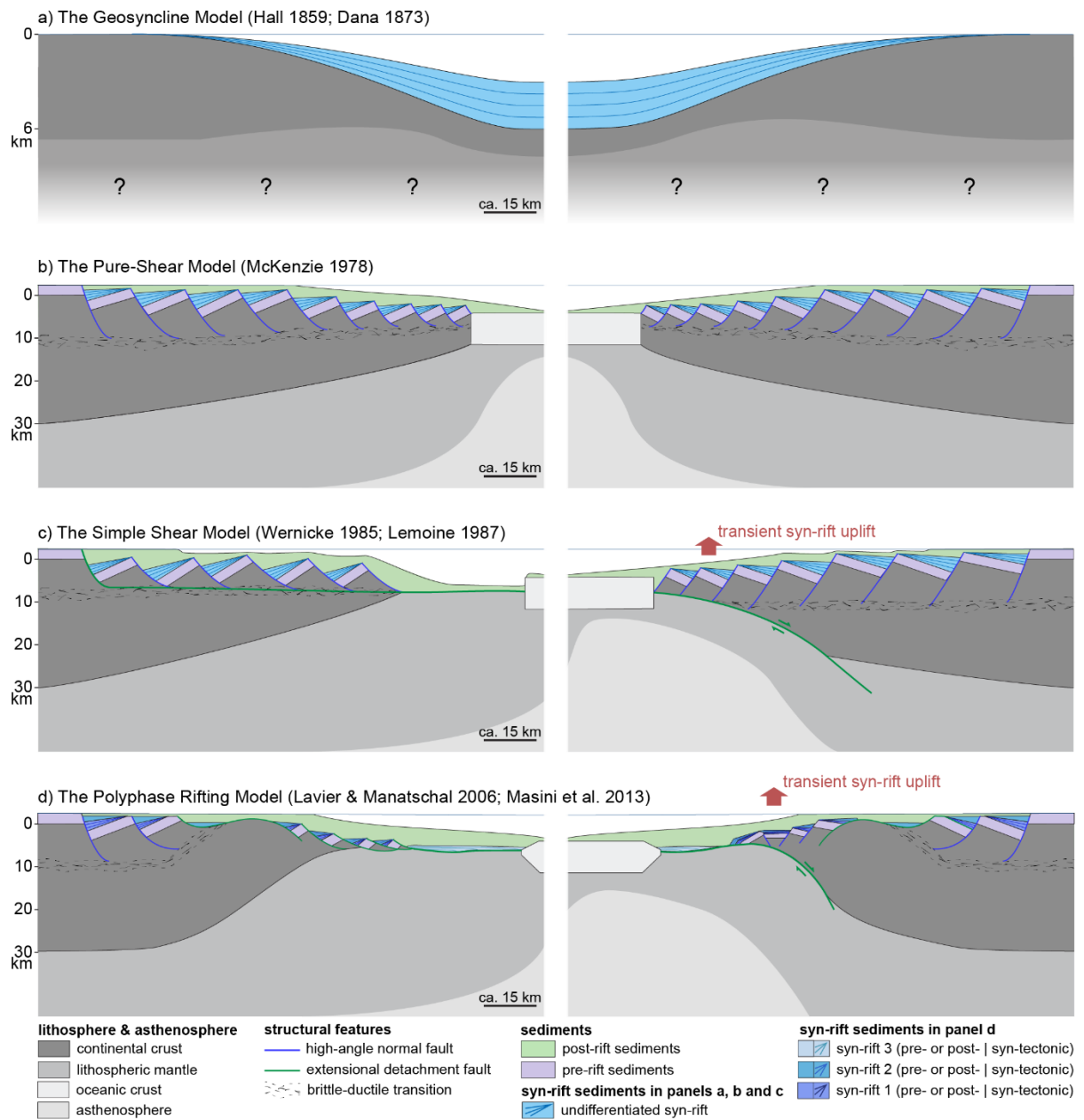
	Necking		Hyperextension		Mantle exhumation		Proto-oceanic				
	phase duration	domain width	phase duration	domain width	phase duration	domain width	Phase duration	domain width			
Alps	6 My (Ribes et al. 2019)	ca. 10 My (Manatschal et al. this vol.)	unknown	5 My (Ribes et al. 2019)	ca. 10 My (Manatschal et al. this vol.)	unknown	18 My (Ribes et al. 2019)	ca. 10 My (Manatschal et al. this vol.)	unknown	X	unknown
Iberia–Newfnd.	ca. 10 My (Mohn et al. 2015, with ref.)	ca. 100 (E) & 45 (W) km (Sutra et al. 2013)	ca. 5 My (Mohn et al. 2015, with ref.)	ca. 60 & 45 km (Sutra et al. 2013)	ca. 25 My (Mohn et al. 2015, with ref.)	ca. 80 (E) & 90(W) km (Sutra et al. 2013)			X		X
NW SCS	7 My (Chao et al. subm.)	N margin: ca. 60 km (Chao et al. Subm.)	4 My (Chao et al. Subm.)	ca. 25 (N) & 30 (S) km (Chao et al. Subm.)			X	X	2 My (Chao et al. subm)		X
Norway	Late Mid-Jurassic–base Cretaceous (ca. 25 My? Péron-Pinvidic et al. 2018, with ref.)	20–80 km (Osmundsen & Péron-Pinvidic 2018)	Base Cretaceous–Late Cretaceous (ca. 60 My? Péron-Pinvidic et al. 2018, with ref.)	unknown	unknown	unknown	unknown	unknown	Late Cretaceous–Paleocene (ca. 30 My? Péron-Pinvidic et al. 2018, with ref.)		unknown
Socotra	< 6 My? (This study)	unknown	ca. 10 My? (This study)	20–30 km (Nonn et al. 2017)	unknown	ca. 10 km (Nonn et al. 2017)			X		X

Table 1: Summary of the duration of the different rift phases and width of the different rift domains at the rift systems presented in this study.

2476
2477
2478
2479
2480

2481
2482

FIGURE CAPTIONS



2483
2484
2485
2486
2487
2488
2489

Figure 1: Schematic illustration of the evolution of stratigraphic models for rifted margins: a) the Geosyncline Model (Dana, 1873; Hall, 1859); b) the Pure-Shear or Depth-Uniform Thinning Model by McKenzie (1978); c) the Simple-Shear Model by Wernicke (1985); and d) the Polyphase Stretching–Thinning–Exhumation Model by Lavier and Manatschal (2006). Note that the scale for sedimentary deposits is vertically exaggerated compared to that of the crust.

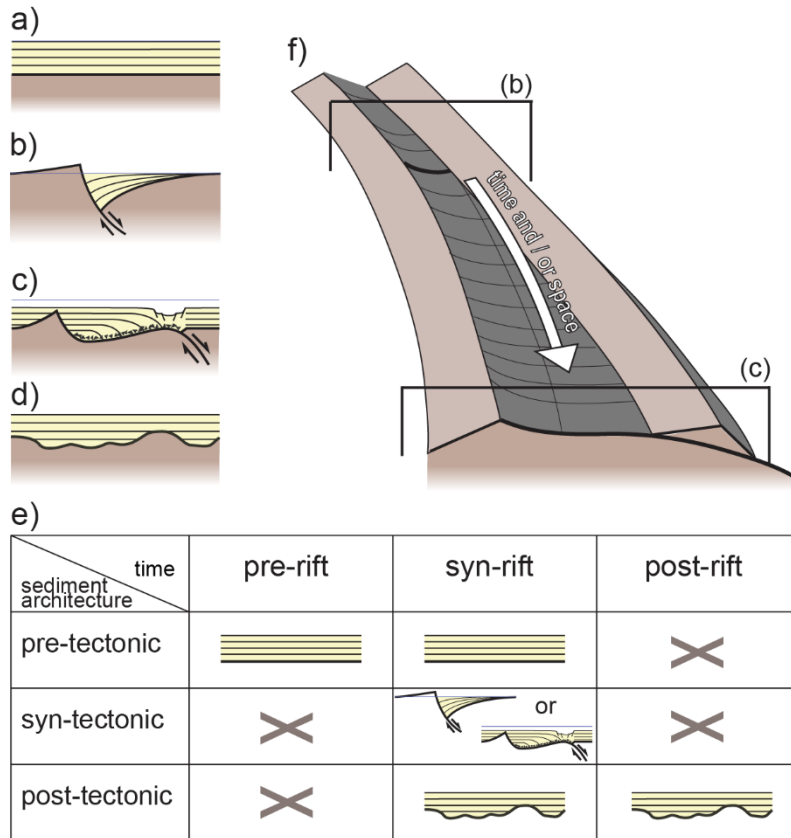


Figure 2: Schematic stratigraphic architectures depending on the tectonic context during sediment deposition: a) pre-tectonic; b) syn-tectonic half-graben wedge-shaped; c) syn-tectonic supra-detachment wedge-shaped; d) post-tectonic. e) relationships between the pre-, syn-, post-rift time intervals and the pre-, syn-, post-tectonic sedimentary architectures; f) schematic illustration of the evolution of a high-angle normal fault into a low-angle extensional detachment fault as extension progresses (modified from Péron-Pinvidic et al., 2007). Note that all schematics represent idealized architectures deposited in sediment-rich systems.

2490
 2491
 2492
 2493
 2494
 2495
 2496
 2497
 2498

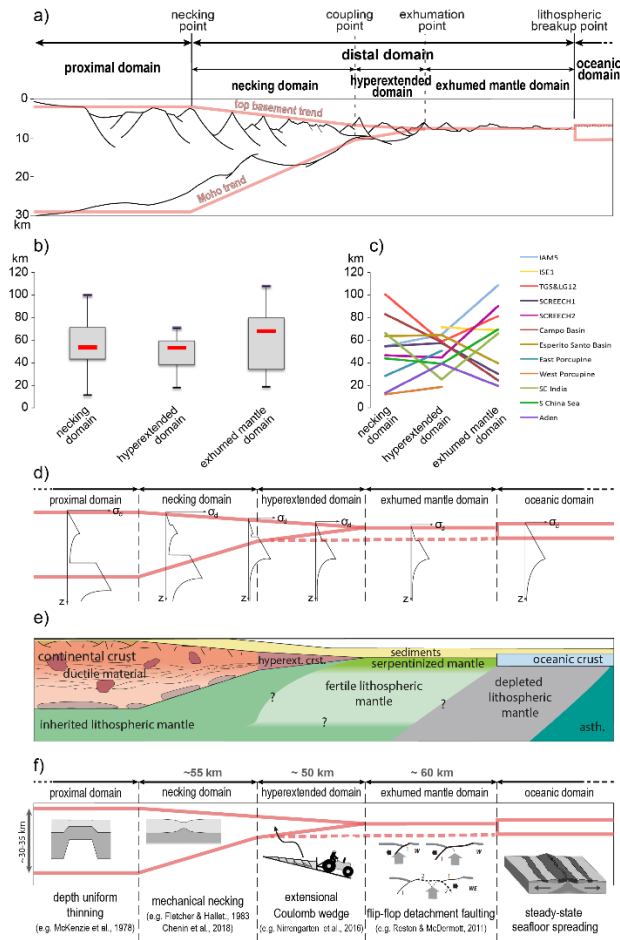


Figure 3: a) Schematic cross section highlighting the primary morphology of magma-poor rifted margins (from Chenin *et al.*, 2017); b) Width of the different distal domains in magma-poor rifted margins (from Chenin *et al.*, 2017); c) Width relationships among the different distal domains in magma-poor rifted margins (from Chenin *et al.*, 2017); d) First-order rheological evolution across a typical magma-poor rifted margin represented by schematic depth-dependent stress profiles; σ_d : deviatoric stress; z : depth; e) Schematic cross section displaying the first-order lithology across a typical magma-poor rifted margin (modified from Chenin *et al.*, 2017). f) Schematic cross section displaying the dominant deformation mechanism associate with the different rift domains of magma-poor rifted margins.

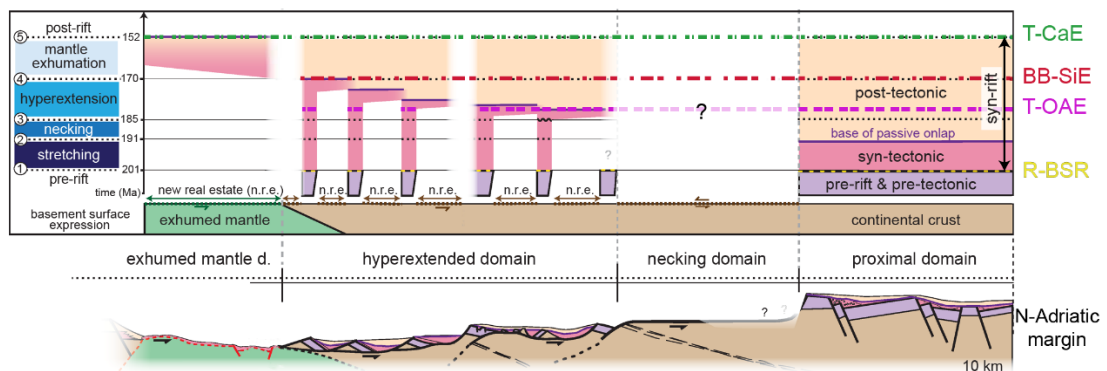
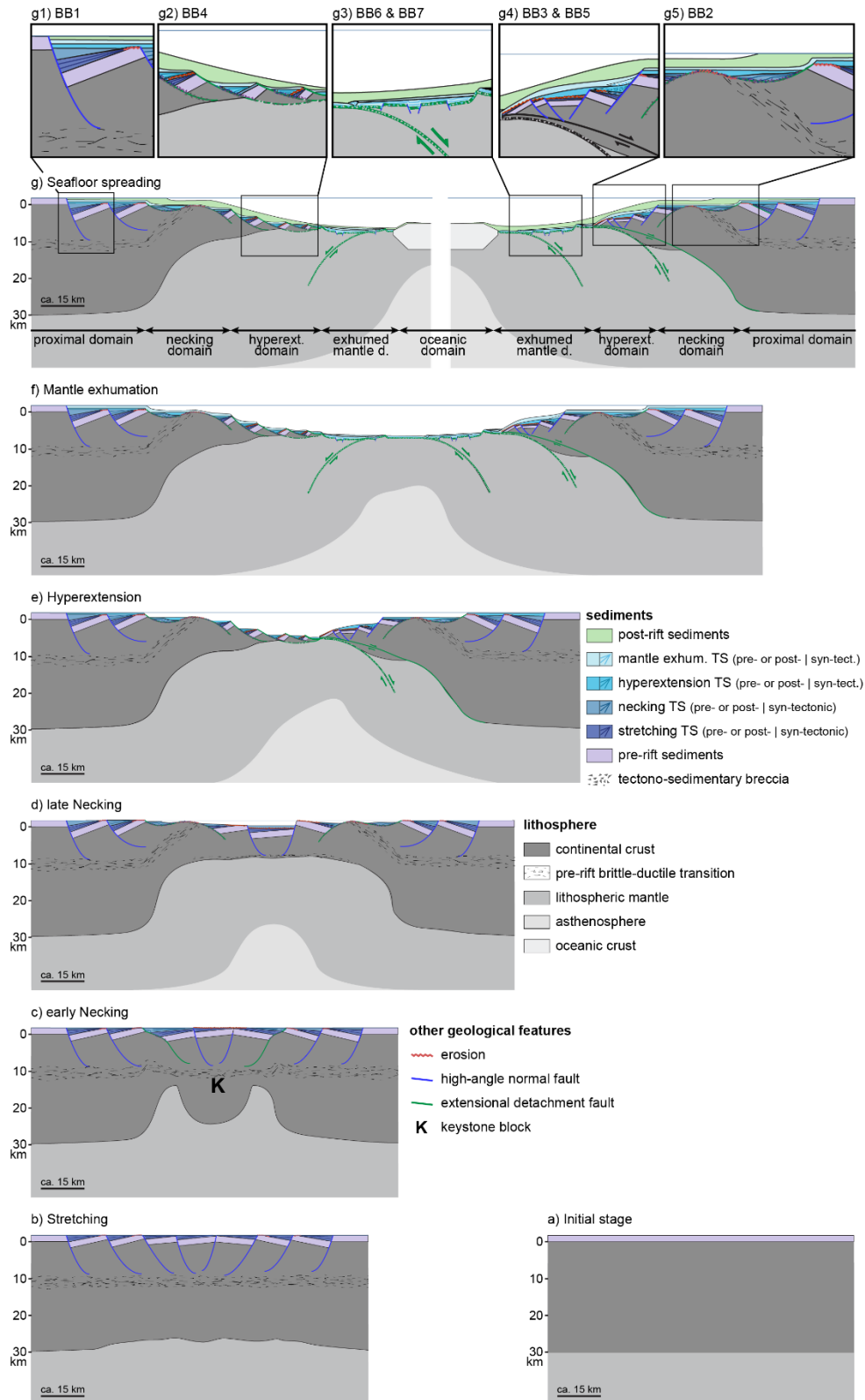


Figure 4: Wheeler diagram representing the spatio-temporal distribution of pre-, syn- and post-tectonic sedimentary sequences across the Adriatic margin of the Alpine Tethys (modified from Ribes *et al.*, 2019b). The dotted lines in the Wheeler diagram represent timelines that correspond to dated global or local events, namely: BB-SiE: Bajocian-Bathonian bio-Siliceous Event; R-BSR: Rhaetian Base of the Syn-rift sequence; T-CaE Tithonian Carbonate Event; T-OAE: Toarcian Oceanic Anoxic Event. Abbreviation n.r.e. stands for *new real estate*.

2499
2500
2501
2502
2503
2504
2505
2506
2507
2508
2509

2510
2511
2512
2513
2514
2515
2516



2518
 2519
 2520
 2521
 2522
 2523
 2524

Figure 5: Schematic evolution of an idealized magma-poor rifting (crustal surface and pre-rift sediment length are conserved among the different stages): a) pre-rift setting; b) stretching phase; c) early necking phase; d) late necking phase; e) hyperextension phase; f) mantle exhumation phase g) seafloor spreading phase. Insets g1-g5 zoom on characteristic “Building Blocks” (BB1-BB7) of rifted margins (see Manatschal *et al.*, this volume, for a description of the different Building Blocks).

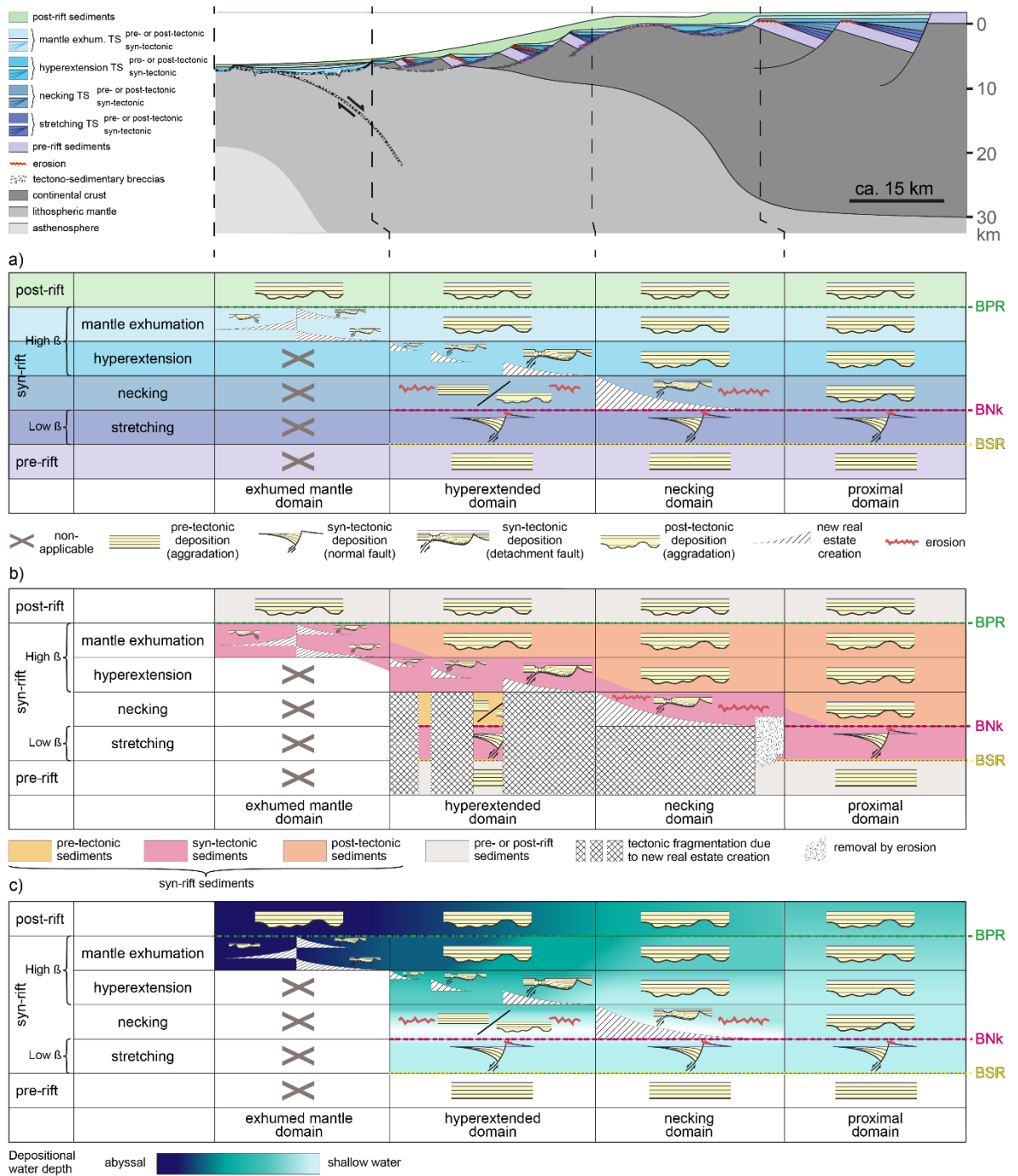
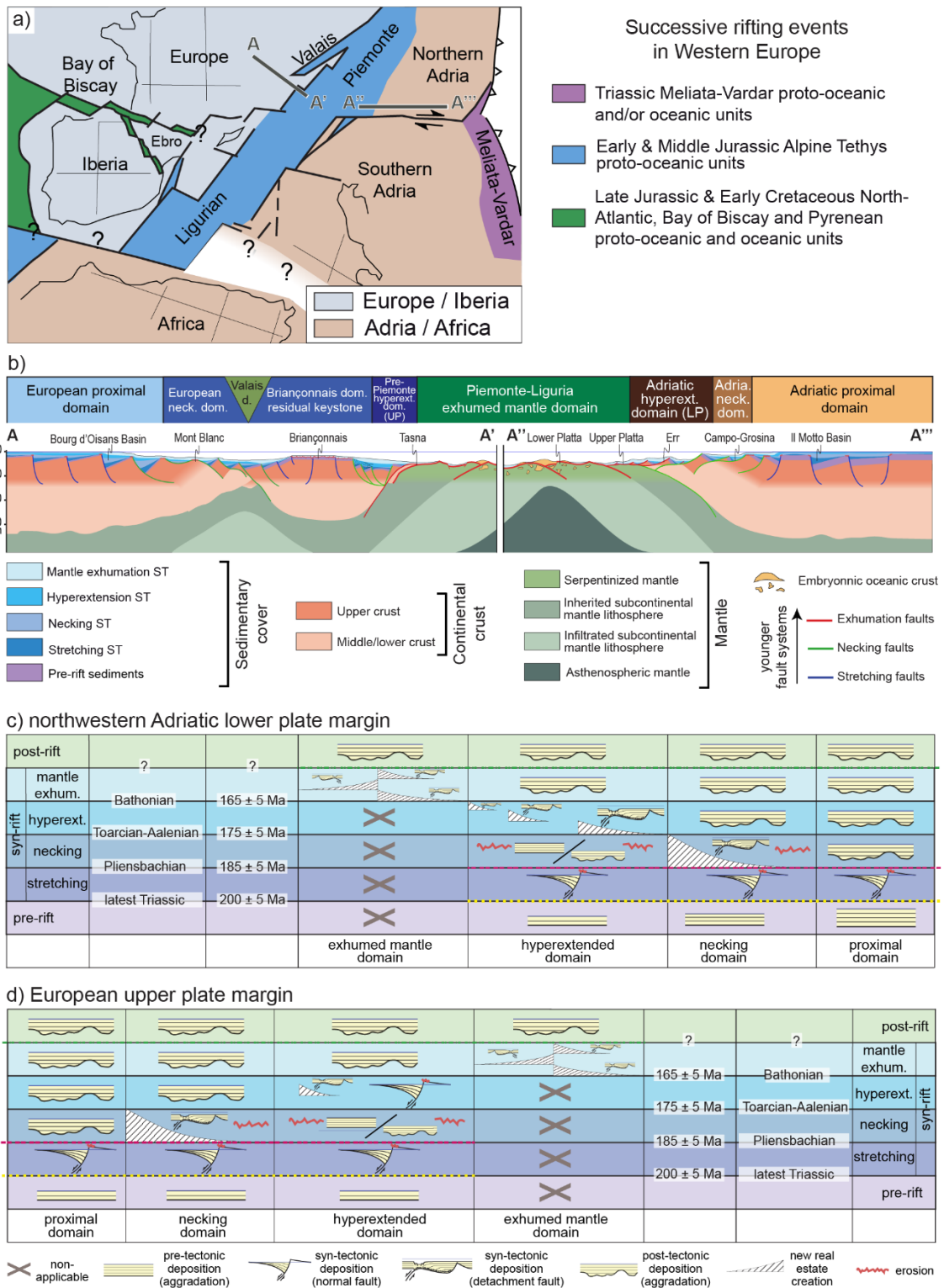
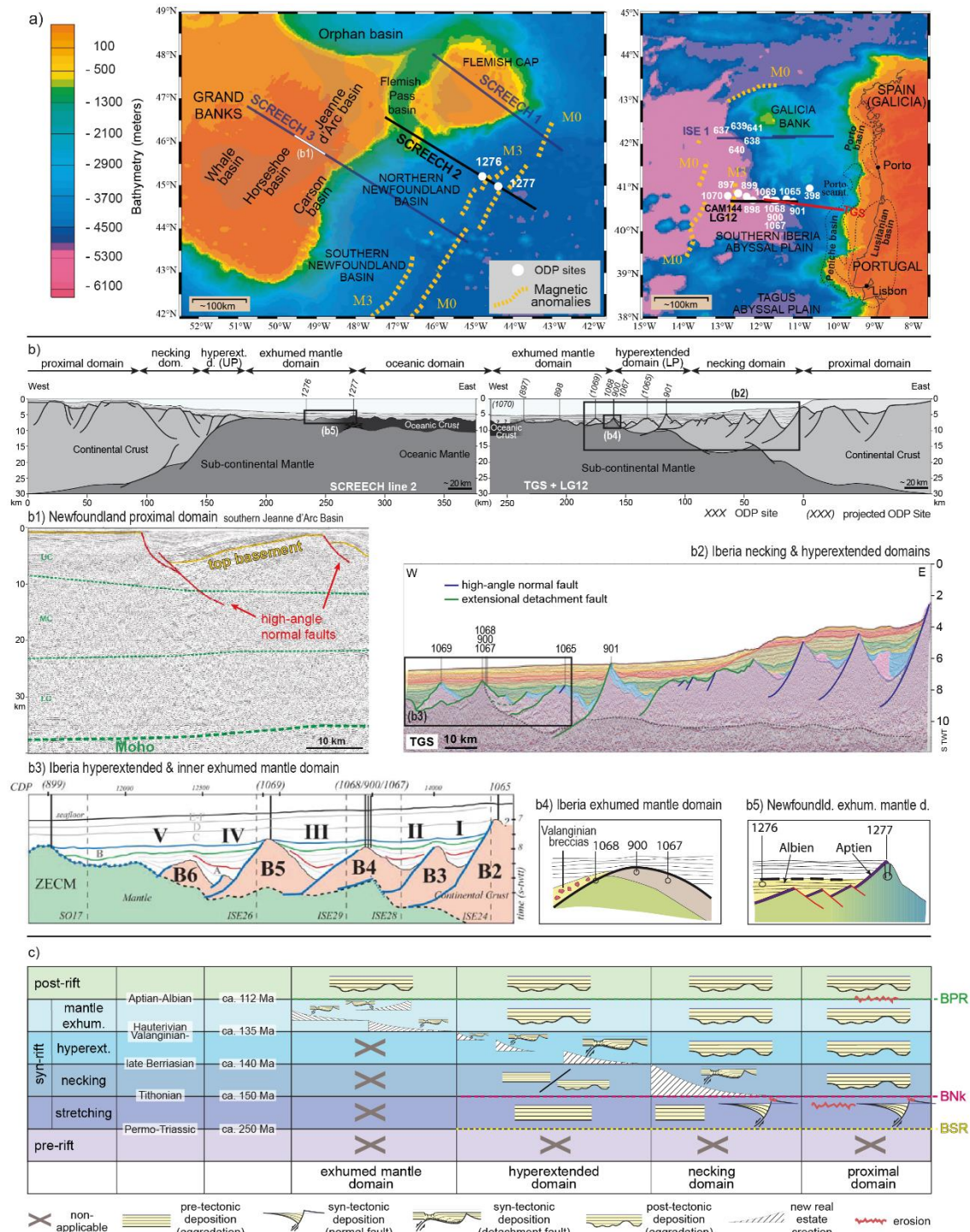


Figure 6: Tables summarizing the main characteristics of each system tract in the different rift domains of our idealized model: a) main structures and related stratigraphic architecture; b) distribution of pre-, syn- and post-tectonic sedimentation and tectonic fragmentation; c) evolution of the depositional water depth.



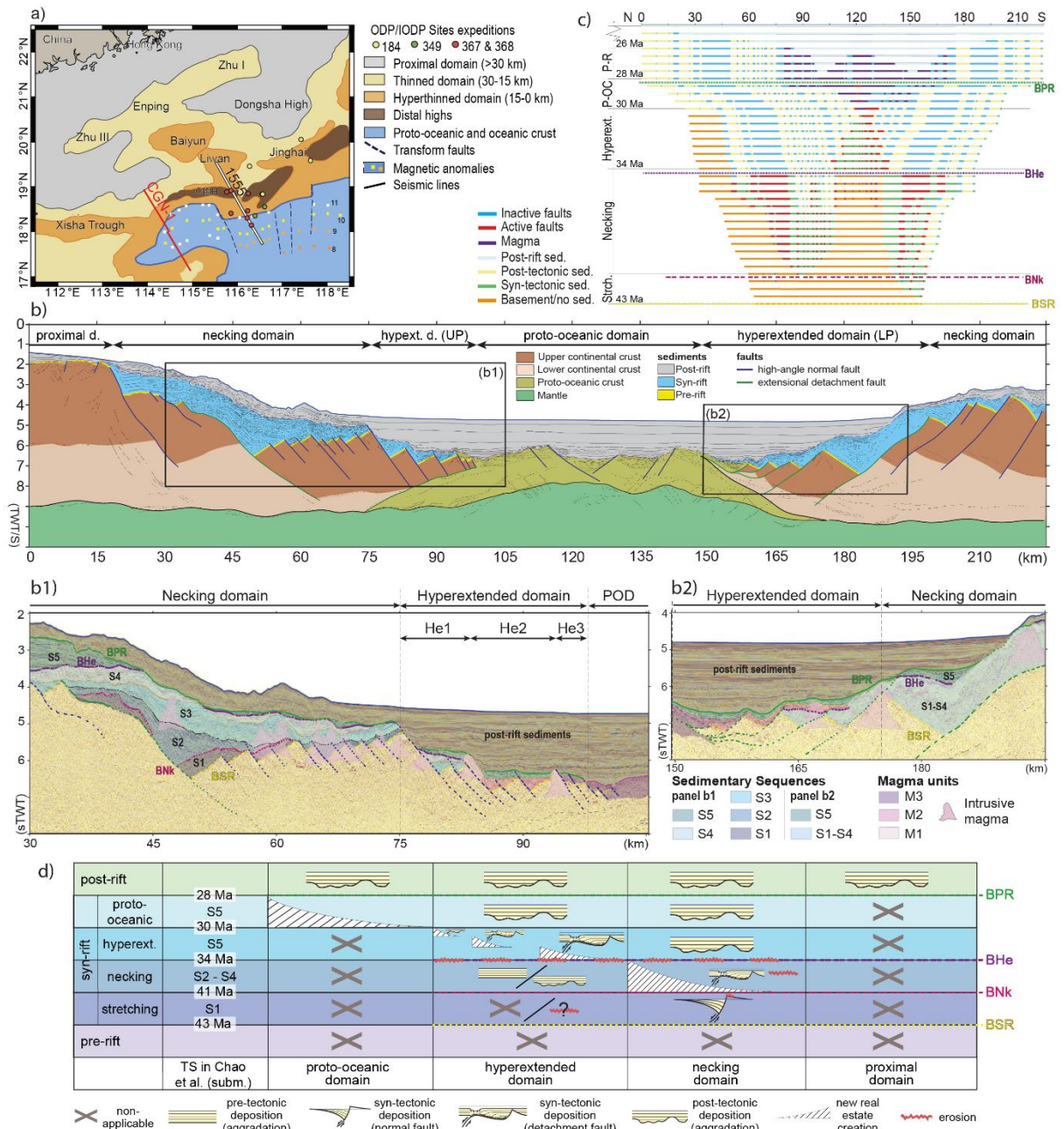
2532
2533
2534
2535
2536
2537
2538
2539
2540
2541

Figure 7: a) Schematic map showing the succession of rifting events in Western Europe (modified from Manatschal and Müntener, 2009).; b) Reconstruction of a synthetic section across the former Alpine Tethys rift system during the Late Jurassic margins. See panel (a) for location and note that section A—A' across the European margin is offset from section A''—A''' across the Adriatic margin. Abbreviations: hyperext.: hyperextended; d.: domain; Low. Aust. N.: Lower Austroalpine nappes; OCT: Ocean–Continent Transition; c) and d) Tables synthesizing the sedimentary architectures in each system tract in the different rift domains of the northwestern Adriatic and European margin, respectively.



2542
 2543
 2544
 2545
 2546
 2547
 2548
 2549
 2550
 2551
 2552
 2553
 2554

Figure 8: a) map of the Iberia–Newfoundland rifted margins and location of the public seismic profiles and drill holes (modified from Sutra *et al.*, 2013); b) interpreted SCREECH 2, TGS and LG 12 seismic sections across the conjugate Iberia–Newfoundland rifted margins (modified from Sutra *et al.*, 2013); b1) close up on the southern Jeanne d’Arc Basin on the SCREECH 3 seismic transect (modified from Deemer *et al.*, 2009); b2) stratigraphic overview of the Iberian necking and hyperextended domains (from Merino-Perez, 2016, and references therein); b3) stratigraphic interpretation of the CAM 144 seismic line imaging the Iberian hyperextended domain (from Péron-Pinvidic *et al.*, 2007); b4) and b5) stratigraphic overview from the exhumed mantle domain of Iberia and Newfoundland, respectively (modified from Sutra *et al.*, 2013); c) Table synthesizing the sedimentary architectures in each system tract in the different rift domains of the Iberian margin.



2555
 2556
 2557
 2558
 2559
 2560
 2561
 2562
 2563

Figure 9: a) Rift domain map showing the location of the CGN-1 transect and IODP Sites (modified from Nirrengarten *et al.* 2020); b) linedrawing of the CGN-1 line by Chao *et al.* (2021); b1) and b2) close-up of the outer necking - inner hyperextended domains of the northern and southern margin, respectively; c) spatio-temporal evolution of active vs inactive faulting and sedimentation along the studied transect (from Chao *et al.* 2021); f) Table synthesizing the sedimentary architectures of each system tract in the different rift domains of the northern margin of the NW-SCS. Abbreviation POD stands for Proto-Oceanic Domain.

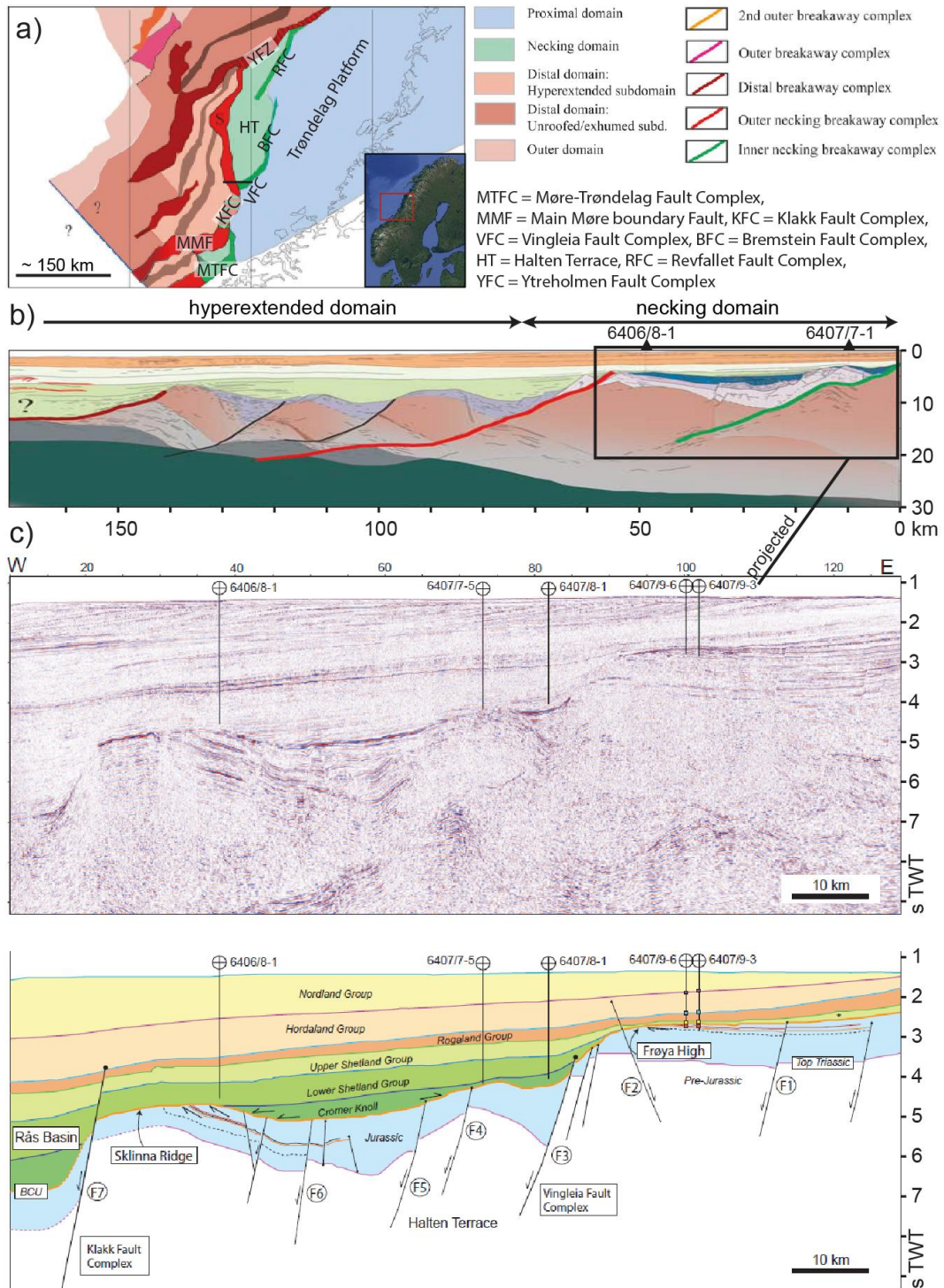
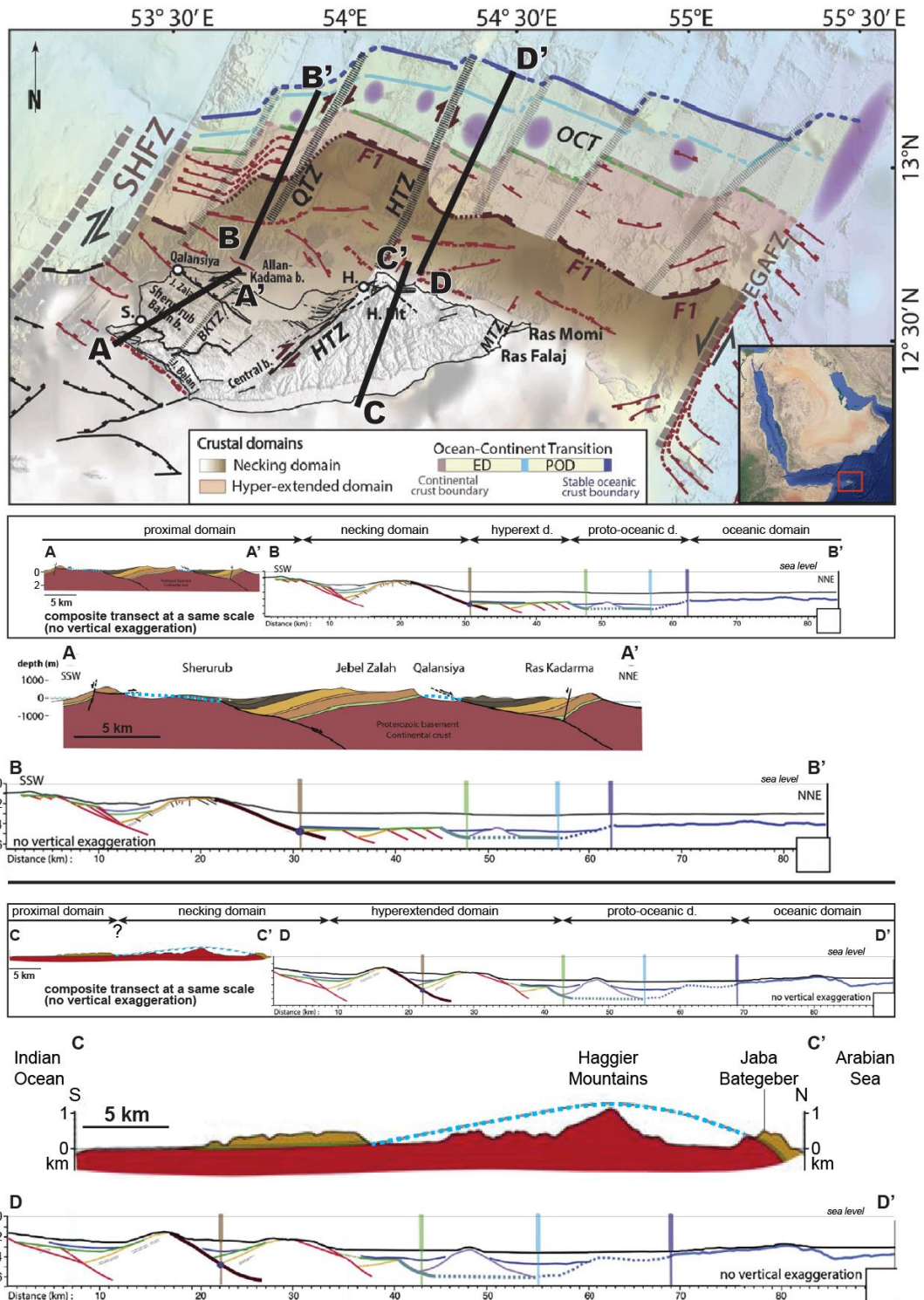


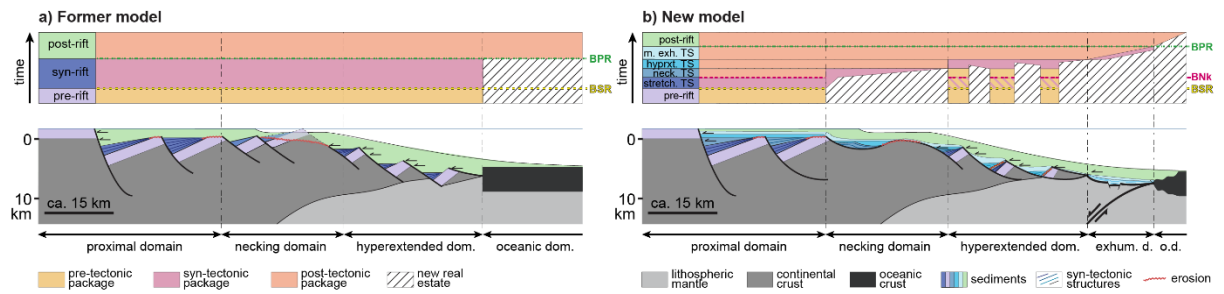
Figure 10: a) Map of the rift domains and intervening breakaway fault complexes at the mid-Norwegian margin (modified from Osmundsen and Péron-Pinvidic, 2018). Inset map from Google Earth; b) Interpreted seismic transect across the necking and hyperextended domains south of the Halten Terrace (no vertical exaggeration; modified from Osmundsen and Péron-Pinvidic, 2018; see panel a for location); c) uninterpreted and interpreted seismic section highlighting pervasive erosion of the Jurassic sequence at the breakaway of both the Vingleia and Klakk fault complexes (from Bell *et al.*, 2014).

2564
 2565
 2566
 2567
 2568
 2569
 2570
 2571
 2572



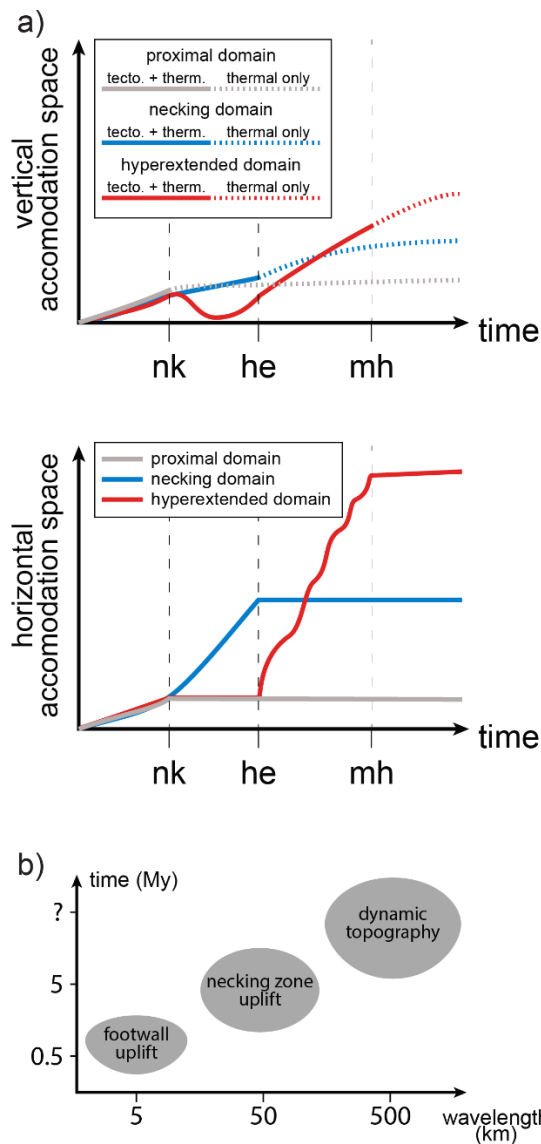
2573
 2574
 2575
 2576
 2577
 2578

Figure 11: Map of the rift domains in the region of Socotra and interpreted transects onshore (A-A' from Nonn *et al.*, 2017; C-C' from (Fournier *et al.*, 2007) and offshore (B-B' and D-D' from Nonn *et al.*, 2017). Transects are first shown at the same scale and without vertical exaggeration for reference. Inset map from Google Earth.



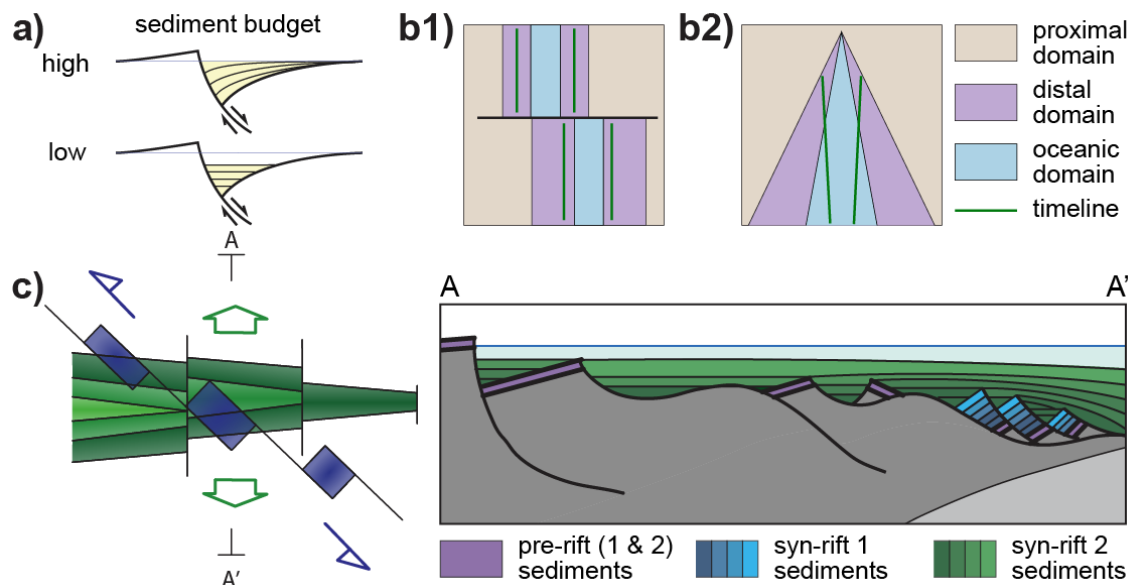
2579
2580
2581
2582
2583

Figure 12: Schematic view of a rifted margin interpretation and corresponding Wheeler diagram according to a) former tectono-stratigraphic models; b) the tectono-stratigraphic presented in this study.



2584
2585
2586
2587
2588
2589

Figure 13: a) Graphs displaying the evolution of vertical and horizontal accommodation creation with time for the different rift domains. Note that vertical accommodation creation may result either from tectonics with a minor thermal component, or from thermal relaxation only. b) Characteristic wavelengths and time of uplift for different tectonic or geodynamic processes.



2590
 2591
 2592
 2593
 2594
 2595
 2596
 2597
 2598

Figure 14: Main pitfalls to be kept in mind when applying a tectono-stratigraphic model to the interpretation of rift systems: a) impact of the ratio between sedimentation- and subsidence rate: sediment-starved systems will incompletely or even not record tectonic activity. b1) impact of segmentation and b2) propagating extension on the correlation of timelines across rift systems. c) impact of spatially overprinting extensional events (i.e., “multi-stage rifting”), which may incorporate sedimentary sequences unrelated to the rifting event considered (modified from Miró *et al.* 2021).